AMMONIUM ION EFFECTS
ON
HYBRIDOMA CELL PHYSIOLOGY

Thesis by

Anne McQueen

In Partial Fulfillment of the Requirements

for the Degree of

Doctor of Philosophy

California Institute of Technology

Pasadena, California

1989

Submitted May 26, 1989

Acknowledgements

Thanks to Jay Bailey for providing guidance and motivation. (His ambitions for my work made me ambitious.) Thanks to Shelley Diamond for introducing me to both cell culture and flow cytometry.

Much appreciation to Nancy DaSilva and Jackie Shanks for sharing this experience with me.

I am very grateful to my loving husband Samir for going through it all over again with me, and to our friends, Khalid, Barbara and Dimitri, for putting up with us.

It is difficult to put into words the indebtedness I feel towards my parents. They have been the greatest influence of my life. They taught me to have high aspirations and never to give up.

To Mom and Dad

Abstract

Ammonium ion is an important inhibitor of mammalian cell growth. Measurements of changes in hybridoma intracellular pH upon NH_4Cl addition (using a flow cytometric assay in which cells are stained with a pH-sensitive fluorescent dye) indicate that NH_4^+ causes a steady-state cytoplasmic acidification. There is a correlation between NH_4Cl effects on growth and on intracellular pH, and these effects are independent of the external pH value, suggesting that NH_4^+, not NH_3 (produced by the dissociation of NH_4^+ at higher external pH values), is the species responsible for growth inhibition.

Ammonium ion has similar effects on batch growth in flasks in an incubator and in a bioreactor at controlled pH and dissolved oxygen concentration. Both decreases in the external pH value and increases in the NH_4Cl concentration inhibit glucose consumption in batch growth. This is hypothesized to be due to intracellular pH decreases. However, cell growth is not dependent on glucose consumption. Changes in the external pH value and in the NH_4Cl concentration, which result in growth inhibition, have no effect on the specific antibody production rate.

A mechanism is proposed and a mathematical model is developed to explain the intracellular pH decreases caused by NH_4^+. This model incorporates a detailed description of the behavior of the Na^+/H^+-exchanger, which is assumed to be the main pH_i controller of the cell. The model is able to reproduce the salient features of the experimental results.

Table of Contents

CHAPTER 1.

Introduction

Part A. Flow effects on the viability and lysis of suspended mammalian cells

A mouse myeloma cell line growing in suspension was subjected intermittently to flow through a sudden contraction and to turbulent flow in a capillary tube. The short-term effects on cell viability and lysis and the long-term effects on growth of the surviving cells were determined. Both the diameter and the length of the capillary tube were varied, leading to changes in the average wall shear stress level and the residence time per pass.

The effects of varying the percent serum and the cell line on the specific lysis rate in the turbulent flow device were determined In addition, the specific lysis rate was measured in a laminar flow device consisting of a smoothly converging and diverging tube. The residence time in the laminar flow device was similar to that in the turbulent flow device. The diameter of the constriction was varied to determine the effect of the average wall shear stress level. The effects of increasing the viscosity of the suspension by adding 70,000 MW dextran were evaluated in both the turbulent and laminar flow devices.

Part B. Ammonium ion effects on hybridoma cell physiology

Previous work has indicated that ammonium ion is an important inhibitor of mammalian cell growth, including hybridoma cell growth [1-6]. The importance of studying the effects of NH_4^+ on cells results from the fact that glutamine has been found to be essential for mammalian cell growth [7,8] and the fact that NH_4^+ is a byproduct of glutamine metabolism. There are two possible mechanisms for growth inhibition by NH_4^+. The first mechanism involves the uptake of the weak base NH_3 into the lysosomes causing alkalinization [9-14], while the second mechanism involves the uptake of the weak acid NH_4^+ into the cytoplasm causing acidification [15]. Previous work on the effects of external pH (pH_e) on growth and on intracellular pH (pH_i) had shown that a 0.2 unit decrease in pH_i is sufficient to inhibit growth [16-20].

The effects of NH_4Cl on the pH_i of hybridoma cells were measured by staining the cells with a fluorescent pH indicator and monitoring their fluorescence as a function of time in the flow cytometer [21,22]. The effects of NH_4Cl on growth were determined for batch growth of cells in flasks in an incubator. It was attempted to correlate the effects of different NH_4Cl concentrations on growth and on pH_i. In addition, the pH_e-dependence of NH_4Cl effects on growth and pH_i was investigated to determine the relative importance of the two possible mechanisms of growth inhibition by NH_4^+. The first mechanism, involving the effects of NH_3 on the lysosome, is expected to be pH_e-independent since the concentration of NH_3, at a given NH_4Cl concentration, decreases as pH_e decreases; while the second mechanism, involving the effects of NH_4^+ on the cytoplasm, should be pH_e-independent since the concentration of NH_4^+, at a given NH_4Cl concentration, is approximately constant as a function of pH_e in the range 6.8 to 7.6 (pK of NH_4^+ is 9.2). The effects of pH_e alone were determined first and these effects were compared with those of NH_4Cl addition at constant pH_e.

The effects of NH_4Cl on cell growth were also studied in a bioreactor at controlled pH and dissolved oxygen concentration, to determine whether the cultures in flasks in an incubator are oxygen-limited and whether this contributes to growth inhibition by NH_4Cl. From the literature [23,24], it was evident that a decrease in pH_i could inhibit glycolysis. Therefore, the effects of NH_4Cl on glucose consumption and lactate production were investigated for cells grown in flasks in an incubator and in the bioreactor. In addition, cell glutamine consumption and NH_4^+ production were measured, since previous studies had indicated that a considerable amount of cell energy is derived from glutamine [25-30]. The effects of NH_4Cl on antibody production were also determined.

To explain how leakage of NH_4^+ into the cell leads to a permanent cytoplasmic acidification, a mechanism was proposed and a mathematical model formulated from it. Boron and DeWeer had previously developed a mathematical model for the effects of NH_4Cl on pH_i, including equations for the passive fluxes of NH_3 and NH_4^+ into and out of the cell and for the active transport of H^+ out of the cell [15]. However, they did not determine the steady-state value of pH_i in the presence of NH_4Cl, and they employed only a rough mathematical description of the H^+ pump. Therefore, their model was extended to include a detailed description of the properties of the Na^+/H^+-exchanger, which is now known to be the main pH_i regulator of the cell [31] and which has been studied extensively [32,33]. The steady-state value of pH_i as a function of NH_4Cl concentration was determined from the model, employing parameter values taken from the literature [33,34]. Boron and DeWeer [15] had shown that the rate of cytoplasmic acidification is primarily a function of the NH_4^+ permeability, which is expected to be cell-line dependent. The model was used to determine the NH_4^+ permeability of the hybridoma cells, by comparing simulation results with experimental data on the steady-state value of pH_i in the presence of 10 mM NH_4Cl. In addition, the dependence of model results on the parameter values chosen was investigated.

REFERENCES

1. Miller, W.M.; Wilke, C.R.; Blanch, H.W.: Transient responses of hybridoma cells to lactate and ammonia pulse and step changes in continuous culture. Bioprocess Engr. 3 (1988) 113-122

2. Glacken, M.W.; Adema, E.; Sinskey, A.J.: Mathematical descriptions of hybridoma culture kinetics for optimization of bioreactors, I. Initial metabolic rates. Biotech. Bioeng. 32 (1988) 491-506

3. Thorpe, J.S.; Murdin, A.D.; Sanders, P.G.; Spier, R.E.: The effect of waste products of cellular metabolism on growth and protein synthesis in a mouse hybridoma cell line. Presented at the 194th National meeting of the American Chemical Society, New Orleans, Louisiana, August 31-September 4, 1987

4. Reuveny, S.; Velez, D.; Macmillan, J.D.; Miller, L.: Factors affecting cell growth and monoclonal antibody production in stirred reactors. J. Immunol. Methods 86 (1986) 53-59

5. Iio, M.; Moriyama, A.; Murakami, H.: Effects on cell proliferation of metabolites produced by cultured cells and their removal from culture in defined media. In: Murakami, H.; Yamane, I.; Barnes, D.W.; Mather, J.P.; Hayashi, I.; Sato, G.H. (Eds.): Growth and differentiation of cells in a defined environment, pp. 437-442. Tokyo: Kodansha and Berlin: Springer 1985

6. Butler, M.; Spier, R.E.: The effects of glutamine utilization and ammonia production on the growth of BHK cells in microcarrier cultures. J. Biotechnology 1 (1984) 187-196

7. McKeehan, W.L.: Glutaminolysis in animal cells. In: Morgan, M.J. (Ed.):

Carbohydrate metabolism in cultured cells, pp. 111-150. New York: Plenum Press 1986

8. Zielke, H.R.; Sumbilla, C.M.; Zielke, C.L.; Tildon, J.T.; Ozand, P.T.: Glutamine metabolism by cultured mammalian cells. In: Haussinger, D.; Sies H. (Eds.): Glutamine metabolism in mammalian tissues, pp. 247-254. Berlin: Heidelberg and New York: Springer 1984

9. Poole, B.; Ohkuma, S.: Effect of weak bases on the intralysosomal pH in mouse peritoneal macrophages. J. Cell Biol. 90 (1981) 665-669

10. Van Leuven, F.; Cassiman, J.-J.; Van Den Berghe, H.: Primary amines inhibit recycling of α_2M receptors in fibroblasts. Cell 20 (1980) 37-43

11. Tietze, C.; Schlesinger, P.; Stahl, P.: Chloroquine and ammonium ion inhibit receptor-mediated endocytosis of mannose glycoconjugates by macrophages: Apparent inhibition of receptor recycling. Biochem. Biophys. Res. Commun. 93 (1980) 1-8

12. King, A.C.; Hernaez-Davis, L.; Cuatrecasas, P.: Lysosomotropic amines cause intracellular accumulation of receptors for epidermal growth factor. PNAS USA 77 (1980) 3283-3287

13. King, A.C.; Hernaez-Davis, L.; Cuatrecasas, P.: Lysosomotropic amines inhibit mitogenesis induced by growth factors. PNAS USA 78 (1981) 717-721

14. Cain, C.C.; Murphy, R.F.: Growth inhibition of 3T3 fibroblasts by lysosomotropic amines: Correlation with effects on intravesicular pH but not vacuolation. J. Cell Physiol. 129 (1986) 65-70

15. Boron, W.F.; DeWeer, P.: Intracellular pH transients in squid giant axons caused by CO_2, NH_3 and metabolic inhibitors. J. Gen. Physiol. 67 (1976) 91-112

16. Taylor, I.W.; Hodson, P.J.: Cell cycle regulation by environmental pH. J. Cell Physiol. 121 (1984) 517-525

17. Musgrove, E.; Seaman, M.; Hedley, D.: Relationship between cytoplasmic pH and proliferation during exponential growth and cellular quiescence. Exp. Cell Res. 172 (1987) 65-75

18. L'Allemain, G.; Paris, S.; Pouyssegur, J.: Growth factor action and intracellular pH regulation in fibroblasts–Evidence for a major role of the Na^+/H^+ antiport. J. Biol. Chem. 259 (1984) 5809-5815

19. Pouyssegur, J.; Franchi, A.; L'Allemain, G.; Paris, S.: Cytoplasmic pH, a key determinant of growth factor-induced DNA synthesis in quiescent fribroblasts. FEBS Lett. 190 (1985) 115-119

20. Gerson, D.F.: The relation between intracellular pH and DNA synthesis rate in proliferating lymphocytes. In: Nuccitelli, R.; Deamer, D.W. (Eds.): Intracellular pH: its measurement, regulation, and utilization in cellular functions, pp. 375-383. New York: Alan R. Liss 1982

21. Rink, T.J.; Tsien, R.Y.; Pozzan, T.: Cytoplasmic pH and free Mg^{2+} in lymphocytes. J. Cell Biol. 95 (1982) 189-196

22. Musgrove, E.; Rugg, C.; Hedley, D.: Flow cytometric measurement of cytoplasmic pH: A critical evaluation of available fluorochromes. Cytometry 7 (1986) 347-355

23. Busa, W.B.: The proton as an integrating effector in metabolic activation. In: Aronson, P.S.; Boron, W.F. (Eds.): Na^+-H^+ exchange, intracellular pH, and cell function, pp. 291-305. New York: Academic Press 1986

24. Moore, R.D.; Fidelman, M.L.; Hansen, J.C.; Otis, J.N.: The role of intracellular

pH in insulin action. In: Nuccitelli, R.; Deamer, D.W. (Eds.): Intracellular pH: its measurement, regulation, and utilization in cellular functions, pp. 385-416. New York: Alan R. Liss 1982

25. Donnelly, M.; Scheffler, I.E.: Energy metabolism in respiration-deficient and wild type Chinese hamster fibroblasts in culture. J Cell Physiol. 89 (1976) 39-52

26. Reitzer, L.J.; Wice, B.M.; Kennell, D.: Evidence that glutamine, not sugar, is the major energy source for cultured HeLa cells. J. Biol. Chem. 254 (1979) 2669-2676

27. Glacken, M.W.; Fleischaker, R.J.; Sinskey, A.J.: Reduction of waste product excretion via nutrient control: Possible strategies for maximizing product and cell yields on serum in cultures of mammalian cells. Biotech. Bioeng. 28 (1986) 1376-1389

28. Miller, W.M.; Wilke, C.R.; Blanch, H.W.: Transient responses of hybridoma cells to nutrient additions in continuous culture: I. Glucose pulse and step changes. Biotech. Bioeng. 33 (1989) 477-486

29. Miller, W.M.; Wilke, C.R.; Blanch, H.W.: Transient responses of hybridoma cells to nutrient additions in continuous culture: II. Glutamine pulse and step changes. Biotech. Bioeng. 33 (1989) 487-499

30. Miller, W.M.; Wilke, C.R.; Blanch, H.W.: Transient and steady-state responses in continuous hybridoma culture. Presented at the 196th national meeting of the American Chemical Society, Los Angeles, California, September 25-30, 1988

31. Boron, W.F.: Transport of H^+ and of ionic weak acids and bases. J. Membrane Biol. 72 (1983) 1-16

32. Grinstein, S.; Rothstein, A.: Mechanisms of regulation of the Na^+/H^+ exchanger. J. Membrane Biol. 90 (1986) 1-12

33. Grinstein, S.; Cohen, S.; Rothstein, A.: Cytoplasmic pH regulation in thymic lymphocytes by an amiloride-sensitive Na^+/H^+ antiport. J. Gen. Physiol. 83 (1984) 341-369

34. Roos, A.; Boron, W.F.: Intracellular pH. Physiol. Reviews 61 (1981) 296-434

CHAPTER 2.

Flow Effects on the Viability and Lysis of Suspended Mammalian Cells

Biotechnology Letters Vol 9 No 12 831-836 (1987)
Received November 12

FLOW EFFECTS ON THE VIABILITY AND LYSIS OF SUSPENDED MAMMALIAN CELLS

Anne McQueen, Eliane Meilhoc, and James E. Bailey

Department of Chemical Engineering
California Institute of Technology
Pasadena, California 91125, USA

ABSTRACT

A mouse myeloma cell line growing in suspension was subjected intermittently to flow through a sudden contraction and turbulent flow in a capillary tube. The probability of lysis per pass through the capillary tube increased with average wall shear stress level and with residence time per pass in the tube. Lysis was first observed at a threshold average wall shear stress level of 1800 dyn/cm^2. Although the flow caused lysis, it had no effect on cell viability.

INTRODUCTION

One of the major challenges in scaling up mammalian cell culture is avoiding cell damage caused by mixing. Agitation is required in bioreactors to provide adequate oxygen and nutrient supply and to keep cells suspended. Since circulation is essential to many bioreactor designs, it is important to understand the effects of flow on mammalian cells.

Effects of laminar and turbulent flows on anchorage-dependent cells have been well documented. Most previous work on cells attached to a substrate was concerned with monolayers of endothelial cells (e.g. Stathopoulos *et al.*, 1985, and Davies *et al.*, 1986). In addition, there have been many studies of cells on microcarriers in stirred tanks, such as those of Croughan *et al.* (1986) and Cherry *et al.* (1987). Much less information is available on flow effects on cells in suspension. Studies in well-defined flow are difficult to do with suspended cells, because the cells must circulate with the medium and therefore often encounter different hydrodynamic environments during the experiment. Settling of the cells is another practical problem in such experiments.

Studies of cells in suspension include investigations of insect cells (Tramper *et al.*, 1986) and mouse hybridoma cells (Smith *et al.*, 1987) in laminar simple shear flow. Previous work on suspended cells in turbulent flow include experiments by Tramper *et al.* (1986) in a stirred tank and one study by Augenstein et al. (1971) in which cells are subjected to multiple passes through a capillary tube. The latter study reported viable cell counts and compared the behavior of two cell lines: HeLa S3 and mouse L929. Cell viability decreased as the number of passes through the capillary tube increased, and the two cell lines exhibited very different sensitivities to flow effects. However, Augenstein *et al.* (1971) did not determine a threshold value of average wall shear stress at which significant loss of viability began to occur since they did not investigate sufficiently small values of average wall shear stress. One objective of the experiments in the present work was to determine this threshold value of average wall shear stress for a mouse myeloma cell line in suspension, using a similar experimental apparatus. As well as viable cell counts, a complementary assay, based on the release of the cytoplasmic enzyme lactate dehydrogenase (LDH) into the medium, was used to monitor cell lysis. This assay was also used by Smith *et al.* (1987).

MATERIALS AND METHODS

Cell culture

A mouse myeloma cell line (ATCC TIB 18) was chosen because myeloma cells are used to make hybridoma cells which produce monoclonal antibodies. The cells were grown in Dulbecco's modified Eagle's basal medium, high glucose option (4.5 g/L glucose) (Irvine Scientific, Irvine, CA) with 20% defined horse serum (HyClone, Logan, Utah) and antibiotics (430 units/mL of penicillin and 22μg/mL of streptomycin) (Irvine Scientific, Irvine, CA), in an incubator kept at 37°C and 10% CO_2. The cells were maintained in exponential growth for 3 days prior to the start of the experiment. Once the cell concentration had reached 5 to 8 $\times$ 10^5 cells/mL, 170 mL of the cell suspension was transferred into the flow loop. The cell suspension was then circulated around the flow loop for two and one half hours, the duration of the experiment.

Flow Loop

The flow loop consisted of (i) a syringe-type Harvard infusion-withdrawal pump, which was used to drive the cells around the flow loop; (ii) the flow device, which provided the flow trauma to which the cells were exposed intermittently; and (iii) a holding flask, which enabled sampling and gas exchange to take place. The holding flask had two bottom ports through which the cell suspension entered and exited. A humidified, filtered 10% CO_2 in air gas mixture was gently sparged over the surface of the cell suspension. A sample tube, inserted into the rubber stopper used to seal the flask, was used to collect a sample aseptically with a needle and syringe. The three components of the flow loop were connected with silicone tubing having an inside diameter of 0.32 cm. The flask and a considerable amount of the tubing were placed in a 37°C water bath. Given the flowrate of 114 ml/min and the total flow loop volume of 170 mL, 150 minutes in the flow loop corresponded to 100 passes of the cell suspension through the flow device. Samples were taken after 5, 50 and 100 passes through the flow loop. The residence time per pass in the flow device was only a very small fraction of the loop circulation time, as will be discussed next.

Flow devices

Two flow devices were used. Most of the results presented were obtained with a capillary tube flow device. This flow device consisted of a sudden contraction into a short length L of stainless steel capillary tubing of inside diameter D (Fig. 1A). Several different capillary tube geometries were studied. The ratio of the tube inside diameter to the cell diameter of 10 microns varied between 50 and 80. The ratio of the silicone tubing inside diameter of 0.32 cm to the capillary tubing inside diameter varied between 4 and 6. Table 1 lists the various diameters used and the corresponding velocities and Reynolds numbers. The tube lengths are also listed in Table 1, together with the corresponding residence time per pass in the flow device, t_{res}. The same length was used for all tube diameters except 0.060 cm. This meant that the residence time per pass varied inversely with the velocity. For the 0.060 cm tube diameter, another residence time per pass was tried at constant average wall shear stress by using an additional tube of this diameter but of different length. Since the Reynolds number is above the critical value of 2200 for flow in a tube (Davies, 1972), the flow is potentially turbulent. Therefore, the turbulent average wall shear stress, $\tau_{w,ave}$, is a useful parameter for characterizing the experiments. The values of $\tau_{w,ave}$ for each of the diameters used are listed in Table 1. From the ratios of length to diameter used, it is clear that the flow is not fully developed turbulent at the outlet of the tubes, since this requires an entrance length of at least 25 to 40 tube diameters (Hinze, 1959). Consequently, $\tau_{w,ave}$ in Table 1 is only an approximate value of the actual average wall shear stress level. It is possible that the average wall shear stress level is higher in the developing turbulent boundary layer.

The second flow device, which was used with the same flow loop, had an opposing jets geometry (Fig. 1B). The diameter of the exit tubes of the opposing jets flow device was varied like that of the capillary tubes, leading to a similar range of flow parameters (Reynolds number and $\tau_{w,ave}$) for the flow in these tubes.

Assays of Flow Effects on Cells

A control flask was left in the incubator for the duration of the experiment. Cells which had been circulated around the flow loop and cells from the control flask were assayed in parallel. The total cell count was measured by hemacytometer.

Percent Viability Measurement

The percent viability was determined using viability dye (eosin yellow) exclusion. Whereas live cells exclude the dye, dead cells, whose membranes are permeable, become stained.

Percent Cell Lysis Measurement

The percent cell lysis was obtained by measuring the release of the cytoplasmic enzyme lactate dehydrogenase (LDH) into the surrounding medium. The enzyme activity in the medium was determined as follows. 25 μL of medium was diluted in 1.4 mL of MOPS buffer. NADH and pyruvate were added to final concentrations of 1.5×10^{-4} mM and 4.2×10^{-3} mM, respectively. The decrease in the absorbance of NADH (at 340 nm) was measured at 37°C. The relative enzyme activity (REA) values, which were equal to the slopes of the records of absorbance as a function of time, were substituted into the following equation for the percent cell lysis.

$$\text{Percent Cell Lysis} = \frac{(\text{N} - \text{NC})}{(\text{S} - \text{NC})} \times 100$$

where NC was the REA value of the unsonicated control sample (not subjected to flow), N was the REA value of the unsonicated experimental sample (subjected to flow), and S was the REA value of the sonicated experimental sample (subjected to flow) (Rhee, 1987). This equation will give the percent cell lysis provided that all cells are lysed in the sonicated sample.

Growth rate assay on the surviving cells

After the end of the experiment, a sample of the surviving cells from the flow loop was allowed to grow in a flask placed in the incubator. The number of viable cells as well as the DNA synthesis rate were determined 24, 36 and 48 hours later.

DNA synthesis rate assay

The DNA synthesis rate was determined by [methyl ^{3}H] thymidine incorporation. The incorporation into triplicate aliquots (4×10^5 cells) was determined as previously described (Meilhoc *et al.*, 1987). The final pellet was solubilized in a mixture of 50 μL of water and 300μL Scintigest solubilizer (Fisher Scientific Company) for 5 hours at 55°C. The radioactivity incorporated into the acid-insoluble material was determined by liquid scintillation spectrometry.

Diameter D, cm	Velocity U, cm/s	Reynolds Number	$\tau_{w,ave}$ dyn/cm^2	Length L, cm	Residence Time per pass, t_{res}, seconds
0.050	920	4780	4290	0.22	0.00024
0.056	775	4340	2880	0.22	0.00028
0.060	672	4030	2250	0.22	0.00033
0.060	672	4030	2250	0.66	0.00099
0.064	590	3780	1780	0.22	0.00037
0.080	378	3020	784	0.22	0.00058

Table 1: Flow parameters

RESULTS

The flow loop design meant that the cells experienced damaging flow effects intermittently rather than continuously. Control experiments indicated that the flow loop, without the flow device, had no effect on any of the cell parameters studied. Therefore, flow effects are considered to be confined to the flow device.

Cell Damage in the Capillary Tube Flow Device

After subjecting cells to capillary tube flow devices having average wall shear stress levels between 800 and 4300 dyn/cm^2, it was found that the flow had no effect on the percent viability of the cells as measured by dye exclusion. However, multiple passes through the flow device did cause a decline in the total cell number, as determined by cell counts in the hemacytometer, and an increase in the percent cell lysis, as measured by LDH release into the medium. This means that, when subjected to the flow, the cells either broke or remained viable. The results obtained from cell counts and from lysis measurements were in good agreement, and both were reproducible from experiment to experiment. Only cell lysis measurements will be presented in the following figures.

Cell lysis measurements indicated that the viable cell number decreased exponentially rather than linearly as a function of the number of passes (Fig. 2). Therefore, the data fits the form:

$$log \frac{x}{x_o} = -kN$$

where N is the number of passes and x/x_o is the fraction of viable cells remaining (not lysed). k is the specific lysis rate (units of (number of passes)$^{-1}$). Alternatively, k may be interpreted as the probability of lysis per pass through the flow device. As shown in Fig. 2, the specific lysis rate depends on the average wall shear stress (noted by each data set).

No cell lysis occured at the lowest average wall shear stress level studied, 800 dyn/cm^2. The threshold level of average wall shear stress, defined as the level at which significant lysis began to occur, was 1800 dyn/cm^2. Above this threshold level of average wall shear stess, the specific lysis rate increased as the average wall shear stress level increased.

In order to assess the relative contributions of the flow through the sudden contraction and the turbulent flow in the tube to cell damage, a preliminary investigation was conducted on the effect of increasing the residence time per pass (i.e. the tube length) in the capillary tube flow device. The damage due to the flow through the sudden contraction is unchanged in these experiments. In Fig. 3, the percent cell lysis is shown as a function of the number of passes for different residence times per pass. It is evident that increases in tube length, at a constant level of average wall shear stress, result in significant increases in cell lysis. This indicates that there is a contribution of the turbulent flow in the tube to cell lysis, as well as (probably) a contribution of the flow through the sudden contraction.

Cell Damage in the Opposing Jets Flow Device

In the opposing jets flow device, at the high flowrates required to obtain lysis, the flow was turbulent and therefore not well defined in this geometry. Similar to the results obtained with the capillary tube flow device, the opposing jets flow device had no effect on cell viability but caused substantial lysis which increased as the diameter of the jets decreased. The opposing jets flow device is included because of a number of important experimental results obtained using it. Two additional assays were performed on the samples subjected to this alternative flow device. The growth rate and DNA synthesis rate of the surviving cells (which were not lysed) were measured for a further 48 hours after the end of the flow loop experiment. It was found that, for a size of the opposing jets at which considerable lysis occurred, there was no effect on either the growth rate or the DNA synthesis rate of the remaining cells measured 24, 36 or 48 hours after the end of the experiment. This means that, in the flow loop with the alternative flow device, cells either lysed or were unaffected by the flow. It remains possible that a transient effect occured during the first 24 hours and this is still under investigation. Although these assays have not been performed so far in experiments with the capillary tube flow device, it is hypothesized that the same results would be obtained under analogous experimental conditions.

. DISCUSSION

The flow geometry examined here consisted of flow through a sudden contraction and through a short length of capillary tubing. The Reynolds number for the flow in the tube was greater than the critical Reynolds number, indicating that the flow was potentially turbulent. Since the length of the tube was less than the required entrance length, the turbulent flow was not fully-developed even at the outlet of the tube. However, the results obtained in this flow device will be compared to measurements made in both laminar flow through a sudden contraction and fully developed turbulent flow in a tube, even though this flow device only approximates those flow types. In addition, the present work will be compared with work on flow effects on cells for other flow types, with other cell lines.

Flow Through a Sudden Contraction

The flow through a sudden contraction (an abrupt entrance into a smaller diameter tube) is an extensional flow. This implies that the magnitude of the rate of strain tensor is greater than the magnitude of the vorticity tensor, rather than equal to it, as it is in simple shear flow. In an extensional flow, by definition, fluid elements and particles suspended in the fluid are extended. In the case of flow through a sudden contraction, the cell will be stretched in the axial (flow) direction and compressed in the radial (transverse) direction. This is because the velocity of the fluid increases and the streamlines of the fluid are squeezed in order to fit through the smaller cross-sectional area of the capillary tube. Han *et al* (1978) studied drops subjected to laminar flow through a sudden contraction. They observed the drops through the transparent walls of the flow device and found that the drops elongated in the contraction, recoiled just beyond it and then assumed an equilibrium configuration in the fully developed region of the flow. If the forces on the drop were sufficient, the drop did not recover from the extensional flow but burst. Drop burst occured at a critical value of the wall shear stess level.

Bentley and Leal (1986) studied drop deformation and burst in a 4-roll mill, which could produce both 2-D pure extensional flow and 2-D flows having nonzero vorticity (approaching simple shear flow). They found that drop burst occurred at a lower critical shear stress level in extensional flow than in flows with vorticity. Both of these studies suggest that extensional flow should be more effective in breaking cells than simple shear flow. Hence, the contribution of the extensional flow in the entry region of the capillary tube flow device may be sufficient to cause cells to lyse in spite of the short residence time in the capillary tube.

Turbulent Flow in a Tube

Augenstein *et al* (1971) used a flow apparatus very similar to that used in this work. The threshold average wall shear stress level found in the present work was below the least damaging conditions used by Augenstein *et al* (1971), all of which caused substantial cell lysis.

Correlation of Cell Lysis with the Kolmogorov Length Scale

The Kolmogorov length scale, which characterizes the size of the smallest, energy-dissipating eddies, was calculated for the tube diameters and velocities used, employing relations determined empirically for fully developed turbulent flow in a tube (Davies, 1972). Since the flow is not fully developed in this case, these values of the Kolmogorov length scale are only approximations to the true values in these tube sizes. In Fig. 4, the specific lysis rate is plotted as a function of the Kolmogorov length scale. It can be seen that the threshold value of the Kolmogorov length scale, at which the specific lysis rate became detectably greater than zero, was 3.5 microns. The cell diameter has been determined by Coulter counter measurements to be 10 microns on average, with some cells as small as 5 microns. Therefore, cell lysis began to occur when the smallest turbulent eddy size fell below the cell diameter. This conclusion is remarkably similar to that of Croughan *et al* (1986), who examined flow effects on cells on microcarriers in a stirred tank. They found that significant loss of viability began to occur when the Kolmogorov length scale of the turbulence in the stirred tank reached a value somewhat smaller than the microcarrier diameter.

Residence Time Required to Obtain Lysis

In the present work, 50 passes through the flow device (total residence time 0.02 seconds) were required to obtain significant lysis at the threshold average wall shear stress level of 1800

dyn/cm^2. In contrast, approximately one hour of continuous shear is required to obtain lysis in laminar simple shear flow experiments on other suspended cell lines. The threshold shear stress values obtained by Tramper *et al.* (1986) for insect cells and by Smith *et al.* (1987) for mouse hybridoma cells were 15 and 8.7 dyn/cm^2 respectively. This difference in residence time required to obtain lysis is probably due to different mechanisms of cell damage in the two cases. Rather than a gradual weakening of the membrane, the cell breaks abruptly in the flow device studied here, due to the severity of the flow conditions.

Acknowledgement: This research was sponsored by the Monsanto Company and by the Caltech Process Biocatalysis Program. A. McQueen is the recipient of a Natural Sciences and Engineering Research Council (NSERC) Postgraduate Scholarship from the Government of Canada.

REFERENCES

Augenstein, D.C., Sinskey, A.J., and Wang, D.I.C. (1971). *Biotechnol. Bioeng.* **8**, 409-418.
Bentley, B.J., and Leal, L.G. (1986). *J. Fluid Mech.* **167**, 241-284.
Cherry, R.S., and Papoutsakis, E.T. (1987). *Biotechnol. Bioeng.* (in press).
Croughan, M.S., Hamel, J.-F., and Wang, D.I.C. (1987). *Biotechnol. Bioeng.* **29**, 130-141.
Davies, J.T. (1972). *Turbulence Phenomena* New York: Academic Press.
Davies, P.F., Remuzzi, A., Gordon, E.J., Dewey, C.F. Jr., and Gimbrone, M.A. (1986). *PNAS (USA)* **83**, 2114-2117.
Han, C.D., and Funatsu, K. (1978). *J. Rheology* **22**, 113-133.
Hinze, J.O. (1959). *Turbulence* New York: McGraw-Hill.
Meilhoc, E., Moulin, M.J., and Osborne, H.B. (1987). *J. Cell. Physio.* **131**, 465-471.
Rhee, B.-G., and McIntire, C.V. (1986). *Chem. Eng. Commun.* **47**, 147-161.
Smith, C.G., Greenfield, P.F., and Randerson, D.H. (1987). *Biotech. Techniques* **1**, 39-44.
Stathopoulos, N.A., and Hellums, J.D. (1985). *Biotechnol. Bioeng.* **27**, 1021-1026.
Tramper, J., Williams, J.B., and Joustra, D. (1986). *Enzyme Microb. Technol.* **8**, 33-36.

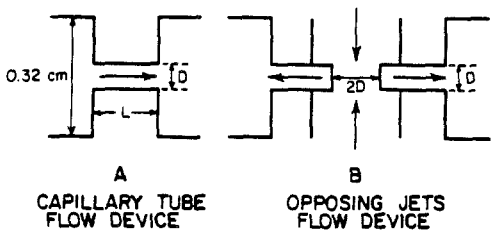

Figure 1: Schematic diagrams of flow devices

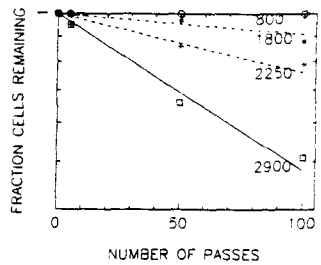

Figure 2: Effect of number of passes through the capillary tube flow device on the percent lysis of mouse myeloma cells. Different symbols denote measurements at different values of average wall shear stress (dyn/cm^2, indicated below each data set).

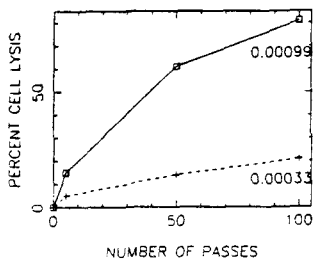

Figure 3: Effect of residence time per pass (seconds, indicated on the figure) in the capillary tube flow device on percent cell lysis as a function of the number of passes.

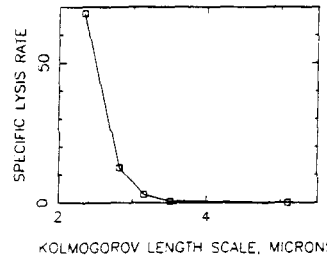

Figure 4: Relationship between the specific lysis rate (units (number of passes)$^{-1}$) of mouse myeloma cells and the approximate Kolmogorov length scale (size of the smallest turbulent eddies) in the capillary tube flow device.

CHAPTER 3.

Dependence of Flow Effects on Suspended Mammalian Cells on Serum Level, Cell Line, Flow Type and Viscosity

ABSTRACT

An investigation of the parametric dependence of cell lysis observed when mammalian cells growing in suspension are subjected intermittently to passage through a flow device was conducted. Two flow devices were tested: one consisting of a sudden contraction into a short length of capillary tubing, in which turbulent flow is obtained, and another consisting of a smoothly converging and diverging tube, in which laminar flow is obtained. Changes in the serum level, in which the cells were grown and subjected to flow trauma, and in the cell line both affected the specific lysis rate (fraction of cells lysed per pass through the flow device) in the turbulent flow device. The threshold value of the average wall shear stress level was approximately the same in the turbulent and laminar flow devices (1500-1800 dyn/cm^2). Increasing the viscosity of the medium with 70,000 MW dextran had no effect on the specific lysis rate in either flow device.

Introduction

One of the major challenges in scaling up mammalian cell culture is avoiding cell damage caused by mixing. Agitation is required in bioreactors to provide adequate oxygen and nutrient supply and to keep cells suspended. Since circulation is essential to many bioreactor designs, it is important to understand the effects of flow on mammalian cells.

Previous work on hydrodynamic effects on cells includes studies of cells attached to a substrate as well as cells in suspension. There have been extensive studies of mammalian cells on microcarriers in a stirred tank, both experimental and theoretical (Cherry *et al.* 1986 and 1988, Croughan *et al.* 1987, 1988, 1989a and 1989b). These papers drew from previous literature on particles in turbulent flow to formulate mechanisms of cell damage and hence to derive the dependence of cell damage on the power dissipation rate per unit mass ϵ, as will be discussed below. Studies of suspended cells, both mammalian cells and other cells, in a stirred tank geometry have also been made, in which are also included attempts to derive a dependence on cell damage on ϵ based on a proposed mechanism (Kramer *et al.* 1988 and Papoutsakis *et al.* 1988 for hybridoma cells and van Suijdam *et al.* 1981 for filamentous molds). Work on the effects of other flow types on suspended mammalian cells includes the studies of Augenstein *et al.* (1971) on two mammalian cell lines in a capillary tube, Smith *et al.* (1988) on hybridoma cells in a Couette device, and McQueen *et al.* (1987) on hybridoma cells in a turbulent capillary tube flow device (including a sudden contraction). In addition to studies of hydrodynamic effects on cells in single-phase environments, the effects of sparging on cells has been investigated by several authors including Handa *et al.* (1987) working with

myeloma and hybridoma cells, Murhammer *et al.* (1988) and Tramper *et al.* (1986 and 1988) working with insect cells and Silva *et al.* working with dunaliella (algae) cells. The effects of changes in the medium viscosity on hydrodynamic damage to cells have been considered by Croughan *et al.* (1989b) for stirred mammalian cells on microcarriers and by Silva *et al.* (1987) for sparged algae cells in suspension, as will be discussed below.

In a previous paper (McQueen *et al.* 1987), the effects of flow on suspended myeloma cells were measured in a flow loop containing a flow device consisting of a sudden contraction into a short length of capillary tubing. Cell lysis was determined from the release of the cytoplasmic enzyme lactate dehydrogenase (LDH). The flow in the capillary tube was developing turbulent, based on the Reynolds number and the length-to-diameter ratio. The following results were obtained:

1) The viable cell number decreased exponentially rather than linearly as a function of the number of passes through the flow device. Therefore, the results were modeled in terms of a specific lysis rate k, which is the fraction of cells that lyse per pass through the tube.

2) A threshold average wall shear stress level $\tau_{w,ave}$ of 1800 dyn/cm^2, at which significant lysis began to occur, was determined using flow devices of varying diameters. Above this value of $\tau_{w,ave}$, the specific lysis rate k increased as $\tau_{w,ave}$ increased.

3) The specific lysis rate k increased as the length of the capillary tube was increased, increasing the residence time per pass t_{res}. This implied that the effects of the turbulent flow in the tube were significant relative to the extensional flow at the inlet.

4) The threshold value of the Kolmogorov length scale η, the length scale of the smallest turbulent velocity fluctuations, at which significant lysis began to occur was found to be 3.5μm, which is on the order of the cell diameter. This was in agreement with common theories on hydrodynamic effects on particles in turbulent flow. Similarly, Croughan *et al.* (1987), who examined flow effects on cells on microcarriers in a stirred tank, observed that significant loss of viability began to occur when the Kolmogorov length scale of the turbulence in the stirred tank reached a value somewhat smaller than the microcarrier diameter.

In the present work, parametric studies of the effect of varying the percent serum and the cell line on the specific lysis rate k were conducted, using the same flow loop and capillary tube turbulent flow device used in the previous paper. In addition, the specific lysis rate k was determined in a laminar flow device consisting of a smoothly converging and diverging tube. The diameter of the tube was varied and the dependence of k on the average wall shear stress level $\tau_{w,ave}$ was determined in order to compare the results in the turbulent and laminar flow devices. The effects of viscosity on the specific lysis rate k were determined in both the laminar and turbulent flow devices. The viscosity of the cell suspension was increased by adding 70,000 MW dextran. Croughan *et al.* (1988) showed that, for cells on microcarriers in a stirred tank, cell damage decreased as the viscosity was increased. Silva *et al.* (1987) studied the effects of viscosity increase (by carboxymethylcellulose addition) on dunaliella (algae) cell growth in two reactor configurations: a Roux bottle in which cells were not circulated but were sparged (using a straight tube with six holes in it) and a miniloop reactor in which cells were circulated (and aerated) by the airlift principle. They observed that, in both cases, cell growth and productivity

increased as viscosity increased, and, in the case of the Roux bottle, the increases in productivity were proportional to the concentration of carboxymethylcellulose added.

MATERIALS AND METHODS

Cell culture

The cell lines studied were as follows: a mouse myeloma cell line (TIB 18) and a murine hybridoma cell line, which produces IgG1 directed at a consensus α-interferon (designated IFN-con1) (Zsebo *et al.* 1986). The cells were grown in Dulbecco's modified Eagle's basal medium, high glucose option (4.5 g/L glucose) (Irvine Scientific, Irvine, CA) with 10% or 5% defined horse serum (TIB 18) or 10% defined fetal calf serum (IFN-con1) (both Hyclone, Logan, Utah) and antibiotics (100 units penicillin/mL and 50 μg streptomycin/mL) (Irvine Scientific, Irvine, CA), in an incubator kept at 37°C and 10% CO_2. The cells were maintained in exponential growth for 3 days prior to the start of the experiment. Once the cell concentration had reached 5 to 8×10^5 cells/mL, 170 mL of the cell suspension was transferred into the flow loop. The cell suspension was then circulated around the flow loop for two and one half hours, the duration of the experiment.

Flow loop

The flow loop was described in the previous paper (McQueen *et al.* 1987). Briefly, it consisted of a syringe-type Harvard infusion-withdrawal pump (to drive the flow) and a holding flask (for sampling and gas exchange), in addition to the flow device. The three components were connected by silicone tubing (0.32 cm inside diameter) and immersed in a 37°C water bath. Given the flowrate of 114 mL/min and the total flow loop volume of 170 mL, 150 minutes in the flow loop corresponded to 100 passes of the cell suspension through the flow device.

Flow devices

Two flow devices were used, one with turbulent flow and the other providing laminar flow. The capillary tube turbulent flow device was described in the previous paper (McQueen *et al.* 1987). Briefly, it consisted of a sudden contraction into a short length of stainless steel capillary tubing of inside diameter D (Fig. 1A). Capillary tubes of serveral different sizes were used. The diameters D are listed in the first part of Table 1, together with the corresponding velocities U and Reynolds numbers. Since the entrance into the capillary tube is abrupt and since the Reynolds number is above the critical value of 2200 for flow in a tube (Davies 1972), the flow is expected to be turbulent or in transition to turbulence. Therefore, the average (over time) wall shear stress value $\tau_{w,ave}$ for turbulent flow was calculated; the values are listed in the first part of Table 1, together with the corresponding values of the power dissipation rate per unit mass ϵ and the Kolmogorov length scale η, the length scale of the smallest energy-dissipating turbulent velocity fluctuations. The length of the capillary tube was 0.22 cm for all diameters used. This implies that the residence time per pass t_{res} varied inversely with the diameter, as shown in the first part of Table 1. In all cases, the time of exposure to the flow was very short. From the ratios of length to diameter used, it is clear that the flow is not fully developed turbulent at the outlet of the tubes, since this requires an entrance length of at least 25 to 40 tube diameters (Hinze 1959). Consequently, $\tau_{w,ave}$ in the first part of Table 1 is only an approximate value of the average wall shear stress level. It is possible that the average wall shear stress level is higher in the developing turbulent boundary layer.

The laminar flow device consisted of a smoothly converging and diverging tube, made of drawn glass (Fig. 1B). Again, devices of several different sizes were used.

The diameters of the constriction between the converging and diverging sections of the tube are shown in the second part of Table 1, which also gives the corresponding velocities and Reynolds numbers. Because of the smoothly converging entrance to the constriction in the tube, the flow remains laminar up to a much higher Reynolds number than 2200 (Davies 1972). Therefore, the wall shear stress value for laminar flow was calculated and the values are listed in the second part of Table 1, together with the corresponding values of the power dissipation rate per unit mass ϵ. The length of the constriction in the tube was 0.22 cm for all diameters used. The residence times per pass t_{res} in the constriction are listed in the second part of Table 1. These values are similar in magnitude to those for the turbulent flow device.

Assays of flow effects on cells

The percent viability measurement and the percent cell lysis measurement were described previously (McQueen *et al.*). However, there was an error in the concentrations of reagents for the cell lysis assay stated in the previous paper. NADH and pyruvate were added to final concentrations of 1.5×10^{-4} M and 4.2×10^{-3} M, respectively, in the assay for LDH.

RESULTS AND DISCUSSION

As described in the previous paper, subjecting the cells to two and one half hours in the flow loop containing the capillary tube turbulent flow device had no effect on the percent viability of the cells as measured by dye exclusion. However, multiple passes through the flow device did cause a decline in the total cell number, as determined by cell counts in the hemacytometer, and an increase in the percent cell lysis, as measured by LDH release into the medium. This means that, when subjected to the flow, the cells either broke or remained viable. Similar behavior was observed when cells were circulated in the flow loop with the laminar flow device. The results obtained from cell counts and from lysis measurements were in good agreement for cells subjected to either laminar or turbulent flow. Only cell lysis measurements will be presented in the following figures.

In Fig. 2, the effect of the percent serum, in which myeloma cells are grown and tested, on the lysis in the capillary tube turbulent flow device is presented. No differences in lysis rates were found for cells grown and tested in 20% and 10% serum (data not shown). Whereas, for cells grown in 10% serum, there is no lysis in 100 passes through the device at a $\tau_{w,ave}$ of 800 dyn/cm^2; for cells grown in 5% serum (in which the doubling time is unchanged), there is a small amount of lysis within 50 passes (specific lysis rate k 0.16×10^{-3} inverse passes). At a $\tau_{w,ave}$ of 1800 dyn/cm^2, the threshold value for significant lysis to occur for cells grown in 10% serum, the specific lysis rate (determined from the slope of the lines in Fig. 1) was 0.50×10^{-3} inverse passes for cells grown in 10% serum and 1.43×10^{-3} inverse passes for cells grown in 5% serum. Therefore, it appears that the fragility of the cells increases as the serum content of the growth and test medium is decreased

below 10%. This suggests that serum exerts a protective effect on cells during exposure to flow trauma. This agrees with the results of Papoutsakis *et al.* (1988) who showed that cell damage decreased and cell yields increased for hybridoma cells in a stirred tank reactor for serum levels greater than 6%.

In Fig. 3, the responses of hybridoma and myeloma cells to circulation through the capillary tube turbulent flow device are presented. The myeloma and hybridoma cells were grown in 10% defined horse or fetal calf serum, respectively. The hybridoma cell line, which has a doubling time of 14 hours, secretes 8.4 $\mu g/10^6$ cells/day of monoclonal antibody while the myeloma cell line is non-secreting and has a doubling time of 12 hours. There is no lysis of the myeloma cell line in 100 passes through the flow device at a $\tau_{w,ave}$ of 800 dyn/cm^2. There is a substantial amount of lysis of the hybridoma cell line within 50 passes (specific lysis rate k=0.63×10^{-3} inverse passes). Significant lysis begins to occur for the myeloma cell line at a $\tau_{w,ave}$ of 1800 dyn/cm^2. The specific lysis rate k (determined from the slope of the lines in Fig. 3) at this average wall shear stress level was 0.50×10^{-3} inverse passes for the myeloma cell line and 2.09×10^{-3} inverse passes for the hybridoma cell line. The hybridoma cells are more easily broken than the myeloma cells under these conditions. Handa *et al.* (1987) also found that cell lines differed in their sensitivity to hydrodynamic effects, in particular their response to sparging in a bubble column fermentor. However, those authors observed greater cell damage for the myeloma cell line (NS1) than for the hybridoma cell line (WC2) derived from it.

In Fig. 4, the effect of wall shear stress level $\tau_{w,ave}$ on cell lysis in the laminar flow device is presented. The results are for the myeloma cell line grown in 10%

serum. The threshold value of the wall shear stress level $\tau_{w,ave}$ at which significant lysis began to occur in the laminar flow device was 1500 dyn/cm^2. At 1500 dyn/cm^2, the specific lysis rate k was 0.22×10^{-3} inverse passes, while k increases to 3.39×10^{-3} inverse passes at 2000 dyn/cm^2. passes. The threshold value of the wall shear stress level in the laminar flow device is very similar to the threshold value of the average wall shear stress level in the turbulent flow device. This is evident in Figure 5, in which the specific lysis rate k is plotted as a function of the average wall shear stress level $\tau_{w,ave}$ for the turbulent (squares) and laminar (crosses) flow devices. Table 1 shows that the specific lysis rate k does not correlate with diameter D, velocity U, or power dissipation rate per unit mass ϵ. The critical values of these parameters at which lysis begins to occur are different for the turbulent and laminar flow devices.

The viscosity of the myeloma cell suspension was increased using 70,000 MW dextran. At a concentration of 2% dextran, the viscosity of medium (with 10% serum) was measured to be 1.5 times the medium viscosity in the absence of dextran (1.2 centipoise versus 0.8 centipoise). Dextran was insoluble at higher concentrations; hence, it was not possible to obtain further increases in viscosity in this fashion. The effect of viscosity on lysis was measured in both the turbulent and laminar flow devices. The 50% increase in viscosity had no effect on the specific lysis rate k in either case.

In the turbulent flow device, the 50% increase in viscosity has no effect on the average wall shear stress level, which is proportional to the density multiplied by the velocity squared. However, the 50% increase in viscosity leads to a 36% increase in the Kolmogorov length scale (at a given capillary tube size), which previous research had shown to be an important parameter governing lysis, based on theory and

experiment (McQueen *et al.* 1987). Croughan *et al.* (1987) proposed a model for the effects of small turbulent eddies on cells on microcarriers in a stirred tank. This model suggested that the specific lysis rate k depended on the Kolmogorov length scale η to the power -3 and hence on the viscosity to the power -2.25, implying that a 50% increase in viscosity should lead to a 60% decrease in the specific lysis rate. Experimental results for FS-4 cells on microcarriers confirmed this dependence of k on viscosity (Croughan *et al.* 1988). Since a 50% increase in viscosity had no effect on the specific lysis rate k for suspended cells in the capillary tube turbulent flow device, it is probable that the mechanism of cell damage in this case is different from that for cells on microcarriers in a stirred tank, which Croughan studied.

A disparity in mechanism between cell damage in our system and in that of Croughan *et al.* (1987) had previously been indicated by the relationship between log k and log ϵ (the power dissipation rate per unit mass) for the turbulent flow device, shown in Fig. 6. Croughan's model and experimental results give a slope of approximately 0.75 for this curve (based on k being proportional to η^{-3} and hence to $\epsilon^{0.75}$). Similarly, Kramer *et al.* (1988) developed a model for suspended cells in a stirred tank, which predicted a slope of 0.5 for the plot of log k versus log ϵ, based on k being a linear function of the shear stress on the cell (as observed in experiments in a Couette flow device), which is proportional to $\epsilon^{0.5}$, assuming a laminar shear field. (Kramer *et al.* assumes that laminar breakup by viscous forces is the controlling mechanism, based on the small size of the cell relative to the length scale of the smallest turbulent velocity fluctuations.) Kramer did not measure the effects of viscosity on cell damage. In contrast to the results of Croughan and Kramer, a slope of 1.7 is obtained from the best fit line to the data in Figure 6.

This is probably because the flow patterns in a capillary tube and in a stirred tank are very different.

In the laminar flow device, the 50% increase in viscosity leads to a 50% increase in the wall shear stress level $\tau_{w,ave}$. The higher viscosity should make the average wall shear stress level in the 0.051 cm diameter laminar flow device similar to that in the 0.046 cm diameter device at the lower viscosity (Table 1), where a much higher specific lysis rate is observed (Fig. 5). Since no increase in lysis is observed in the 0.051 cm diameter device upon increasing the viscosity 50%, these results suggest that $\tau_{w,ave}$ is not the only parameter governing cell lysis.

Acknowledgement: The authors wish to thank Prof. David James of the University of Toronto, Canada for his help. A. McQueen is the recipient of a Natural Sciences and Engineering Research Council (NSERC) Postgraduate Scholarship from the Government of Canada.

REFERENCES

Augenstein, K.C., Sinskey, A.J., and Wang, D.I.C. (1971). *Biotechnol. Bioeng.* **8**, 409-418.

Cherry, R.S., and Papoutsakis, E.T. (1986). *Bioprocess Eng.* **1**, 29-41.

Cherry, R.S., and Papoutsakis, E.T. (1988). *Biotechnol. Bioeng.* **32**, 1001-1014.

Croughan, M.S., Hamel, J.-F., and Wang, D.I.C. (1987). *Biotechnol. Bioeng.* **29**, 130-141.

Croughan, M.S., Hamel, J.-F., and Wang, D.I.C. (1988). *Biotechnol. Bioeng.* **32**, 975-982.

Croughan, M.S., and Wang, D.I.C. (1989a). *Biotechnol. Bioeng.* **33**, 731-744.

Croughan, M.S., Sayre, E.S., and Wang, D.I.C. (1989b). *Biotechnol. Bioeng.* **33**, 862-872.

Davies, J.T. (1972). *Turbulence Phenomena* New York: Academic Press.

Handa, A., Emery, A.N., and Spier, R.E. (1987). *Dev. Biol. Std* **66**, 243-253.

Hinze, J.O. (1959). *Turbulence* New York: McGraw-Hill.

Kramer, H., Schurl, U., Einsele, A., Widmer, F., and Eppenberger, H.M. (1988). *Biotechnol. Bioeng.*, in press.

McQueen, A., Meilhoc, E., and Bailey, J.E. (1987). *Biotechnol. Letters* **9**, 831-836.

Murhammer, D.W., and Goochee, C.F. (1988). Presented at the annual meeting of the American Institute of Chemical Engineers, Nov. 27-Dec. 2, 1988, Washington, D.C., paper no. 138e.

Papoutsakis, E.T., and Kunas, K.T. (1988). Presented at the annual meeting of the American Institute of Chemical Engineers, Nov. 27-Dec. 2, 1988, Washington, D.C., paper no. 137e.

Silva, H.J., Cortinas, T., and Ertola, R.J. (1987). *J. Chem. Tech. Biotechnol.* **40**, 41-49.

Smith, C.G., Greenfield, P.F., and Randerson, D.H. (1987). *Biotech. Techniques* **1**, 39-44.

Tramper, J., Williams, J.B., and Joustra, D. (1986). *Enzyme Microb. Technol.* **8**, 33-36.

Tramper, J., Smit, D., Straatman, J., and Vlak, J.M. (1988). *Bioprocess Eng.* **3**, 37-41.

Van Suijdam, J.C., and Metz, B. (1981). *Biotechnol. Bioeng.* **23**, 111-148.

Zsebo, K.M., Lu, H.-S., Fieschko, J.C., Goldstein, L., Davis, J., Duker, K., Suggs, S.U., Lai, P.-H., and Bitter, G.A. (1986). *J. Biol. Chem.* **261**, 5858-5865.

Table 1: Flow parameters.

Diameter D, cm	Velocity U, cm/s	Reynolds Number	$\tau_{w,ave}$ dyn/cm^2	ϵ cm^2/s^3 $\times 10^{-8}$	Kolmogorov length scale η, μm	Residence time per pass, t_{res}, seconds
Turbulent flow devices						
0.056	775	4340	2880	1.59	2.8	0.00028
0.060	672	4030	2250	1.01	3.2	0.00033
0.064	590	3780	1780	0.66	3.5	0.00037
0.080	378	3020	784	0.15	5.1	0.00058
Laminar flow devices						
0.046	1160	5290	2030	2.05		0.00019
0.051	937	4760	1480	1.09		0.00023
0.061	650	3970	853	0.91		0.00034

Figure 1: Schematic diagrams of flow devices

A: Turbulent flow device

B: Laminar flow device

Figure 2: Effect of percent serum on cell lysis in the turbulent flow device

The log of the fraction cells remaining is plotted as a function of the number of passes through the turbulent flow device (Fig. 1A) for mouse myeloma cells grown in and subjected to flow trauma in media containing different percent horse serum: 10% serum (solid lines) and 5% serum (dashed lines). For comparison, two different average wall shear stress levels (Table 1) were used: 1800 dyn/cm^2 (stars and circles) and 800 dyn/cm^2 (plus signs and squares). Cell lysis was measured as described in the Materials and Methods. The specific lysis rates k are calculated from the slopes of the curves in this figure.

Figure 3: Effect of cell line on cell lysis in the turbulent flow device

The log of the fraction cells remaining is plotted as a function of the number of passes through the turbulent flow device (Fig. 1A) for mouse myeloma cells (solid lines) or mouse hybridoma cells (dot-dashed lines), both grown in 10% serum (horse and fetal bovine, respectively). For comparison, two different average wall shear stress levels (Table 1) were used: 1800 dyn/cm^2 (stars and circles) and 800 dyn/cm^2 (plus signs and squares). Cell lysis was measured as described in the Materials and Methods. The specific lysis rates k are calculated from the slopes of the curves in this figure.

Figure 4: Effect of average wall shear stress level on cell lysis in the laminar flow device

The log of the fraction cells remaining is plotted as a function of the number of passes through the laminar flow device (Fig. 1B) for mouse myeloma cells grown in 10% horse serum at different average wall shear stress levels: 2000 dyn/cm^2 (plus signs), 1500 dyn/cm^2 (squares) and 850 dyn/cm^2 (stars). Cell lysis was measured as described in the Materials and Methods. The specific lysis rates k are calculated from the slopes of the curves in this figure.

Figure 5: Comparison of turbulent and laminar flow devices

The specific lysis rate k is plotted against the average wall shear stress level (Table 1) in the turbulent (solid line) and laminar (dashed line) flow devices (Fig. 1). Cell lysis was measured as described in the Materials and Methods. The values of k are calculated from the slope of the curve of the log fraction cells remaining versus the number of passes, obtained from Figure 4 for the laminar flow device. The data for the turbulent flow device were presented in a previous paper (McQueen *et al.* 1987).

Figure 6: Relationship between the specific lysis rate and the power dissipation rate per unit mass

The log of the specific lysis rate k in the turbulent flow device (Fig. 1A) is plotted aganinst the log of the average power dissipation rate per unit mass (Table 1), for comparison with the model of Croughan *et al.* (1987). Cell lysis was measured as described in the Materials and Methods. The values of k are the same as in Fig. 5 and are taken from a previous paper (McQueen *et al.* 1987).

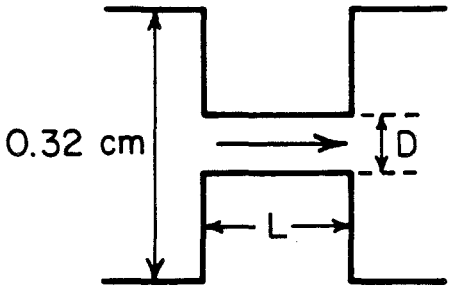

A

CAPILLARY TUBE
FLOW DEVICE

Figure 1A

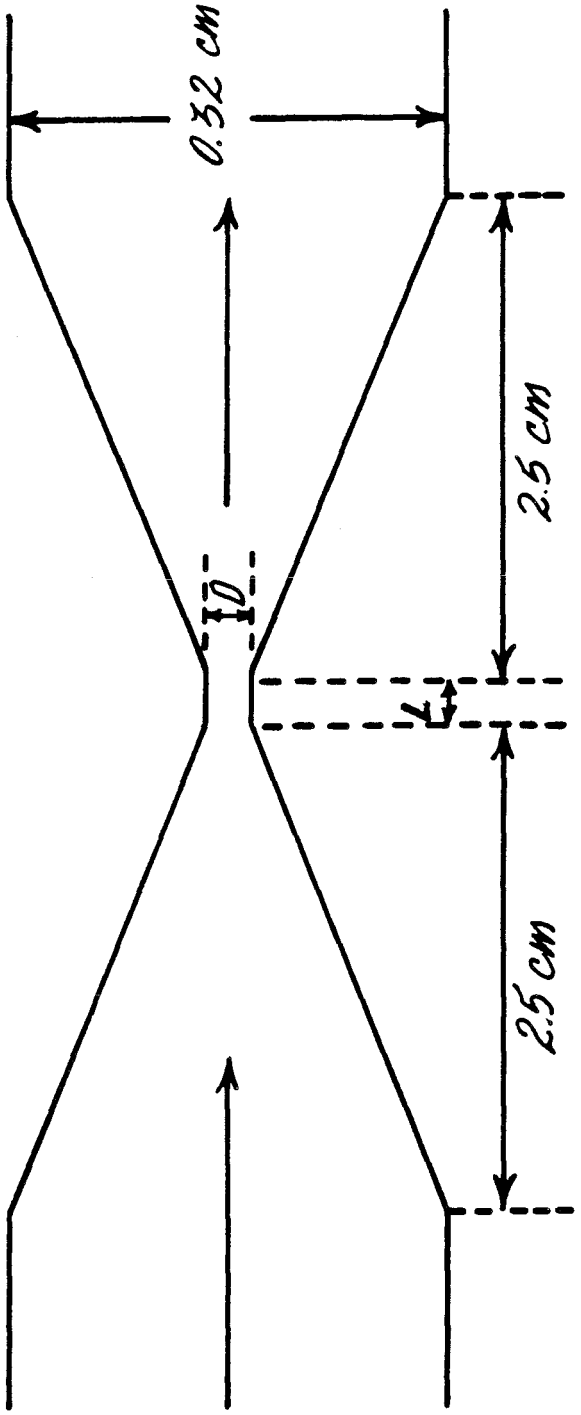

Figure 1B

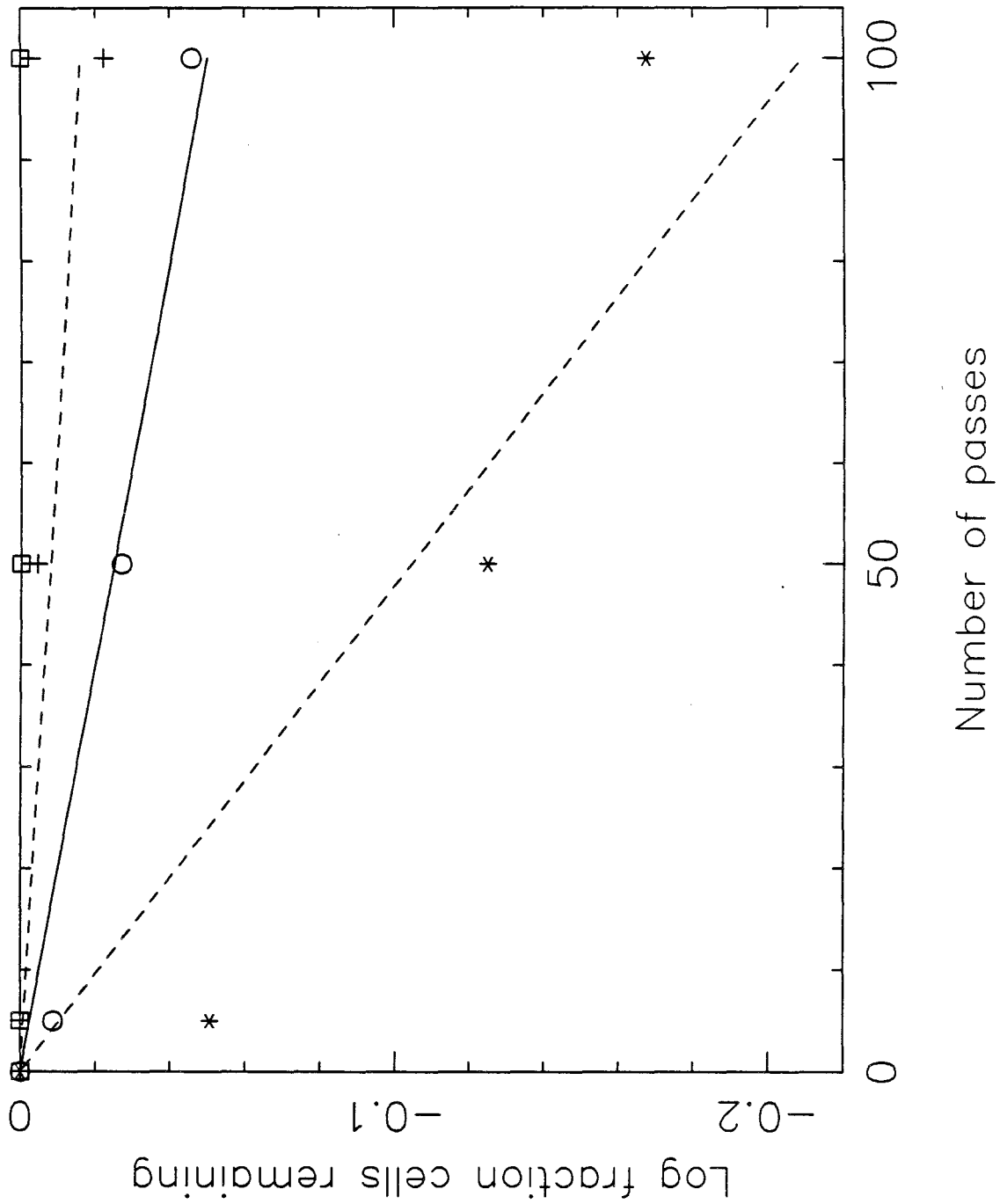
Log fraction cells remaining
0
−0.1
−0.2
Number of passes
0
50
100

Figure 2

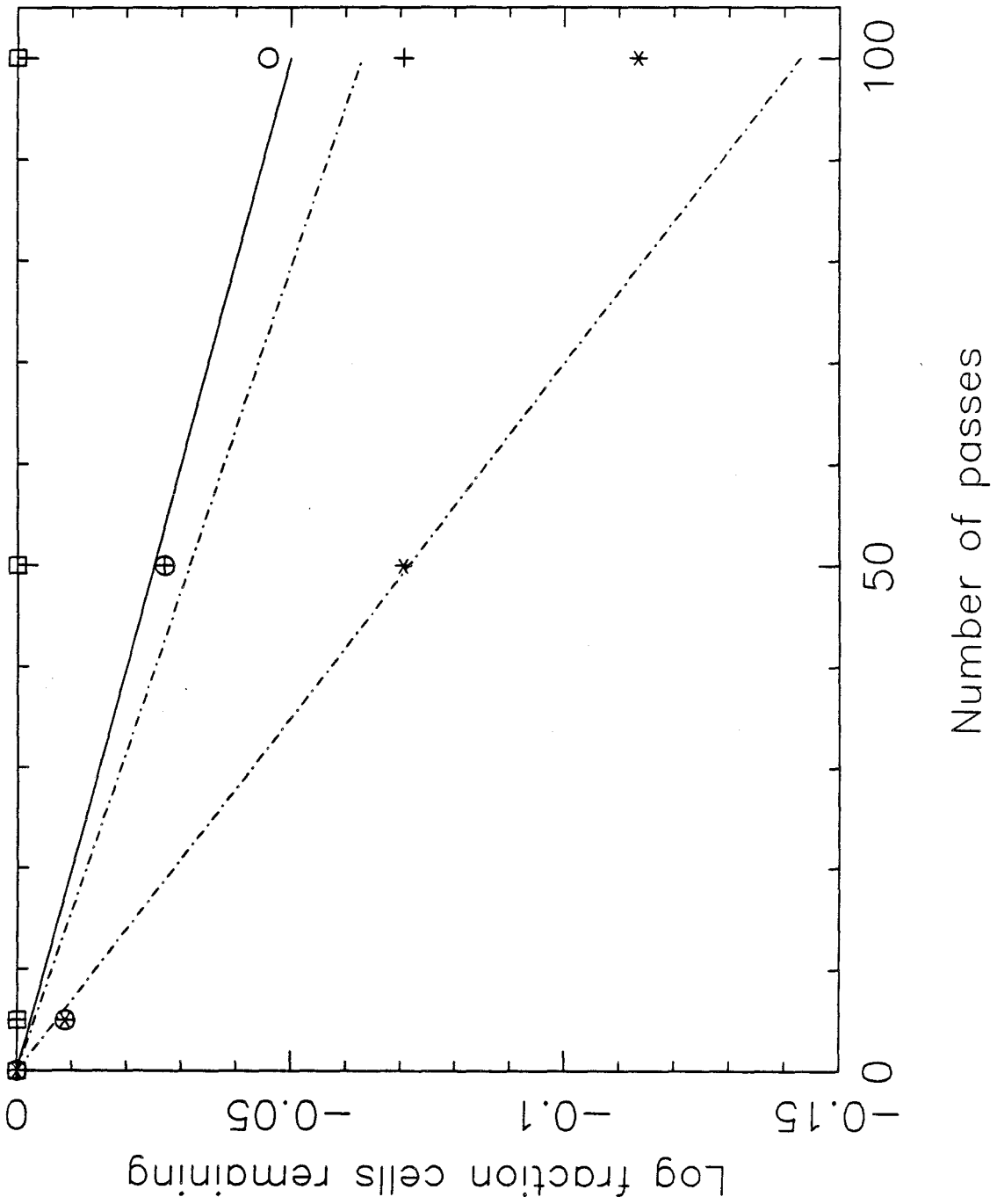
Log fraction cells remaining
0
−0.05
−0.1
−0.15
Number of passes
0
50
100

Figure 3

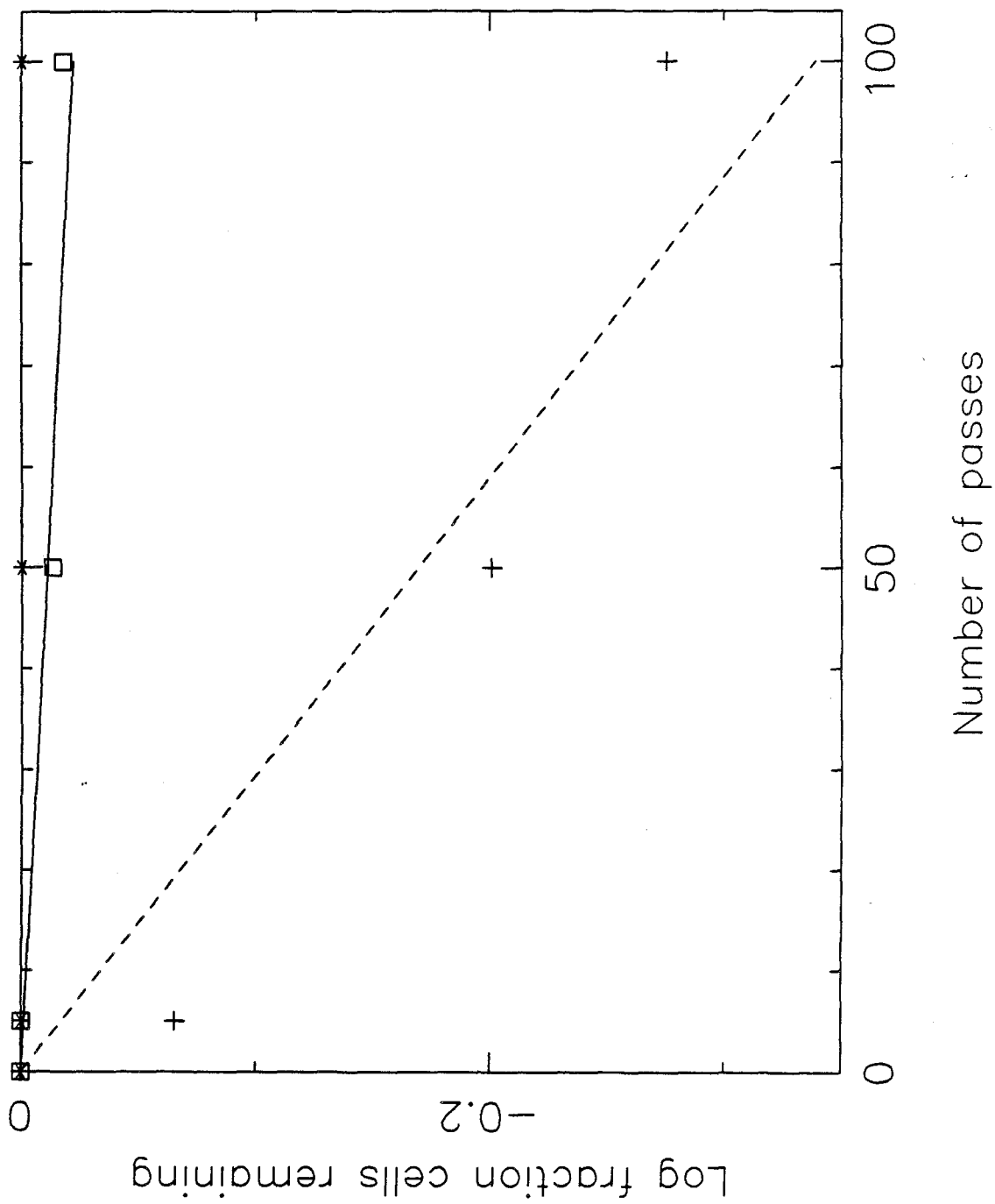

Figure 4

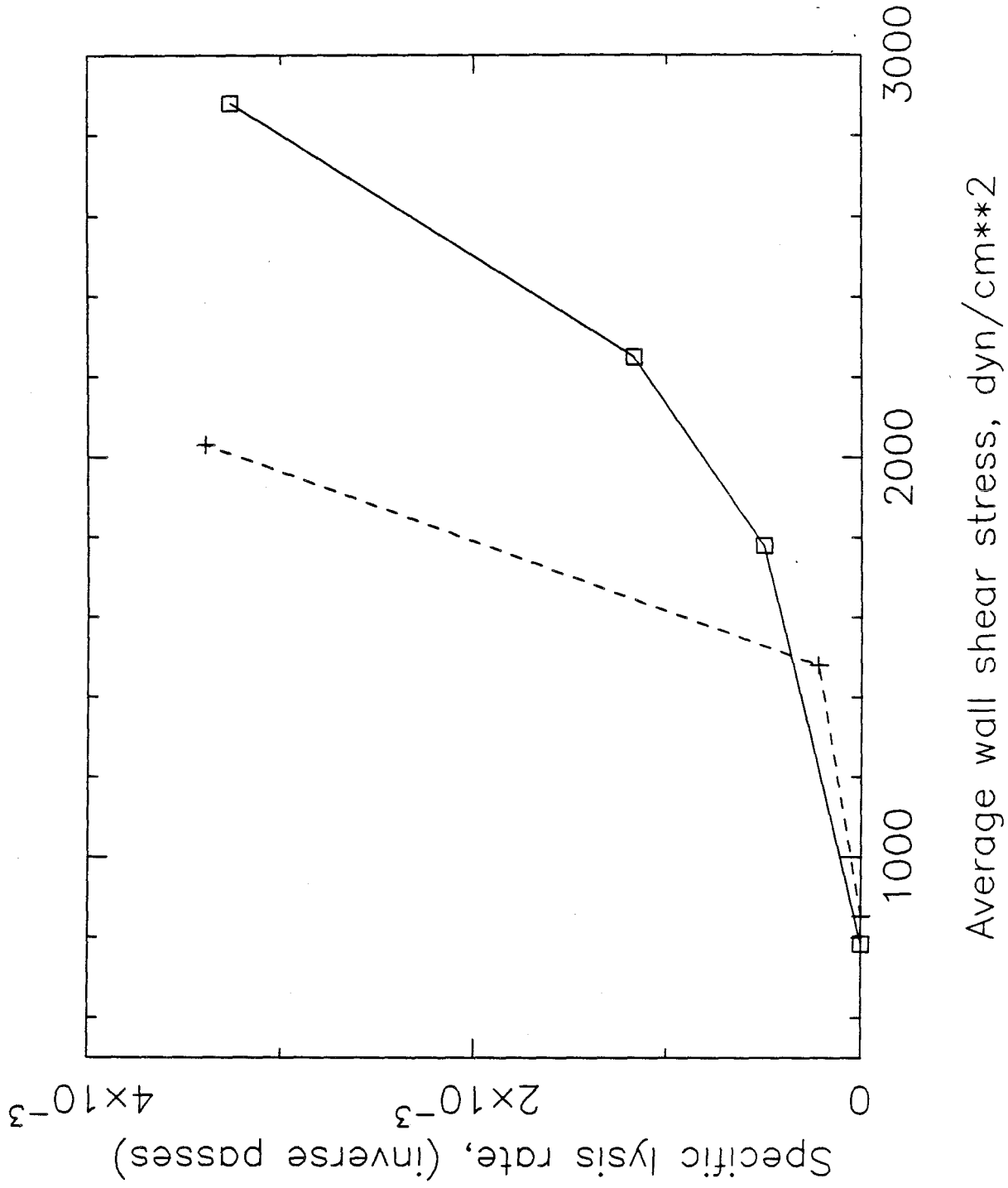
Specific lysis rate, (inverse passes)
0
2×10⁻³
4×10⁻³
Average wall shear stress, dyn/cm**2
1000
2000
3000

Figure 5

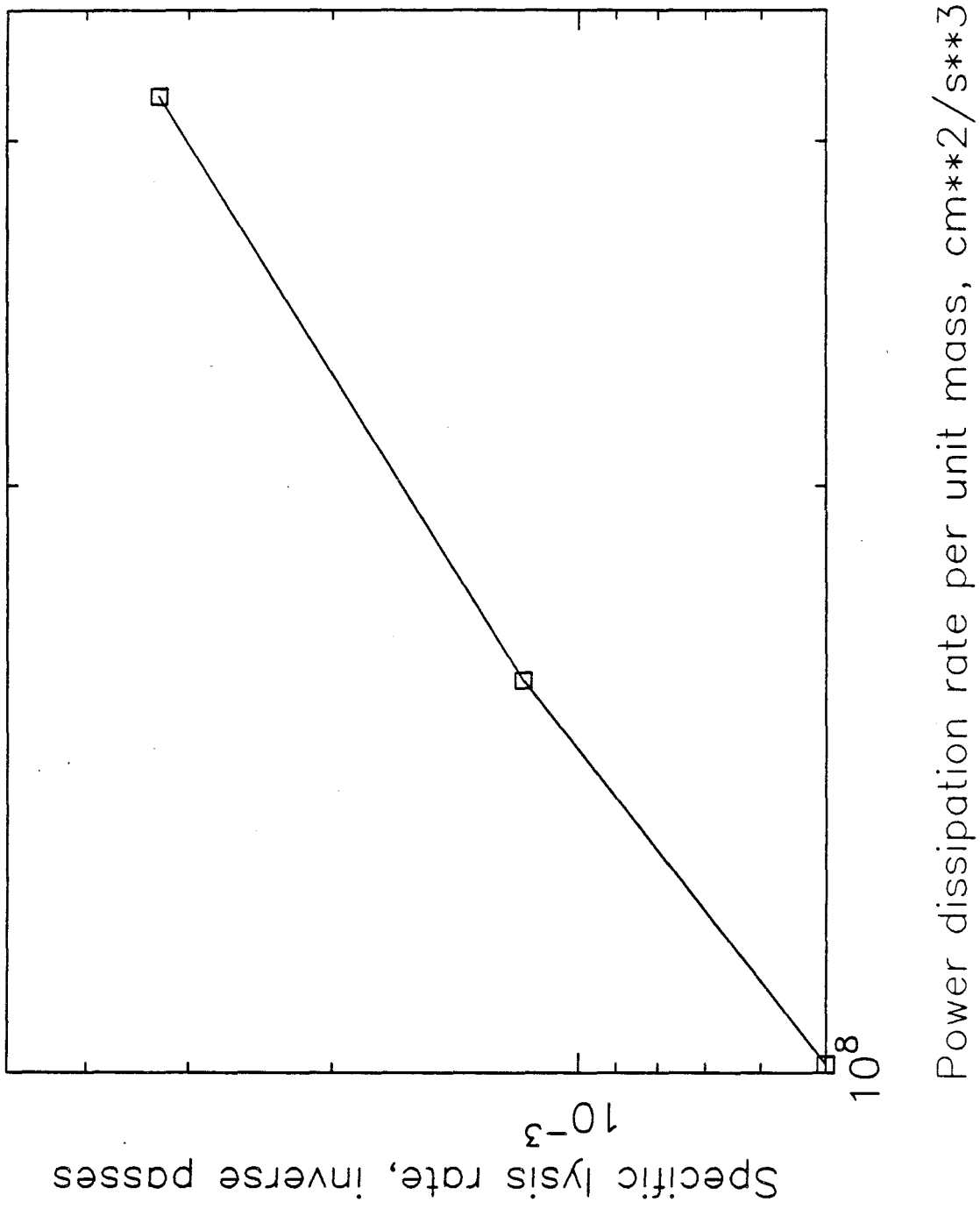
Specific lysis rate, inverse passes
10^-3
10^8
Power dissipation rate per unit mass, cm**2/s**3

Figure 6

CHAPTER 4.

Growth Inhibition of Hybridoma Cells by Ammonium Ion: Correlation with Effects on Intracellular pH

ABSTRACT

The effect of NH_4Cl addition on intracellular pH (pH_i) was determined by flow cytometric measurements of the fluorescence of a pH-sensitive dye. The effects of NH_4Cl on growth were determined for batch growth of cells in flasks in an incubator. The addition of NH_4Cl caused a cytoplasmic acidification. A new lower steady-state value of pH_i was attained within 20-40 minutes of NH_4Cl addition. A correlation was found between the effects of NH_4Cl on growth and on pH_i: whereas 3 mM NH_4Cl had little effect on growth and on pH_i, 10 mM NH_4Cl caused a substantial growth inhibition and a pH_i decrease of 0.2-0.3 units. The effects of NH_4Cl on growth and on pH_i were found to be independent of the external pH value (pH_e) over the range 6.8 to 7.6, except that 10 mM NH_4Cl was more toxic at pH_e 7.6. The addition of NH_4Cl caused an increase in the average cell volume at pH_e 7.6 but had no effect on the average cell volume at pH_e's 6.8 and 7.2. For comparison, the effects of pH_e alone on growth and on pH_i were determined. There was little difference in cell growth at pH_e's 6.8, 7.2 and 6.6. At pH_e 6.6, there was a substantial growth inhibition. Some measurements of the effects of pH_e on pH_i were made although the steady-state value of pH_i as a function of pH_e was not determined, due to limitations in the pH_i-measuring technique. These measurements showed that pH_i remained constant from pH_e 7.6 to 6.8 but fell by 0.2 units at pH_e 6.6, in agreement with the growth results.

Introduction

Previous work has indicated that ammonium ion is an important growth inhibitor of mammalian cells, including mouse hybridoma cells [1-6]. The objective of the present work is to investigate the reasons for this growth inhibition by NH_4^+. The importance of studying the effects of NH_4^+ on cells results from the fact that glutamine has been found to be an essential nutrient for cultured mammalian cells [7] and the fact that NH_4^+ is a byproduct of glutamine metabolism. Glutamine is necessary for both its anabolic and catabolic role [8]. The consumption of 1 mole of glutamine will release between 1 and 2 moles of NH_4^+ [7,8]. The rate of consumption of glutamine as a function of glutamine concentration in the medium has been observed to follow Monod kinetics [2,9]. As the glutamine consumption increases, the stoichiometry of NH_4^+ production remains the same [2,9,10]. In previous work, the optimal glutamine concentration for cell growth was found to be 4mM for both BHK and hybridoma cells [6,11].

A possible reason for NH_4^+ toxicity to cells is due to the effect of weak bases, such as NH_3 and other amines, on lysosomes [12-17]. The uncharged amines permeate the lysosomes and cause an increase in intralysosomal pH (pH_{il}). This effect depends on the neutral base concentration in the medium, which in turn is determined by the total base concentration added to the medium and the pH of the medium (the external pH (pH_e) [12]. As the amines accumulate in the lysosomes, they also cause osmotic swelling of the lysosomes, referred to as vacuolation. The pH_{il} increase is thought to be the reason for amine inhibition of receptor-mediated endocytosis of macromolecules [13,14] including growth factors [15]. King *et al.* [16] have shown that those amines that cause an inhibition of receptor-mediated

endocytosis of growth factors also cause an inhibition of growth-factor induced DNA synthesis in human fibroblast cells. Cain and Murphy [17] found a correlation between the concentration of amines required to increase intralysosomal pH and the concentrations required to inhibit growth factor stimulation of quiescent mouse fibroblast cells.

Alternatively, the effect of amines on growth may be due to their effects on intracellular (cytoplasmic) pH (pH_i) rather than due to their effect on intralysosomal pH. Boron and DeWeer [18] observed that NH_4Cl caused an increase in the pH_i of squid giant axon cells followed by a slow decrease, which they explained by leakage of NH_4^+ into the cell. The rate of decrease of pH_i is a function of the permeability of the membrane to NH_4^+, which is expected to be cell-line dependent. Boron and DeWeer's results suggest the possibility that a net cytoplasmic acidification may occur but they did not determine the steady-state value of pH_i after long-term continuous exposure to NH_4Cl. Since NH_4^+ rather than NH_3 is the species responsible for cytoplasmic acidification, these effects are a function of the NH_4Cl concentration only and are approximately independent of the external pH value in the physiological range (6.8 to 7.6), since the concentration of NH_4^+ (pK=9.2) at a given NH4Cl concentration does not vary substantially over this range.

The effects of cytoplasmic acidification (due to factors other than NH_4^+) on cell growth have been investigated by many authors. There are three reasons for suspecting that intracellular pH may be a controlling factor in cell proliferation. First, one of the early events in human fibroblast cell response to growth factors is the stimulation of the Na^+/H^+ exchanger, leading to a cytoplasmic alkalinization of approximately 0.2 units [19]. Second, growth of human tumour, Chinese Hamster

lung fibroblast, and mouse spleen lymphocyte cells has been found to be severely dependent on external pH, and this has been shown to reflect the effects of external pH on intracellular pH [20-24]. Third, *in vitro* measurements of the pH dependence of cellular enzymes suggest that intracellular pH could be a controlling factor *in vivo* [25]. From all three lines of evidence, it is clear that there is a critical alkaline pH_i value below which cells will not grow, that a 0.2 unit decrease in pH_i is sufficient to inhibit growth, and that inhibition of cell growth by low pH_i leads to accumulation of cells in G1 phase.

The purpose of this study is to determine the effects of NH_4Cl on hybridoma cell growth and to attempt to correlate these with effects of NH_4Cl on hybridoma intracellular pH, a cell parameter that previous authors have shown to be a determining factor in cell growth. Two different approaches were used for growth and pH_i measurements. The effects of NH_4Cl on growth and cell cycle distribution were determined in 4-day batch experiments in flasks in an incubator at 37°C. The effect of NH_4Cl on pH_i was determined in 6-hour experiments at 25°C in which cells were first stained with a fluorescent pH indicator. Subsequently, NH_4Cl was added and its effect on indicator fluorescence as a function of time, relative to that of a control sample, was evaluated on the flow cytometer. It was not possible to measure NH_4Cl effects on pH_i at 37°C because the dye rapidly leaked out of the cells at this temperature. Even at 25°C, corrections had to be made for leakage effects. The pH_i of cells stained after longer exposure to NH_4Cl could not be measured accurately due to limitations in the pH_i measuring technique, as will be discussed below. However it is possible to compare results from long-term growth experiments and short-term pH_i experiments because the pH_i measurements indicate the rapid attainment of

a steady-state. (Note that previous measurements of intralysosomal pH were also made in short-term experiments and the rapid attainment of a steady-state was also observed).

Since the pK of NH_4^+ is 9.2 (literature value in water) the concentration of NH_3 will be very small relative to that of NH_4^+ at all pH_e values (6.6 to 7.6) in the present work. Therefore, the NH_4^+ concentration will be considered to be approximately equal to the NH_4Cl concentration.

MATERIALS AND METHODS

Cell lines

A hybridoma cell line (ATCC TIB 131), which produces monoclonal antibody against all forms of intermediate filaments, was chosen.

Growth assay

The cells were grown in Dulbecco's modified Eagle's basal medium (DMEM), high glucose option (4.5 g/L glucose) (Irvine Scientific, Irvine, California), with 10% defined horse serum (HyClone, Logan, Utah) and antibiotics (100 units penicillin/mL and 50 μg streptomycin/mL) (Irvine Scientific, Irvine, California), in an incubator kept at 37°C and 10%CO_2. To determine the effect of pH_e on growth, the cells were resuspended in the same medium containing different bicarbonate concentrations, to which 20mM buffer were added (20 mL/L from a 1M stock), as indicated in Table 1. The pH of the 1M buffer stock solutions was adjusted (as indicated in Table 1) to give the desired pH when added to the medium at a 20mM concentration. Control experiments were performed to show that variations in the $NaHCO_3$ concentration over the range 4.4mM to 44mM had no effect on cell growth. It was shown that cells grown at the same pH_e but at different bicarbonate concentrations had the same batch growth curves, proving that pH_e not $NaHCO_3$ concentration was the controlling factor.

DNA content distribution assay

Cell nuclei were prepared and stained as described in Ref. 26. 3×10^6 cells were washed twice by centrifugation (5 min., 4°C, 200 g) with HEPES (15mM),

pH7.4, NaCl (135mM). The final pellet was resuspended in 100μL ice cold lysis buffer (TRIS 10mM, pH 7.4, $MgCl_2$ 4mM, $CaCl_2$ 2mM, sucrose 0.6 M, EDTA 5 mM, Triton X-100 0.005%). After four minutes on ice, the nuclei were collected by centrifugation (7 min., 4°C, 360 g), and washed with 500μL of lysis buffer without Triton. The nuclei were resuspended in 270μL of assay buffer (TRIS mM, pH 7.4, $MgCl_2$ 4 mM, $CaCl_2$ 2mM). The nuclear RNA was then digested (5 min., RT) with bovine pancreatic ribonuclease A (Sigma) (1.3 mg/mL), and the DNA was stained with ethidium bromide (3×10^5 M). The stained nuclei were washed once with assay buffer and resuspended in assay buffer. The stained nuclei were analysed on a Cytofluorograph 50H (Ortho), using a Lexel Model 95 argon ion laser (200 mW stabilized power at 488nm) and optical signal processing with a 590 highpass filter. The DNA histograms obtained were computer-fitted to determine the fraction of cells in G1, S and G2+M phases.

Final protocol for pH_i assay

The fluorescent indicator, BCECF-AM [27] was used to measure pH_i in a flow cytometric assay. The cells were grown, stained and washed under the same conditions. The reason that cells grown and/or stained under different conditions cannot be used in this pH_i assay is explained in the next section. After staining, the cells were divided into aliquots and subjected to different pH_e values and NH_4Cl concentrations. The method used for sample preparation and flow cytometric analysis was similar to that described by Musgrove *et al.* [28], who employed a ratio of fluorescences at 520 and 620nm as a measure of pH_i.

1) Cells were kept in exponential growth by daily passaging for 3 days prior to the experiment and were at a concentration between 8.0×10^5 and 1.2×10^6 on the day

of the experiment. The cells were harvested in late exponential phase prior to the large decreases in pH_e that occur in stationary phase and which might affect the pH_i of the cells.

2) The cells were counted and centrifuged and the old medium was removed.

3) The cells were washed in complete DMEM medium, 4.5 g/L glucose, 10% horse serum, with 25mM $NaHCO_3$ and 20mM HEPES buffer, pH 7.2 (see above section on growth assay).

4) The cells were resuspended in the above medium at 1×10^7 cells/mL and 10μM BCECF-AM was added from a 10mM stock solution in DMSO. (The final concentration of DMSO was 0.1%.)

5) The cells were incubated at 37°C for 5 minutes to allow intracellular hydrolysis of the acetoxymethyl ester form of the dye to BCECF. All manipulations were carried out at 25°C except the centrifugations, which were at 4°C.

6) The cells were centrifuged and the supernatant removed.

7) The cells were divided into aliquots and washed in the same medium.

8) The aliquots of cells were resuspended in one of the following: complete DMEM medium with different $NaHCO_3$ concentrations and 20mM buffer at different pH values, Na^+ buffers at different pH values (see below), or K^+ buffers at different pH values containing 10μM nigericin for calibration (see below). Cells resuspended in medium or Na^+ buffers will be referred to as regular samples. Cells resuspended in K^+ buffers containing nigericin will be referred to as calibration samples.

9) The initial reading of the fluorescence of all samples was made within 60 minutes to avoid the effects of leakage. The problem of leakage and the methods used to compensate for its effects will be discussed in the next section.

10) For flow cytometric analysis, the 488nm line of the argon ion laser was used at 20mW power. The filters used were a 560nm dichroic filter, to divide the beam into greater than 560nm and less than 560nm parts, a 520nm bandpass filter for fluorescence 1 (numerator of the ratio) and a 590nm highpass filter for fluorescence 2 (denominator of the ratio). The 620nm bandpass filter was not used for fluorescence 2 because this would give a low signal-to-noise ratio. Ultimately, it was decided not to use the ratio of fluorescences as a measure of pH_i, for reasons discussed in the next section. The average value of fluorescence 1 (520nm) was used instead.

Other differences between our protocol and that of Musgrove *et al.* [28] include a shorter incubation time at 37°C, which was found to be optimal to avoid excessive leakage, and the use of medium with serum during all manipulations, due to the effects of growth factors on pH_i.

The immediate (very short-term) effects of pH_e on pH_i were determined from the fluorescence values of samples resuspended in media or Na^+ buffers at different pH_e values measured immediately (within 60 minutes) after resuspension. It was not possible to obtain more long-term data on the effects of pH_e on pH_i due to the differential leakage rates as a function of pH_e, described in the next section. More long-term effects of NH_4Cl on pH_i were determined by following the fluorescence of treated and control (untreated) samples in medium at the same pH_e as a function of time and using normalized fluorescence values (defined in the next section) to compensate for the effects of leakage.

The calibration method used is that developed by Thomas *et al.* [29]. It is based on the principle that when the ionophore nigericin is added to the cells, it establishes the equilibrium: $[H^+]_i/[H^+]_e = [K^+]_i/[K^+]_e$. If cells are resuspended in

a high K^+ buffer such that $[K^+]_i = [K^+]_e$, then pH_i is equal to pH_e. In practice, it is difficult to exactly match the intracellular K^+ concentration. However, the mismatched K^+ concentration will affect only absolute pH_i measurements (as in measurements of the effect of pH_e on pH_i), not relative pH_i measurements (as in measurements of the effect of NH_4Cl concentration on pH_i).

The Na^+ buffers contained the following: NaCl 130 mM, KCl 5 mM, $CaCl_2$ 1.3 mM, $MgSO_4$ 0.8mM $NaH_2PO_4.H_2O$ 1.0 mM, glucose 5.6 mM; to which 20 mM of one of the following buffers was added: MES pH 5.5, MES pH 6.1, MES pH 6.4, PIPES pH 6.6, PIPES pH 6.8, HEPES pH 7.2, TRICINE pH 7.6, TRICINE pH 8.0, or TRICINE pH 8.5. The K^+ buffers contained the following: NaCl 5 mM, KCl 130 mM, $CaCl_2$ 1.3 mM, $MgSO_4$ 0.8 mM, KH_2PO_4 1.0 mM, glucose 5.6 mM; to which 20 mM of one of the following buffers was added: MES pH 6.4, PIPES pH 6.8, HEPES pH 7.2, or TRICINE pH 7.6.

Development of pH_i assay

The use of the fluorescent indicator BCECF-AM to measure pH_i was first introduced in a paper by Rink *et al.* in 1982 [27]. In 1986, Musgrove *et al.* [28] published a paper in which BCECF-AM was used in a flow cytometric assay for the first time. Musgrove *et al.* employed a ratio of fluorescences at 520nm and 620nm (obtained using bandpass filters at these wavelengths) as a measure of pH_i, in order to correct for cell-to-cell variations in volume and intracellular dye concentration (dye uptake). The single disadvantage they reported with BCECF-AM was the low sensitivity to pH_i of the 520nm/620nm ratio, which gave a resolution of only 0.4 pH units. We modified their procedure, using a 590 highpass filter instead of the 620nm bandpass filter to give better signal-to-noise ratios.

Two examples of typical histograms obtained for fluorescences 1 (520nm) and 2 (greater than 590 nm) are presented in Fig. 1 A and B (A1 and B1, A2 and B2, respectively). The magnitude of fluorescence 2 is much smaller than that of fluorescence 1, since 520nm represents the peak of the emission spectrum. Therefore, a much higher gain value had to be used for fluorescence 2 (3.2-3.5) than for fluorescence 1 (1.2-1.5). The two-parameter contour plots of the data are shown in Fig. 2 A and B. Figures 1A and 2A show a regular sample at pH_e 7.2, while figures 1B and 2B show a calibration sample at pH_e 6.4. (The pH_i of the calibration samples is approximately equal to pH_e, as explained in the previous section.) In Fig. 2, it can be seen that the cells in both the regular and calibration samples fall along a single straight line, indicating that there is little cell-to-cell heterogeneity in pH_i. The value of the ratio of fluorescence 1 to fluorescence 2 can be determined graphically from the slope of this line. Alternatively, the average values of fluorescences 1 and 2 can be determined from the histograms and their ratio calculated. These two methods are found to give similar results and therefore the second method will be chosen since it gives more accurate results. The narrow distribution in the ratio of fluorescence 1 to fluorescence 2 indicated by the contour plot implies that it is not necessary to calculate this ratio on a single-cell basis. The sample at the lower pH_i (Figures 1B and 2B) has lower values of fluorescences 1 and 2 as well as a decreased ratio value.

The ratio of the fluorescences (1/2) (in arbitrary units) of the calibration samples is plotted as a function of pH_e in Fig. 3, for both 10μM and 5μM dye concentration. Although the above contour plot shows that the ratio of fluorescences (1/2) is independent of cell volume; the data in Fig. 3 shows that this ratio is not

independent of the intracellular dye concentration. This implies that the fluorescence ratio cannot be used to correct for differences in dye uptake, as suggested by other authors. This means that the fluorescence of cells grown and stained under different conditions cannot be compared since their dye uptake may vary. As a result, variables such as pH_e and NH_4Cl can only be introduced at the time of resuspension, after a uniform cell dye content has been assured. This is the reason that only short-term experiments on the effects of pH_e and NH_4Cl on pH_i were made, in which cells were first stained and then divided into aliquots and subjected to different conditions during a 6-hour experiment. The details of the procedure are described in the previous section.

A further problem with the fluorescence ratio is its relative insensitivity to pH_i: the ratio decreases at pH_i 6.4 to only 20% of its value at pH_i 7.6 (Figure 3). In Fig. 3, the absolute values of fluorescence 1 (in arbitrary units) of the calibration samples are presented for both $5\mu M$ and $10\mu M$ dye concentration. As indicated in Fig. 3, fluorescence 1 is very sensitive to pH_i, decreasing at pH_i 6.4 to approximately 50% of its value at pH_i 7.6. Hence, in all subsequent experiments, the absolute value of fluorescence 1 (fluorescence 2 has much smaller magnitude) will be used to estimate pH_i. $10\mu M$ dye concentration was used throughout. (Henceforth, fluorescence 1 will be referred to simply as fluorescence.)

The fluorescence of a single cell depends on three factors: cell volume, intracellular dye concentration, and pH_i, in the following manner:

$$\text{fluorescence} = k \times \text{cell volume} \times \text{intracellular dye concentration} \times f(pH_i)$$

where k is some constant and f is a function describing the pH dependence of dye fluorescence. To use the fluorescence as a measure of pH_i, the effects of cell volume

and intracellular dye concentration must be eliminated. Controls were performed to ensure that the mean cell volume (average fluorescence is used here) did not change during the course of the 6-hour experiment or as a result of pH_e change or NH_4Cl addition. (Mean cell volume was measured in the Coulter counter.) An initially uniform intracellular dye concentration was obtained by growing and staining cells under the same conditions. However, after resuspension, the fluorescence of the cells decreases as a function of time, as shown in Fig. 4, and this has been determined to be caused by leakage of the dye out of the cells (by spectrofluorometric measurements on the supernatant after centrifuging out the cells). In addition, as Fig. 4 shows, the rate of leakage depends on the pH_e value. Dye content decreases after 200 minutes by 10% at pH_e 6.8 and by 30% at pH_e 7.6.

To solve the problem of dye leakage, two different approaches were used. In the case of pH_e effects on pH_i, the absolute fluorescence of samples resuspended at different pH_e values was compared immediately after resuspension, before substantial leakage occured, to the absolute fluorescence of the calibration samples (whose pH_i is known) run at the same time. Therefore, only very short-term effects of pH_e on pH_i could be determined. The calibration curve of fluorescence versus pH_i (approximately equal to pH_e for the calibration samples), such as that shown in Fig. 3, must be obtained daily due to variations in instrument setup and gain value. In the case of NH_4Cl effects on pH_i, a normalization method was used to compensate for changes in fluorescence due to dye leakage rather than due to changes in pH_i. Therefore, it was possible to determine more long-term effects of NH_4Cl on pH_i. In the normalization method, the fluorescence of the sample treated with NH_4Cl was divided by that of the control sample (untreated) at the same pH_e (since leakage

depends on pH_e), as in the following equation:

$$\begin{pmatrix}\text{normalized fluorescence value} \\ \text{of sample}\end{pmatrix} = \frac{\text{absolute value of fluorescence 1 of sample}}{\text{abs. value of fluorescence 1 of control sample}}$$

$$(= 1 \text{ for control sample})$$

This normalization method was adopted after experiments on the effects of leakage on the calibration samples showed that, while the absolute fluorescence values of the calibration samples decreased as a function of time (Fig. 5), their normalized fluorescence values, defined in the following equation, remained the same (Fig. 6).

$$\begin{pmatrix}\text{normalized fluorescence value} \\ \text{of calibration sample}\end{pmatrix} = \frac{\text{abs. value of fluor. 1 of calibr. sample}}{\text{abs. val. of fluor. 1 of calibr. sam. at } pH_e \text{ 7.6}}$$

$$(= 1 \text{ for calibration sample at } pH_e \text{ 7.6})$$

In Figure 6, it can be seen that the normalized fluorescence values of the calibration samples remain approximately constant for 4 hours although 30-40% of the dye has leaked out (Fig. 5). (Note: The normalization of the fluorescence of the calibration samples by the fluorescence of the calibration sample at pH_e 7.6 (pH_i approximately equal to 7.6) makes good sense since experimental results (to be discussed below) indicate that the pH_i of regular samples in medium at pH_e values from 7.6 to 6.8 is approximately 7.6 prior to NH_4Cl treatment.) As a result, the calibration data in terms of normalized fluorescence values, presented in Fig. 6, can be used to estimate pH_i differences between samples, based on a comparison of their normalized fluorescence values. Table 2 shows how a percent difference in normalized fluorescence value (due to pH_e change or NH_4Cl addition) can be converted into a difference in pH_i (ΔpH_i). The calibration data in Table 2 (percent difference in normalized fluorescence value versus ΔpH_i), used to obtain relative

pH_i values, has been found to be approximately constant from day to day (unlike the calibration curve of fluorescence versus pH_i, such as that in Fig. 3, used to obtain absolute pH_i values).

RESULTS

The two important independent variables to be studied to assess ammonium ion effects on growth and intracellular pH are medium NH_4Cl concentration and external pH. Since external pH, by itself, may affect cell growth, these effects will be discussed first.

Effect of pH_e on cell growth and cell cycle distribution

Cells were grown in an incubator with 10% CO_2 at various pH_e values in media containing different concentrations of bicarbonate and 20mM of different buffers, as described in the Materials and Methods. pH_e remained constant for the first 48 hours of the batch then decreased gradually. The final values of pH_e were an average of 0.4 units lower than the initial, nominal pH_e values. In Fig. 7, the effect of pH_e on cell growth is presented. There is little difference in the growth curves at pH_e 7.6 and 7.2 except that there is a drop in the viable cell density on the fourth day of the batch culture at pH_e 7.6. While some reduction in growth rate is observed at pH_e 6.8, relative to higher pH_e values, growth is not severely inhibited until pH_e 6.6. At pH_e 6.6, the fraction of viable cells also decreases (data not shown). At pH_e 6.4, no cell growth is observed and all cells die within 48 hours (data not shown).

The effect of pH_e on average cell volume (determined on the Coulter counter) as a function of time is presented in Fig. 8. It can be seen that average cell volume decreases both as the nominal pH_e value decreases and as a function of time at a given nominal pH_e value. These decreases in cell volume as a function of time in part reflect the declining pH_e values described above. However, since the average cell volume at higher nominal pH_e values falls more quickly during the course of

the batch than at lower nominal pH_e values; by the end of the batch, the average cell volume values become similar at all nominal pH_e values. This implies that, if specific growth rates were calculated on a cell mass basis rather than a cell number basis, differences between high pH_e and low pH_e values would be reduced.

The cell cycle distribution was measured by a flow cytometric assay of DNA content. In Fig. 9, the fraction of cells in G1 phase is plotted as a function of time in batch. Whereas at pH_e 6.6, the fraction of cells in G1 is always high (above 0.35), the fraction in G1 is initially low (below 0.2) at pH_e values 6,8, 7.2, and 7.6 and increases throughout the batch reaching values similar to those of the pH_e 6.6 experiment on day 3.

Effect of NH_4Cl on cell growth and cell cycle distribution at different pH_e values

The effect of the addition of 3 and 10mM NH_4Cl on cell growth at pH_e values 6.8, 7.2 and 7.6 is presented in Figures 10A, 10B and 10C. At all pH_e values, it can be seen that, whereas 3mM NH_4Cl had little effect on cell growth, 10mM NH_4Cl caused severe growth inhibition. The toxicity of 10mM NH_4Cl varies as a function of pH_e. At pH_e 7.6, although some cell growth occurs during the first 24 hours, 10mM NH_4Cl causes partial cell death between 24 and 48 hours and complete cell death within 72 hours (data not shown). In Fig. 11, the average cell volume at pH_e 7.6 is plotted as a function of time for 0, 3 and 10mM NH_4Cl. It can be seen that average cell volume increases as the concentration of NH_4Cl increases. At pH_e 7.2, whereas 3mM NH_4Cl had no effect on average cell volume, 10mM NH_4Cl caused a small increase (data not shown). At pH_e 6.8, 3 and 10mM NH_4Cl had no effect on cell volume (data not shown).

In Figures 12A, 12B, and 12C, the fraction of cells in G1 phase is plotted as a

function of time at pH_e values 6.8, 7.2 and 7.6 for different NH_4Cl concentrations. At pH_e values 6.8 and 7.2 (Figures 12A and 12B), 10mM NH_4Cl causes the early accumulation of cells in G1 phase, and 3mM NH_4Cl has little effect on cell cycle distribution. Whereas at 0 and 3mM NH_4Cl the fraction in G1 did not reach 0.35 until day 4 of the batch, the fraction in G1 reached 0.35 on day 2 at 10mM NH_4Cl. The accumulation of cells in G1 phase resembled that observed at pH_e 6.6 in the absence of NH_4Cl, except that, in that case, the fraction in G1 reached 0.35 within 24 hours. At pH_e 7.6, 3mM NH_4Cl also has little effect on cell cycle distribution (Fig. 12C). The cell fragility and early cell death at 10mM NH_4Cl made it impossible to obtain cell cycle distribution data under these conditions. The reason that the fraction of cells in G1 phase is lower at 3mM NH_4Cl than at 0mM NH_4Cl at later times in the batch (pH_e values 6.8, 7.2 and 7.6) is the slower rate of growth observed at 3mM NH_4Cl, which leads to a delay in reaching batch stationary phase in which cells accumulate in G1 phase.

Effect of pH_e on pH_i

The effects of pH_e on pH_i were determined by resuspending samples, which had been grown and stained under identical conditions (medium containing 25mM $NaHCO_3$ and 20mM HEPES buffer pH 7.2, preincubated in a 10% CO_2 atmosphere, as described in the Materials and Methods) before dividing into aliquots, in buffered media containing bicarbonate or Na^+ buffers, at different pH_e levels. Na^+ buffers were used for comparison because they have a wider range of pH_e values than medium equilibrated with 10% CO_2. The samples were read within 60 minutes after resuspension, before differential leakage rates could make the results difficult to interpret. Therefore, only short-term effects of pH_e on pH_i were determined. The

data in terms of the ratio of fluorescence 1 to fluorescence 2 show the same general trends as intracellular pH values estimated from the absolute value of fluorescence 1. The results for the latter are presented in Fig. 13.

For cells in medium, there is little change in pH_i over the range of pH_e 6.8 to 7.8. A comparison with the daily calibration curve, such as that shown in Fig. 3, indicates that pH_i is approximately 7.6 over this range. This estimate was obtained reproducibly from day to day. At pH_e values below 6.8, there is a gradual decrease in fluorescence. Compared to values at pH_e 6.8 and above, fluorescence declines 8% at pH_e 6.6 and 16% at pH_e 6.4, corresponding to pH_i decreases of approximately 0.2 and 0.4 units, respectively, by comparison to Table 2.

In the case of cells in Na^+ buffers, pH_i also remains approximately constant at 7.6 over the pH_e range 6.8 to 8.5. At pH_e 6.6, there is a small decrease in fluorescence. At pH_e values 6.1 and 5.5, there is a dramatic drop in fluorescence (23% and 51%, respectively), indicating 0.6 and 1.1 unit decreases in pH_i, respectively, by reference to Table 2.

Effect of NH_4Cl on pH_i at different pH_e values

To measure the effect of NH_4Cl on pH_i, samples that had been grown, stained and washed under identical conditions (medium containing 25mM $NaHCO_3$ and 20mM HEPES buffer pH 7.2, preincubated in a 10% CO_2 atmosphere, as described in the Materials and Methods) were resuspended in buffered media without NH_4Cl at three different pH_e levels: 6.8, 7.2 or 7.6 and divided into aliquots. After measuring the initial fluorescence, 3, 10 or 30mM NH_4Cl was added to samples at each of the pH_e values, while one sample at each pH_e value was kept aside to use as a control. The fluorescence as a function of time of the samples with 3, 10 or 30mM

NH_4Cl was compared to that of the control sample (without NH_4Cl) at the same pH_e.

In the first set of experiments, the short-term effects of NH_4Cl on pH_i were determined: the fluorescence of each sample was measured immediately after adding NH_4Cl and every 5 minutes thereafter. The data in terms of the ratio of fluorescence 1 to fluorescence 2 show the same general trends as the data in terms of the absolute value of fluorescence 1. The results for the latter are presented in Fig. 14 at pH_e 7.2. The addition of NH_4Cl leads to a brief cytoplasmic alkalinization followed by a rapid cytoplasmic acidification. pH_i levels off within 20-40 minutes of NH_4Cl addition. During this time, the effects of leakage could be neglected. In Fig. 14, the results after 60 minutes of incubation with NH_4Cl are also included. The fluorescence value after 60 minutes has been normalized to correct for leakage. Both the extent of the initial alkalinization and the extent of the ultimate acidification increase with the NH_4Cl concentration. While the initial part of the transients are similar at 3 and 10 NH_4Cl; after 20 minutes, the curves diverge. At 3mM NH_4Cl, there is a recovery to a higher pH_i value, which remains approximately constant from 40 to 60 minutes. At 10mM NH_4Cl, there is no further change in pH_i. At 30mM NH_4Cl, pH_i decreases continuously from 5 to 30 minutes then increases somewhat from 30 to 60 minutes.

In the second set of experiments, the long-term effects of NH_4Cl on pH_i were estimated by measuring the fluorescence of control and treated samples at 60 minute intervals after NH_4Cl addition for up to 6 hours. The effects of leakage on the fluorescence as a function of time were eliminated by normalizing the fluorescence of the samples containing NH_4Cl, dividing their fluorescence values by that of the

control sample (without NH_4Cl) at the same pH_e.

In Figures 15A, 15B and 15C, the long-term effects of 3, 10, and 30mM NH_4Cl on intracellular pH are presented at pH_e values 6.8, 7.2 and 7.6, respectively. It is clear from Figures 15A-15C that pH_i reaches an approximate steady-state within 60 minutes of NH_4Cl addition. The steady-state normalized fluorescence values are listed in Table 3. The acidification due to NH_4Cl is dose-dependent. However, the dose dependence does not vary with external pH. In all cases, whereas 3mM NH_4Cl has little effect of pH_i (2-7% decrease), 10mM causes a substantial acidification (11-14% decrease) and 30mM depresses pH_i still further (20-26% decrease). These decreases correspond to reductions in pH_i of 0-0.1 units at 3mM NH_4Cl, of 0.2-0.3 units at 10mM NH_4Cl and of 0.5-0.7 units at 30mM NH_4Cl, based on the calibration data listed in Table 2.

Proof that fluorescence changes upon addition of NH_4Cl are due to pH_i changes and not due to differential indicator leakage rates as a function of NH_4Cl concentration is provided by the following two lines of evidence. First, the NH_4Cl effects occur on a different time scale, as seen by comparing Figures 4 and 14. Second, when a sample that has been treated with NH_4Cl is resuspended in the absence of NH_4Cl, its fluorescence value returns to that of the control sample, reflecting the pH_i recovery and implying negligible influence of NH_4Cl on the indicator leakage rate.

in the measurements of the effects of NH_4Cl on average cell volume at pH_e 7.6. However, NH_4Cl had negligible effects on cell volume at pH_e values 6.8 and 7.2. Therefore, although vacuolation may be the cause of the toxicity of 10mM NH_4Cl at pH_e 7.6, it is unlikely to be responsible for the growth inhibition resulting from 10mM NH_4Cl at pH_e's 6.8 and 7.2.

The results for effect of NH_4Cl on cell growth are compared with those of other authors in Table 5. The same basis was used as in Table 4. The results of other authors were obtained in medium at standard pH_e values 7.2-7.4. The compilation of previous work indicates that, in general, for mouse hybridoma cells and for mouse myeloma cells in the presence of serum [2-5], 2-4mM NH_4Cl are required for growth inhibition, while 5-8mM NH_4Cl are required for cell death. Some other cells appear to be more sensitive to NH_4Cl: mouse myeloma cells in the absence of serum [5] and anchorage-dependent BHK cells [6]. In contrast, TIB 131 hybridoma cells seem to be less sensitive to NH_4Cl. At pH_e 7.2, they show only very slight (10%) growth inhibition with 3mM NH_4Cl and no cell death even at 10mM NH_4Cl (although growth is severely inhibited–78%–at this concentration). Cain and Murphy's results for mouse fibroblast cells at pH_e 7.4 appear to be similar to ours [17] at pH_e 7.2. These investigators observed a correlation between the effects of 3 and 10mM NH_4Cl on cell growth and on intralysosomal pH (pH_{il}). While 1mM NH_4^+ had no effect on pH_{il} or on cell growth, 3 and 10mM NH_4Cl caused 0.3 and 0.6 unit increases in pH_{il} and 30 and 58% growth inhibition, respectively. 30mM NH_4Cl caused a 0.9 unit increase in pH_{il} and approximately 100% growth inhibition. Miller [1] observed that hybridoma cells in continuous culture could be adapted to an NH_4Cl concentration of 8mM in a period of 5 days following a step

change but could not recover from a pulse of 18mM NH_4Cl applied subsequently. (80% of cells died within 48 hours although the NH_4Cl concentration fell to 10mM during this time.)

Results from this study show that the intracellular pH of TIB 131 hybridoma cells remains constant at 7.6 as pH_e decreases until pH_e falls below 6.8, as determined from a comparison of fluorescence values immediately (within 60 minutes) after resuspension. At pH_e 6.6, there is a pH_i decrease of approximately 0.2 units. Hence, there is a correlation between the effects of pH_e on growth and on pH_i based on these very short-term measurements of pH_e effects on pH_i. Whether pH_i remains unaffected by pH_e values from 6.8 to 7.6 over longer times is not known. The fact that pH_i shows a decrease immediately upon resuspension at pH_e values below 6.8 suggests that the cell cannot maintain very large pH gradients (greater than 0.8 units) across the plasma membrane.

The addition of NH_4Cl to hybridoma cells leads to a rapid cytoplasmic acidification, as predicted by Boron and DeWeer's [18] model for cells with a high permeability to NH_4^+. Although these pH_i measurements are made in relatively short-term experiments (6 hours), the results have implications for the long-term behavior of pH_i because pH_i reaches a new, lower steady-state value within 60 minutes of NH_4Cl addition. Whereas 3mM NH_4Cl has little effect on pH_i, 10mM NH_4Cl causes a 0.2-0.3 unit decrease in pH_i. Therefore, there is a correlation between the effects of NH_4Cl on growth and on pH_i. In agreement with previous work, a decrease in pH_i causes growth inhibition. The magnitude of the pH_i decrease required to inhibit growth, 0.2-0.3 units for both pH_e and NH_4Cl effects, is also consistent with the work of other authors on the relationship between pH_i and growth [20-24].

Our results demonstrate the existence of an alternative mechanism (designated 2 below) for NH_4Cl effects on growth, different from the existing mechanism (designated 1 below), which is based on the effects of NH_3 on the lysosome, which interfere with receptor-mediated endocytosis of growth factors. The salient features of these two mechanisms are presented in the following table.

	Mechanism 1	Mechanism 2
Compartment whose pH is affected	lysosome	cytoplasm
Direction of pH change	alkalinization	acidification
Agent responsible	NH_3	NH_4^+
pH_e dependence	yes	no

The first mechanism is pH_e-dependent because it involves the effects of NH_3, and the concentration of NH_3 at a given NH_4Cl concentration decreases as pH_e decreases due to the shift in equilibrium between NH_3 and NH_4^+. Therefore, mechanism 1 suggests that the concentration of NH_4Cl required to inhibit growth should increase as pH_e decreases. The second mechanism is relatively pH_e-independent, for pH_e values in the physiological range, since the concentration of NH_4^+ (pK=9.2), at a given NH_4Cl concentration, does not vary much over this range. It is important to note that these two mechanisms are complementary, not mutually exclusive, since both NH_3 and NH_4^+ are present at significant concentrations at higher pH_e values. The pH_e dependencies of the effects of NH_4Cl on growth and on pH_i were measured here in order to distinguish between the two mechanisms.

At all pH_e values (6.8, 7.2, and 7.6), 3mM NH_4Cl has little effect on growth and on pH_i, while 10mM NH_4Cl has a substantial effect on both. Therefore, since

the effects of NH_4Cl are not pH_e-dependent, the results in the present work indicate growth inhibition due to NH_4Cl based on the second mechanism. The results are in direct contradiction with the first mechanism since the amount of growth inhibition observed should correlate with the NH_3 concentration in that mechanism, and this is not found to be true. The concentration of NH_4Cl required to inhibit growth does not increase as pH_e decreases. This implies that NH_3 cannot be the sole agent responsible for growth inhibition, but intracellular acidification, due to NH_4^+ permeation, must also be significant. At pH_e 7.6, the first mechanism contributes to the toxic effects of 10mM NH_4Cl. However, the first mechanism is insufficient to explain the growth inhibition observed at the lower pH_e values (6.8 and 7.2). Hence, the second mechanism is an important addition to complete the picture.

Acknowledgements: This research was supported by the National Science Foundation. Anne McQueen was supported in part by a Natural Sciences and Engineering Research Council of Canada (NSERC) fellowship.

REFERENCES

1. Miller, W.M.; Wilke, C.R.; Blanch, H.W.: Transient responses of hybridoma cells to lactate and ammonia pulse and step changes in continuous culture. Bioprocess Engr. 3 (1988) 113-122

2. Glacken, M.W.; Adema, E.; Sinskey, A.J.: Mathematical descriptions of hybridoma culture kinetics for optimization of bioreactors, I. Initial metabolic rates. Biotech. Bioeng. 32 (1988) 491-506

3. Thorpe, J.S.; Murdin, A.D.; Sanders, P.G.; Spier, R.E.: The effect of waste products of cellular metabolism on growth and protein synthesis in a mouse hybridoma cell line. Presented at the 194th National meeting of the American Chemical Society, New Orleans, Louisiana, August 31-September 4, 1987

4. Reuveny, S.; Velez, D.; Macmillan, J.D.; Miller, L.: Factors affecting cell growth and monoclonal antibody production in stirred reactors. J. Immunol. Methods 86 (1986) 53-59

5. Iio, M.; Moriyama, A.; Murakami, H.: Effects on cell proliferation of metabolites produced by cultured cells and their removal from culture in defined media. In: Murakami, H.; Yamane, I.; Barnes, D.W.; Mather, J.P.; Hayashi, I.; Sato, G.H. (Eds.): Growth and differentiation of cells in a defined environment, pp. 437-442. Tokyo: Kodansha and Berlin: Springer 1985

6. Butler, M.; Spier, R.E.: The effects of glutamine utilization and ammonia production on the growth of BHK cells in microcarrier cultures. J. Biotechnology 1 (1984) 187-196

7. McKeehan, W.L.: Glutaminolysis in animal cells. In: Morgan, M.J. (Ed.):

Carbohydrate metabolism in cultured cells, pp. 111-150. New York: Plenum Press 1986

8. Zielke, H.R.; Sumbilla, C.M.; Zielke, C.L.; Tildon, J.T.; Ozand, P.T.: Glutamine metabolism by cultured mammalian cells. In: Haussinger, D.; Sies H. (Eds.): Glutamine metabolism in mammalian tissues, ppl 247-254. Berlin: Heidelberg and New York: Springer 1984

9. Himes, V.B.; Hu, W.-S.: Glutamine utilization by CHO cells in perfused microcarrier cultures. Presented at the 196th national meeting of the American Chemical Society, Los Angeles, California, September 25-30, 1988

10. Miller, W.M.; Wilke, C.R.; Blanch, H.W.: The transient responses of hybridoma cells to nutrient additions in continuous culture: II. Glutamine pulse and step changes. Biotech. Bioeng. 33 (1989) 487-499

11. Dalili, M.; Ollis, D.F.: Flow cytometric analysis of hybridoma growth and monoclonal antibody production. Presented at the 196th national meeting of the American Chemical Society, Los Angeles, California, September 25-30, 1988

12. Poole, B.; Ohkuma, S.: Effect of weak bases on the intralysosomal pH in mouse peritoneal macrophages. J. Cell Biol. 90 (1981) 665-669

13. Van Leuven, F.; Cassiman, J.-J.; Van Den Berghe, H.: Primary amines inhibit recycling of α_2M receptors in fibroblasts. Cell 20 (1980) 37-43

14. Tietze, C.; Schlesinger, P.; Stahl, P.: Chloroquine and ammonium ion inhibit receptor-mediated endocytosis of mannose glycoconjugates by macrophages: Apparent inhibition of receptor recycling. Biochem. Biophys. Res. Commun. 93 (1980) 1-8

15. King, A.C.; Hernaez-Davis, L.; Cuatrecasas, P.: Lysosomotropic amines cause

intracellular accumulation of receptors for epidermal growth factor. PNAS USA 77 (1980) 3283-3287

16. King, A.C.; Hernaez-Davis, L.; Cuatrecasas, P.: Lysosomotropic amines inhibit mitogenesis induced by growth factors. PNAS USA 78 (1981) 717-721

17. Cain, C.C.; Murphy, R.F.: Growth inhibition of 3T3 fibroblasts by lysosomotropic amines: Correlation with effects on intravesicular pH but not vacuolation. J. Cell Physiol. 129 (1986) 65-70

18. Boron, W.F.; DeWeer, P.: Intracellular pH transients in squid giant axons caused by CO_2, NH_3 and metabolic inhibitors. J. Gen. Physiol. 67 (1976) 91-112

19. Moolenaar, W.H.; Defize, L.H.K.; Van Der Saag, P.T.; De Laat, S.W.: The generation of ionic signals by growth factors. In: Aronson, P.S.; Boron, W.F. (Eds.): Na^+-H^+ exchange, intracellular pH, and cell function, pp. 137-156. New York: Academic Press 1986

20. Taylor, I.W.; Hodson, P.J.: Cell cycle regulation by environmental pH. J. Cell Physiol. 121 (1984) 517-525

21. Musgrove, E.; Seaman, M.; Hedley, D.: Relationship between cytoplasmic pH and proliferation during exponential growth and cellular quiescence. Exp. Cell Res. 172 (1987) 65-75

22. L'Allemain, G.; Paris, S.; Pouyssegur, J.: Growth factor action and intracellular pH regulation in fibroblasts–Evidence for a major role of the Na^+/H^+ antiport. J. Biol. Chem. 259 (1984) 5809-5815

23. Pouyssegur, J.; Franchi, A.; L'Allemain, G.; Paris, S.: Cytoplasmic pH, a key determinant of growth factor-induced DNA synthesis in quiescent fribroblasts. FEBS Lett. 190 (1985) 115-119

24. Gerson, D.F.: The relation between intracellular pH and DNA synthesis rate in proliferating lymphocytes. In: Nuccitelli, R.; Deamer, D.W. (Eds.): Intracellular pH: its measurement, regulation, and utilization in cellular functions, pp. 375-383. New York: Alan R. Liss 1982

25. Busa, W.B.: The proton as an integrating effector in metabolic activation. In: Aronson, P.S.; Boron, W.F. (Eds.): Na^+-H^+ exchange, intracellular pH, and cell function, pp. 291-305. New York: Academic Press 1986

26. Hugues, B.; Osborne, H.B.: Dexamethasone inhibits a heme-independent event necessary for terminal differentiation of murine etythroleukemia cells. Biochem. Biophys. Res. Commun. 102 (1981) 1342-1349

27. Rink, T.J.; Tsien, R.Y.; Pozzan, T.: Cytoplasmic pH and free Mg^{2+} in lymphocytes. J. Cell Biol. 95 (1982) 189-196

28. Musgrove, E.; Rugg, C.; Hedley, D.: Flow cytometric measurement of cytoplasmic pH: A critical evaluation of available fluorochromes. Cytometry 7 (1986) 347-355

29. Thomas, J.A.; Buchsbaum, R.N.; Zimniak, A.; Racker, E.: Intracellular pH measurements in Ehrlich Ascites tumor cells utilizing spectroscopic probes generated in situ. Biochemistry 18 (1979) 2210-2218

30. Miller, W.M.; Blanch, H.W.; Wilke, C.R.: A kinetic analysis of hybridoma growth and metabolism in batch and continuous suspension culture: Effect of nutrient concentration, dilution rate and pH. Biotech. Bioeng. 32 (1988) 947-965

Table 1: Composition of media used for growth assay.

Desired pH_e	mM $NaHCO_3$	Buffer added	pH of buffer
6.4	4.4	MES	6.1
6.6	4.4	PIPES	6.6
6.8	10	PIPES	6.8
7.2	25	HEPES	7.2
7.6	44	TRICINE	8.5
7.8	44	TRICINE	8.8

Table 2: Calibration data in terms of normalized fluorescence values.

pH_e	$\Delta pH_e = pH_e - 7.6$ $= \Delta pH_i$	Normalized fluorescence value of calibration sample	Percent difference in normalized fluorescence value
7.6	0.0	1.00	0
7.2	-0.4	0.82	18
6.8	-0.8	0.72	28
6.4	-1.2	0.43	57

Table 3: Steady-state normalized fluorescence values.

pH_e	6.8	7.2	7.6
mM NH_4^+			
0	1.00	1.00	1.00
3	0.98	0.93	0.95
10	0.89	0.88	0.86
30	0.74	0.80	0.78

Table 4: Effect of pH_e on cell growth.

Cell line	pH	Viable cells/mL		Ratio of final to initial	Percent growth inhibition	Reference
		Initial	48 hours			
Human	7.2	1.0	5.0	5.0	0	Taylor
melanoma	6.5	1.0	2.0	2.0	60	1984 [20]
PMC-22	6.3	1.0	1.4	1.4	72	
Mouse	7.2	0.5	5.2	10.4	0	Present
hybridoma	6.8	0.5	3.7	7.4	29	work
TIB 131	6.6	0.5	1.1	2.2	79	

Table 5: Effect of NH_4^+ on cell growth.

Cell line	mM NH_4^+ required for growth inhibition	Percent growth inhibition	mM NH_4^+ required for cell death	Percent cell death	Reference
Mouse hybridoma	4	48	–	–	Glacken 1988 [2]
Mouse hybridoma	4	24	8	25	Thorpe 1987 [3]
Mouse hybridoma	3	42	5	20	Reuveny 1986 [4]
Mouse myeloma	2.4 2.4	28 64	in serum-containing in serum-free		Iio 1985 [5]
B Hamster kidney	1 2	33 67	–	–	Butler 1984 [6]
Mouse Fibroblast	3 10	30 58	–	–	Cain 1986 [17]
Mouse hybridoma TIB 131					
pH_e					
6.8	3	20	–	–	Present
	10	60			work
7.2	3	10	–	–	
	10	78			
7.6	3	55	–	–	
	10	88			

Figure 1: Histograms of fluorescences 1 and 2 for 2 samples at different pH_i values

A1: Histogram of fluorescence 1 for sample A

A2: Histogram of fluorescence 2 for sample B

A3: Histogram of fluorescence 1 for sample A

A4: Histogram of fluorescence 2 for sample B

Sample A: Regular sample, cells resuspended in medium, pH 7.2 (composition in Table 1).

Sample B: Calibration sample, cells resuspended in K^+ buffer containing nigericin, pH 6.4 (composition in Materials and Methods).

The samples were grown, stained with 10μM BCECF-AM, divided, resuspended and analyzed on the flow cytometer as described in Materials and Methods.

Figure 2: Two-parameter contour plots (fluorescences 1 and 2) for 2 samples at different pH_i values

A: Contour plot for sample A

B: Contour plot for sample B

The samples were the same as in Fig. 12.

Figure 3: Calibration curves in terms of the ratio of fluorescence 1 to fluorescence 2 and in terms of the absolute value of fluorescence 1

The ratio of fluorescence 1 to fluorescence 2 (ratio of averages of histograms or slope of contour plot) of the calibration samples is plotted as a function of pH_e for cells stained with either 10μM (squares) or 5μM (crosses) dye concentration (dashed

lines). The absolute value of fluorescence 1 (average of histogram) of the calibration samples is plotted as a function of pH_e for cells stained with either 10μM (squares) or 5μM (crosses) dye (solid lines). The calibration samples are samples resuspended in K^+ buffers containing nigericin, as described in Materials and Methods. The samples were grown, stained with BCECF-AM, divided, resuspended and analyzed on the flow cytometer as described in Materials and Methods.

Figure 4: Effect of leakage on the fluorescence of samples in medium

The fluorescence (average of histogram of fluorescence 1) of cells resuspended in media at pH_e 7.6 (solid line), 7.2 (dashed line) and 6.8 (dot-dashed line) was plotted as a function of time, expressed as a fraction of the initial value. The samples were grown, stained with 10μM BCECF-AM, divided, resuspended and analyzed on the flow cytometer as described in Materials and Methods.

Figure 5: Calibration curves in terms of the absolute value of fluorescence 1 as a function of time

The absolute value of fluorescence 1 (average of histogram) of the calibration samples is plotted as a funtion of pH_e for different times after resuspension: immediately after (solid line), 45 minutes after (dashed line), 90 minutes after (dot-dashed line) and 230 minutes after (dotted line). The calibration samples are samples resuspended in K^+ buffers containing nigericin, as described in Materials and Methods. The samples were grown, stained with 10μM BCECF-AM, divided, resuspended and analyzed on the flow cytometer as described in Materials and Methods.

Figure 6: Effect of leakage on the fluorescence of the calibration samples

The data in Figure 16 are re-plotted as follows. The current value of the fluorescence of a given calibration sample at a certain pH_e is divided by the current value of the calibration sample at pH_e 7.6, and these normalized fluorescence values are plotted as a function of time.

Figure 7: Effect of external pH on cell growth

The viable cells/mL ($\times 10^{-5}$) are shown as a function of time for pH_e 7.6 (solid line), 7.2 (dashed line), 6.8 (dot-dashed line) and 6.6 (dotted line). The cells were grown as described in Materials and Methods in media with 20mM buffer at different pH_e values. The composition of the media were as described in Table 1. The total cell concentration was determined on the Coulter Counter and the percent viability was determined with a hemacytometer using eosin yellow as a viability stain.

Figure 8: Effect of external pH on average cell volume

The average cell volume (μm^3) is plotted as a function of time for cells grown in medium at pH_e 7.6 (solid line), 7.2 (dashed line), 6.8 (dot-dashed line) and 6.6 (dotted line). The cells were grown as described in Figure 7. The average cell volume was determined on the Coulter counter.

Figure 9: Effect of external pH on the cell cycle distribution

The fraction of cells in G1 phase is plotted as a function of time for cells grown in medium at pH_e 7.6 (solid line), 7.2 (dashed line), 6.8 (dot-dashed line) and 6.6 (dotted line). The cells were grown as described in Figure 7. The fraction of cells in G1 phase was determined by computer fit of the DNA content distribution obtained by flow cytometric analysis of cell nuclei stained with ethidium bromide, as described in Materials and Methods.

Figure 10: Effect of ammonium chloride on cell growth at pH_e values 6.8, 7.2 and 7.6

The viable cells/mL ($\times 10^{-5}$) are shown as a function of time for cells grown in medium (composition as in Table 1) at pH_e 6.8 (Fig. 10A), 7.2 (Fig. 10B) or 7.6 (Fig. 10C), containing 0mM (solid lines), 3mM (dashed lines), or 10mM (dot-dashed lines) NH_4Cl. The cells were grown as described in Materials and Methods. The total cell concentration was determined with the Coulter counter and the percent viability was determined with a hemacytometer using eosin yellow as a viability stain.

Figure 11: Effect of ammonium chloride on the average cell volume at pH_e 7.6

The average cell volume (μm^3) is plotted as a function of time for cells grown in medium at pH_e 7.6, containing 0mM (solid line), 3mM (dashed line) or 10mM (dot-dashed line) NH_4Cl. The cells were grown as described in Figure 10.

Figure 12: Effect of ammonium chloride on the cell cycle distribution at pH_e values 6.8, 7.2 and 7.6

The fraction of cells in G1 phase is plotted as a function of time for cells grown in medium at pH_e 6.8 (Fig. 12A), 7.2 (Fig. 12B) or 7.6 (Fig. 12C), containing 0mM (solid lines), 3mM (dashed lines) or 10mM (dot-dashed lines) NH_4Cl. The cells were grown as described in Figure 10. The fraction of cells in G1 phase was determined by computer fit of the DNA content distribution obtained by flow cytometric analysis of cell nuclei stained with ethidium bromide, as described in Materials and Methods.

Figure 13: Effect of external pH on intracellular pH

The fluorescence (average value of histogram of fluorescence 1) of cells was determined immediately after resuspension at different pH_e values in media (solid line) (compositions in Table 1) or Na^+ buffers (dashed line) (compositions in Materials and Methods). The samples were grown, stained with 10μM BCECF-AM, divided, resuspended and analyzed on the flow cytometer as described in Materials and Methods. (Note that the solid and dashed lines should be superimposed from pH_e values 6.8 to 7.8 but have been drawn apart for clarity.)

Figure 14: Short-term effects of ammonium chloride on intracellular pH at pH_e 7.2

The fluorescence (average value of histogram of fluorescence 1) of cells resuspended in medium at pH_e 7.2 (composition in Table 1), to which 3mM (dashed line) 10mM (dot-dashed line) or 30mM (dotted line) NH_4Cl were added at time 0, was plotted as a function of time. The cells were grown, stained with 10μM BCECF-AM, resuspended, divided and analyzed on the flow cytometer as described in Materials and Methods. A different symbol is used for the points at 60 minutes because, in this case, the fluorescence has been normalized (by dividing by the current value of the control sample at the same pH_e) to correct for leakage, whose effects could no longer be neglected (see text).

Figure 15: Long-term effects of ammonium chloride on intracellular pH at pH_e values 6.8, 7.2 and 7.6

The fluorescence (average value of histogram of fluorescence 1) of cells resuspended in medium (composition in Table 1), at pH_e 6.8 (Fig. 15A), 7.2 (Fig. 15B) or 7.6 (Fig. 15C), to which 3mM (dashed lines), 10mM (dot-dashed lines) or 30mM

(dotted lines) NH_4Cl was added at time 0, was normalized by dividing by the current value of the control sample (without NH_4Cl) at the same pH_e and plotted as a function of time. The cells were grown, stained with 10μM BCECF-AM, resuspended, divided and analyzed as described in Materials and Methods.

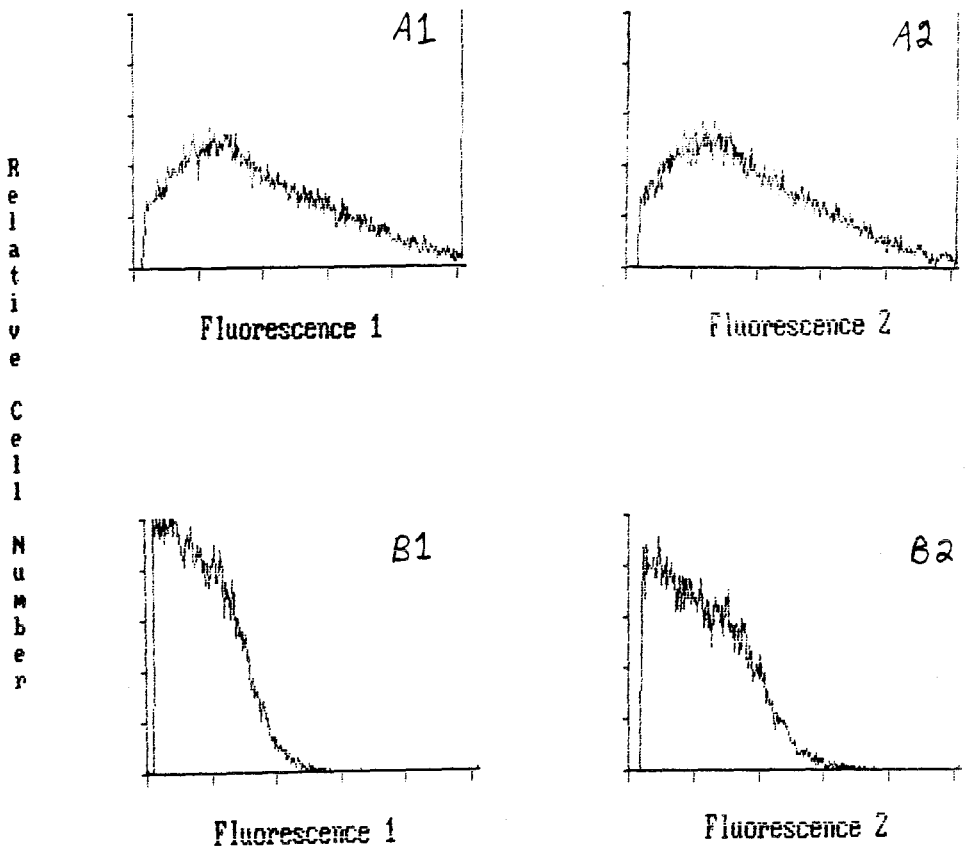
A1
A2
Relative Cell Number
Fluorescence 1
Fluorescence 2
B1
B2
Fluorescence 1
Fluorescence 2

Figure 1

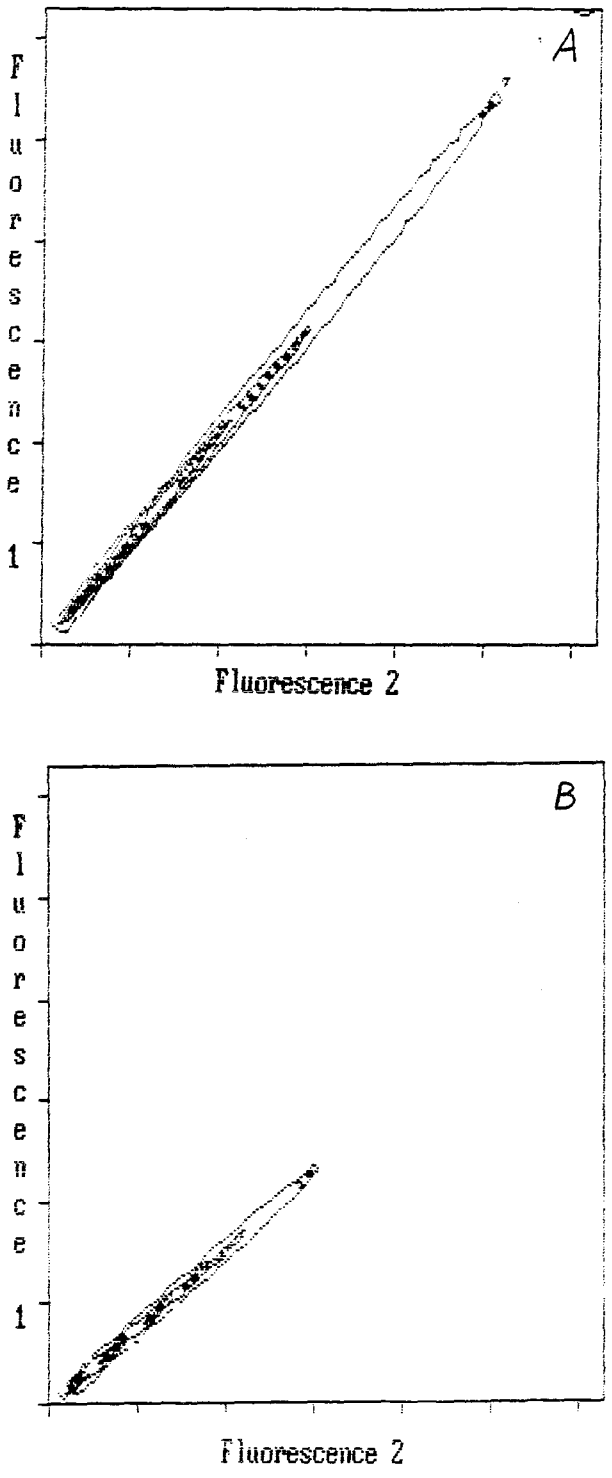
A
Fluorescence 1
Fluorescence 2
B
Fluorescence 1
Fluorescence 2

Figure 2

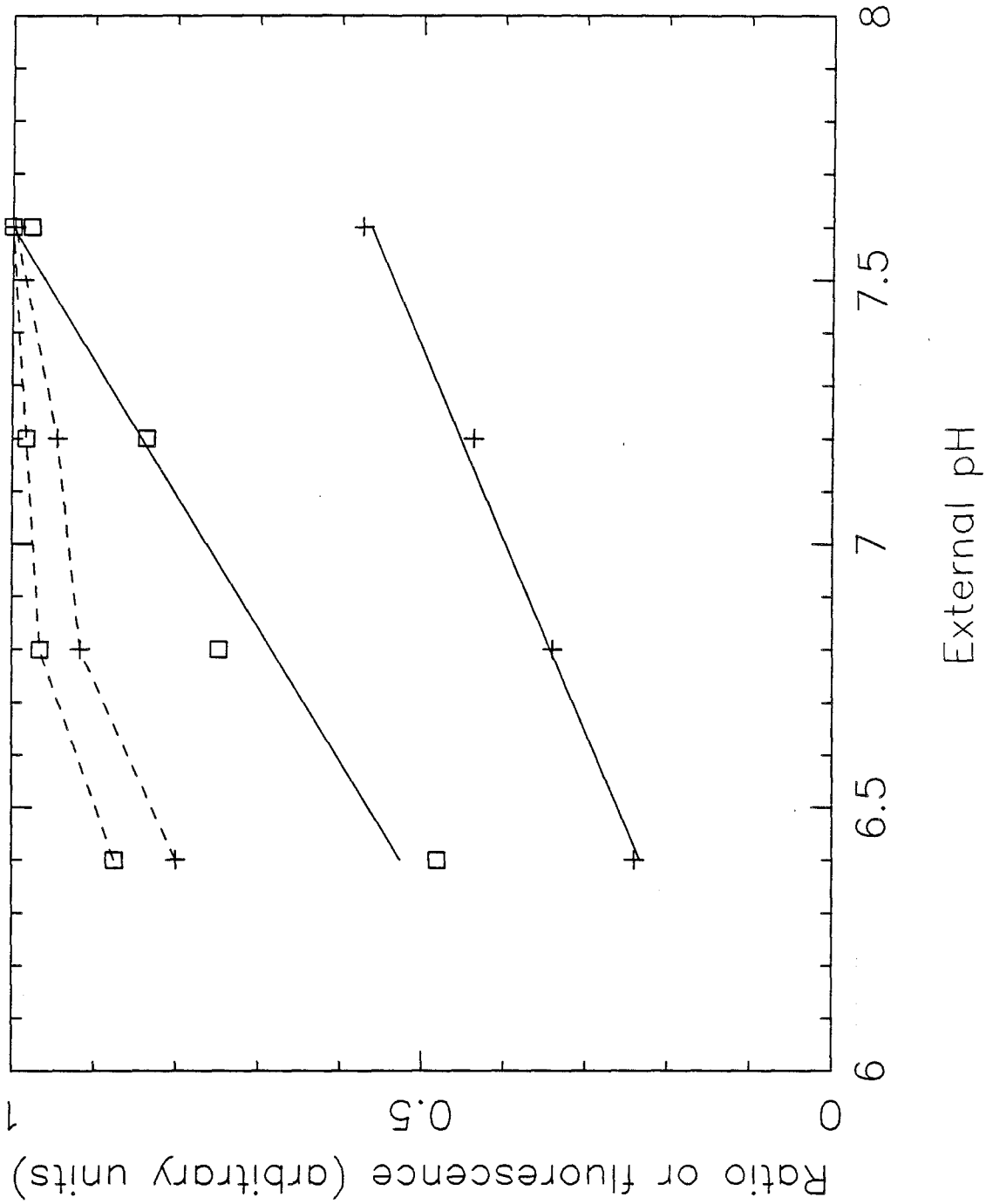
Ratio or fluorescence (arbitrary units)
0
0.5
1
6
6.5
7
7.5
8
External pH

Figure 3

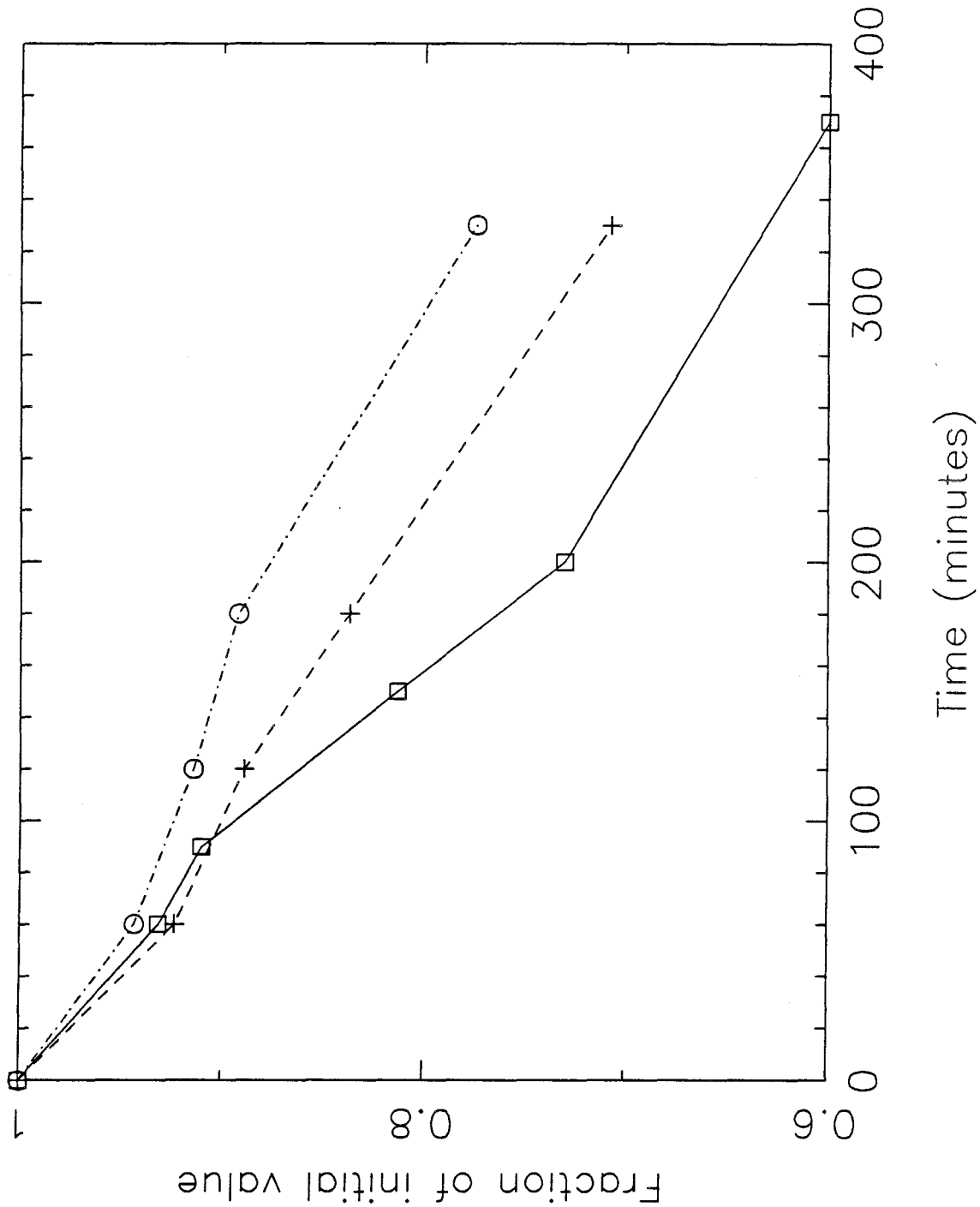
Fraction of initial value
1
0.8
0.6
0
100
200
300
400
Time (minutes)

Figure 4

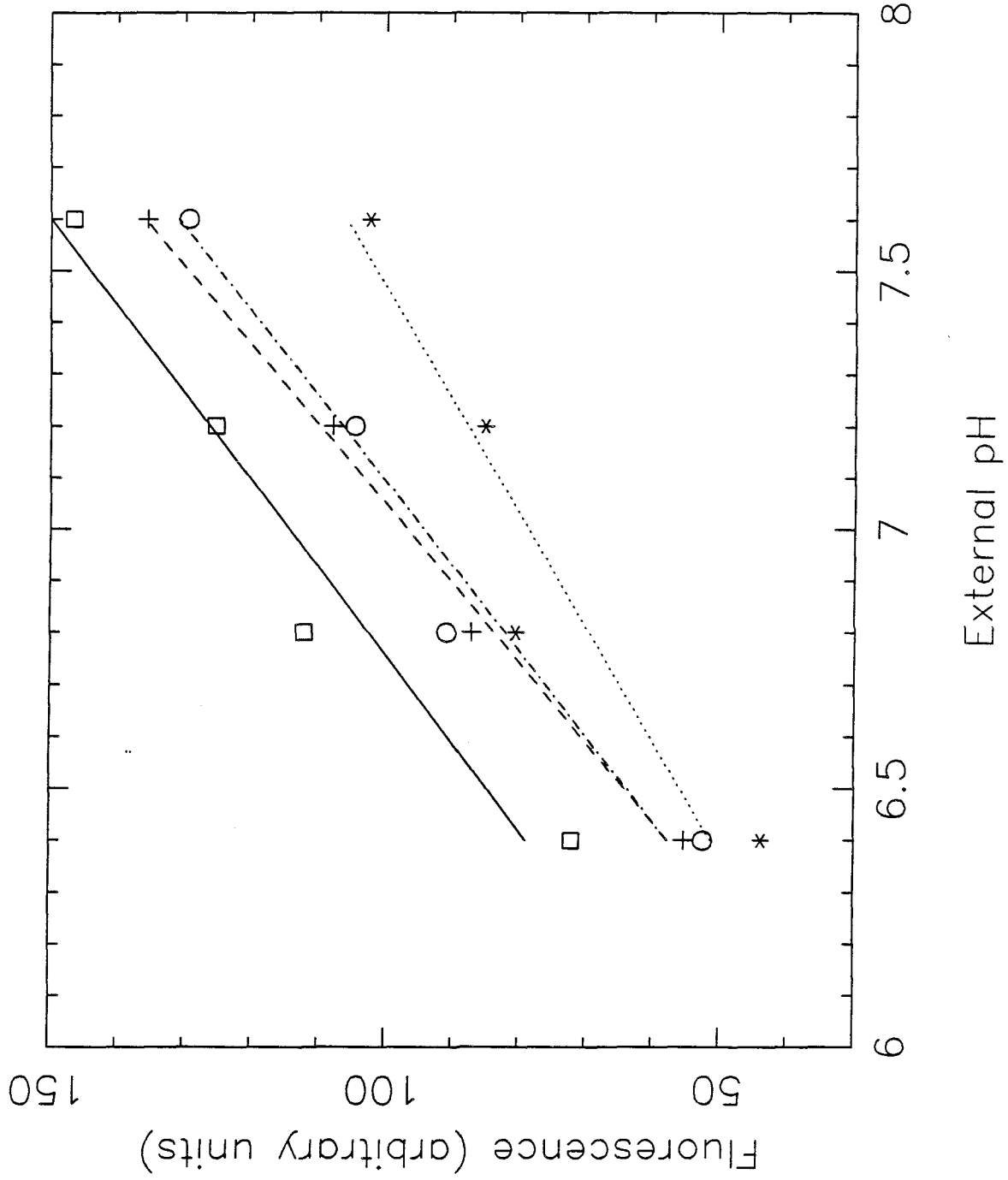
Fluorescence (arbitrary units)
150
100
50
External pH
6
6.5
7
7.5
8

Figure 5

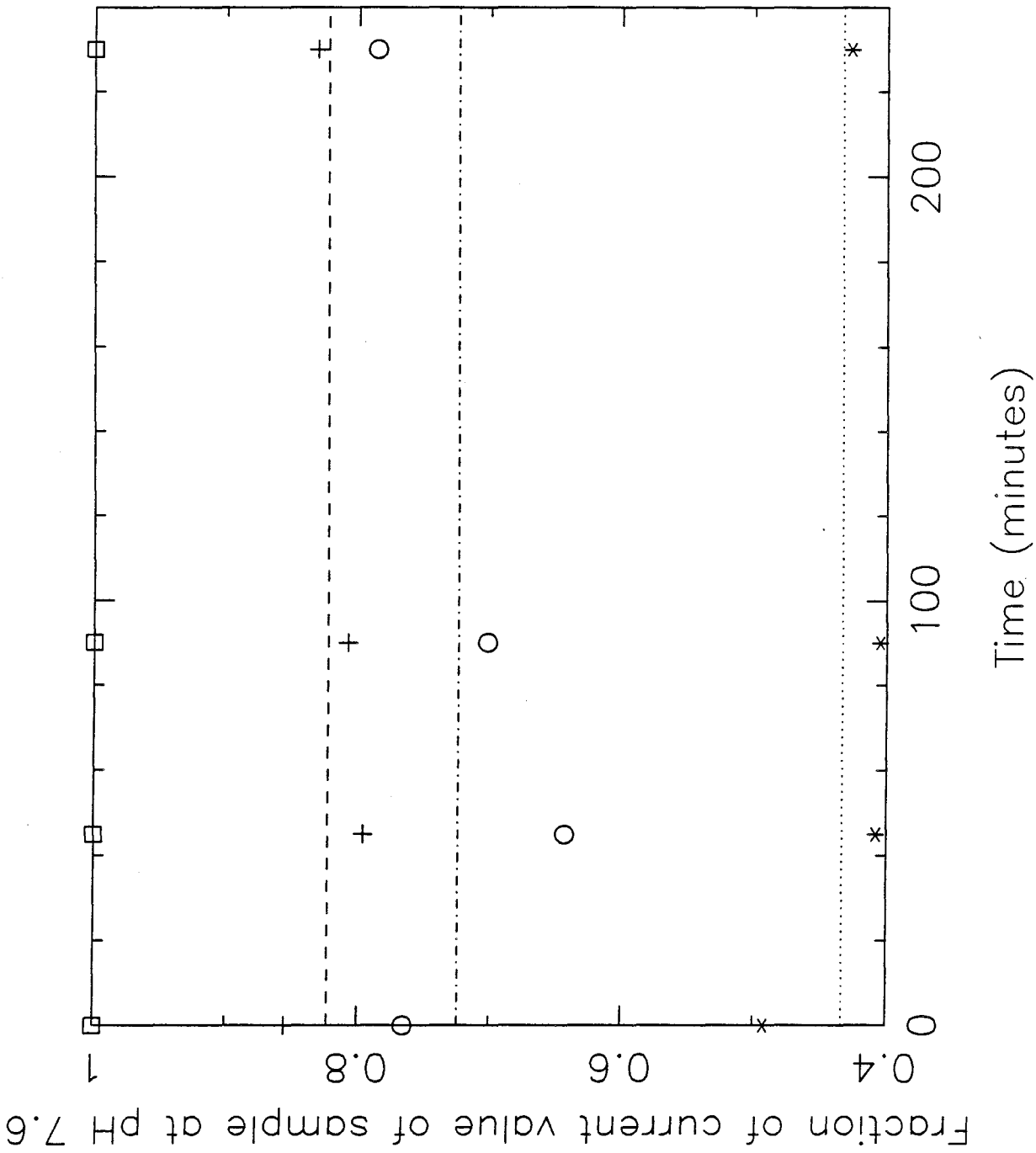
Fraction of current value of sample at pH 7.6
0.4
0.6
0.8
1
0
100
200
Time (minutes)

Figure 6

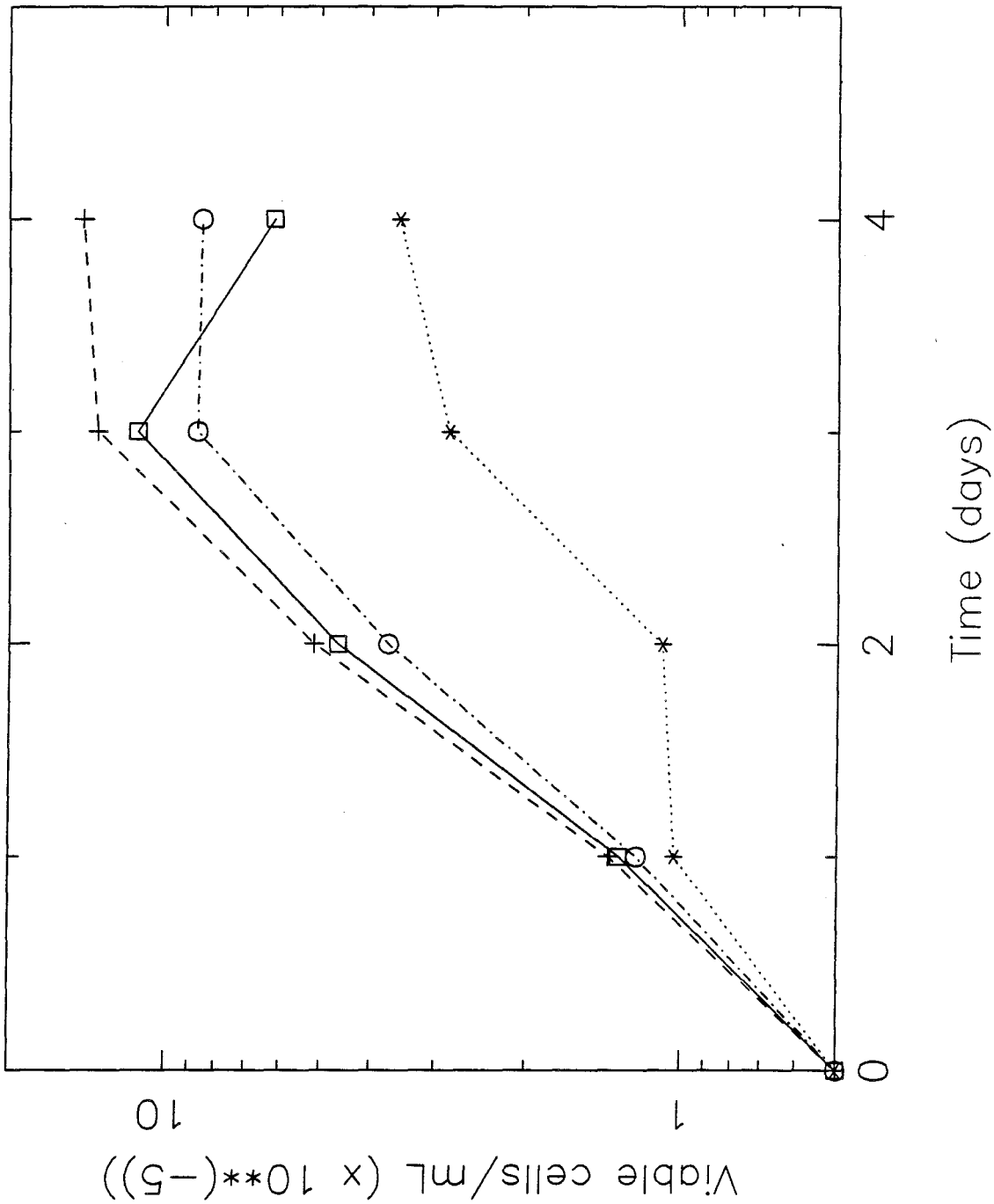

Figure 7

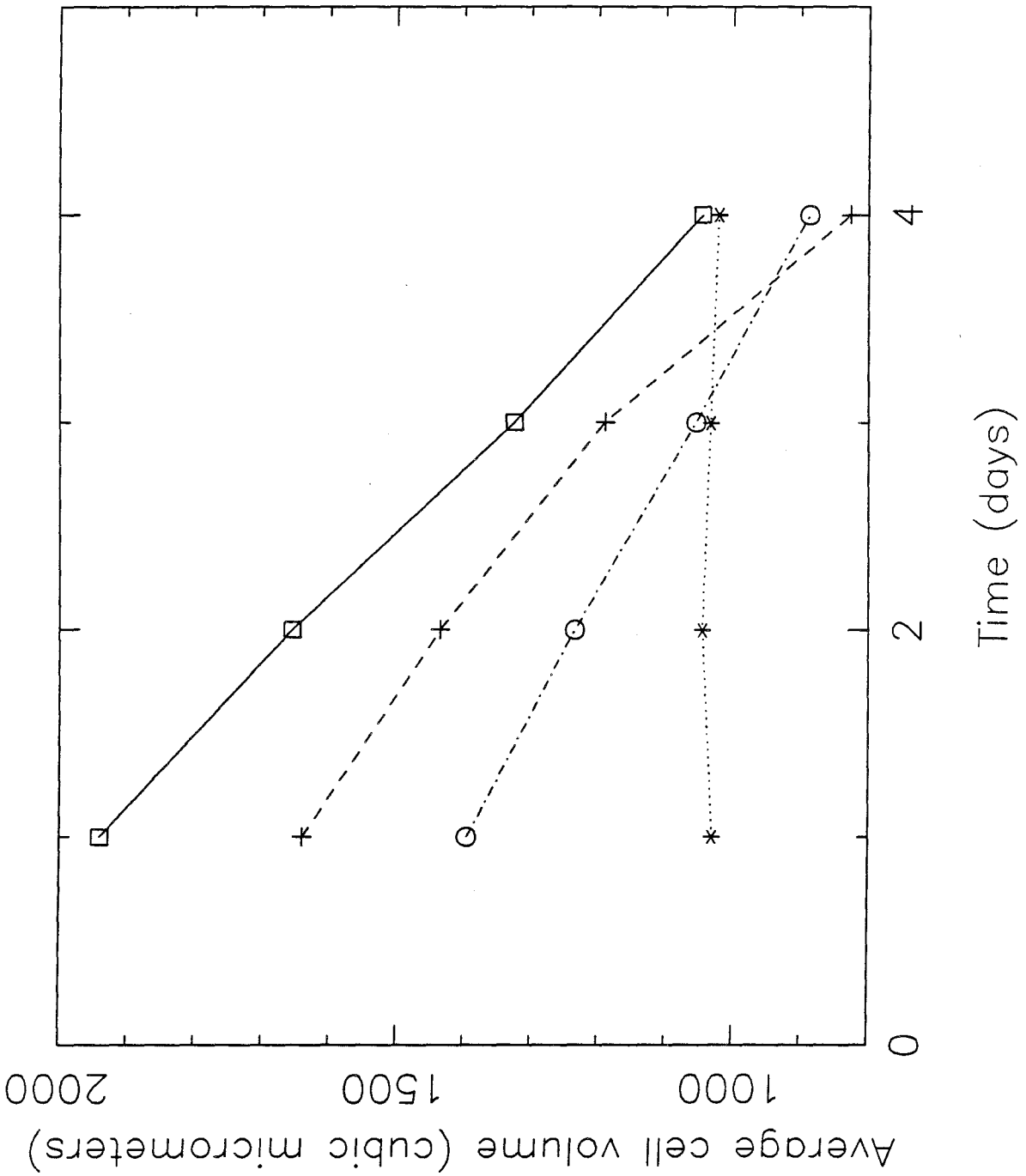
Average cell volume (cubic micrometers)
1000
1500
2000
0
2
4
Time (days)

Figure 8

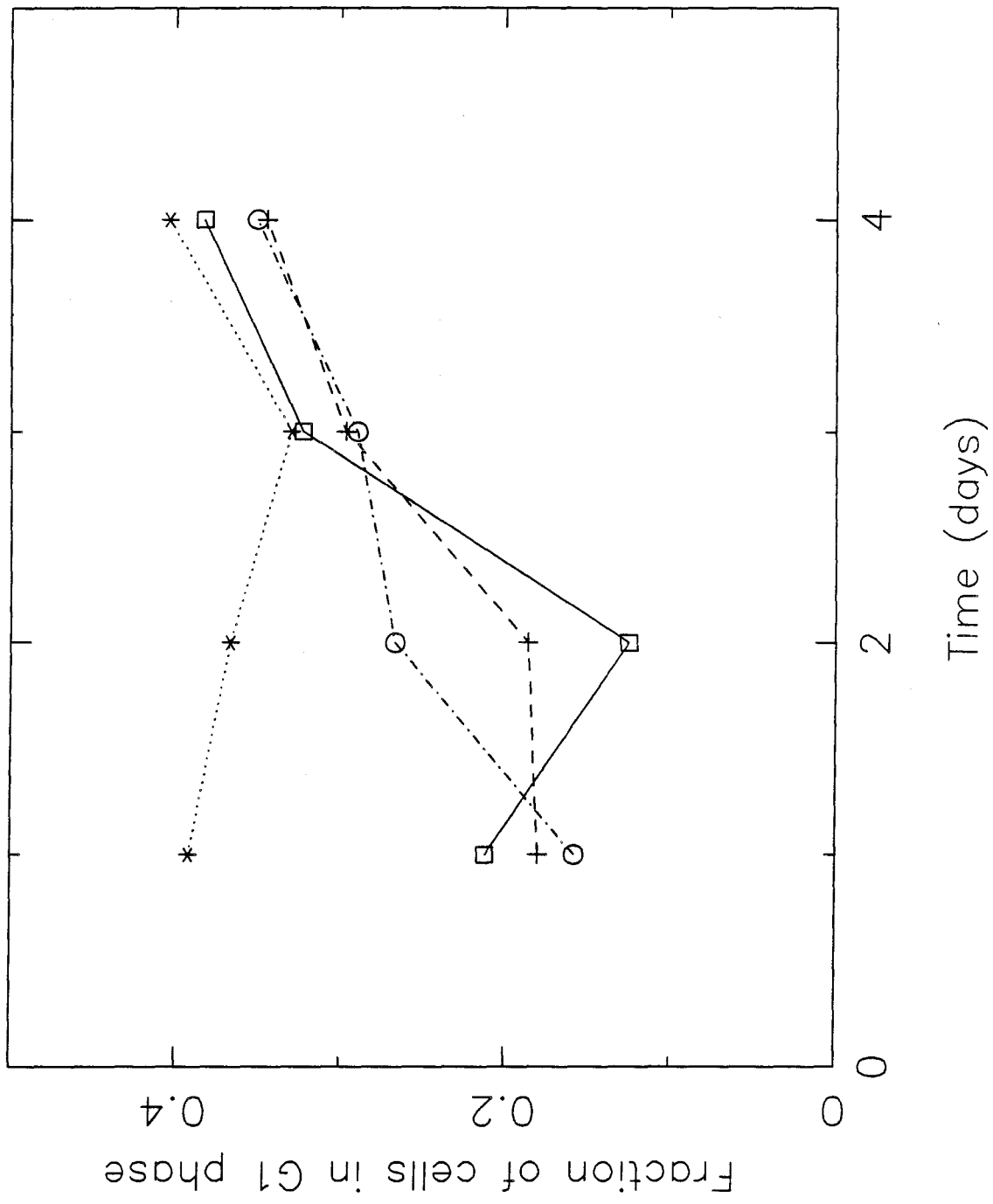

Figure 9

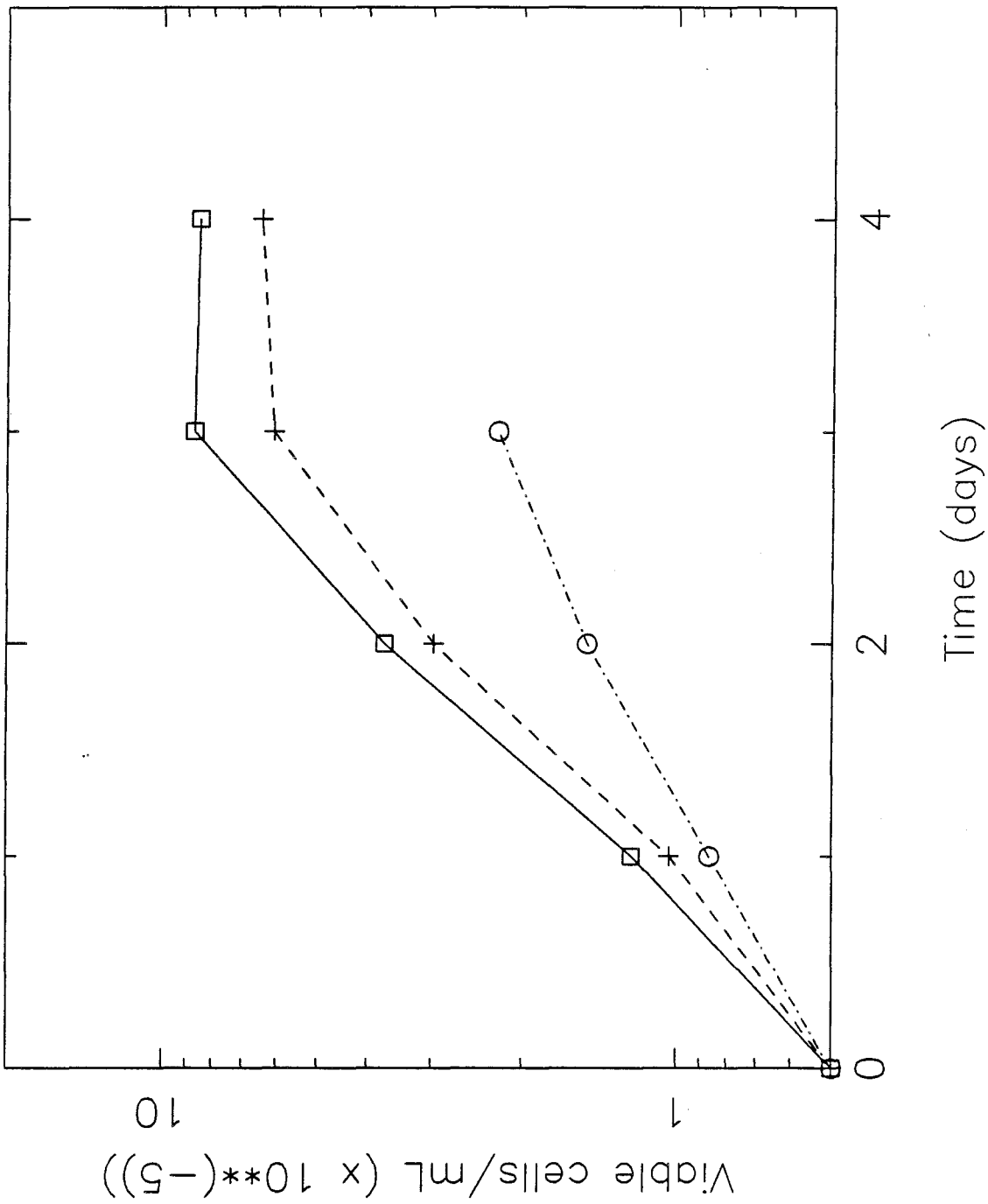

Figure 10A

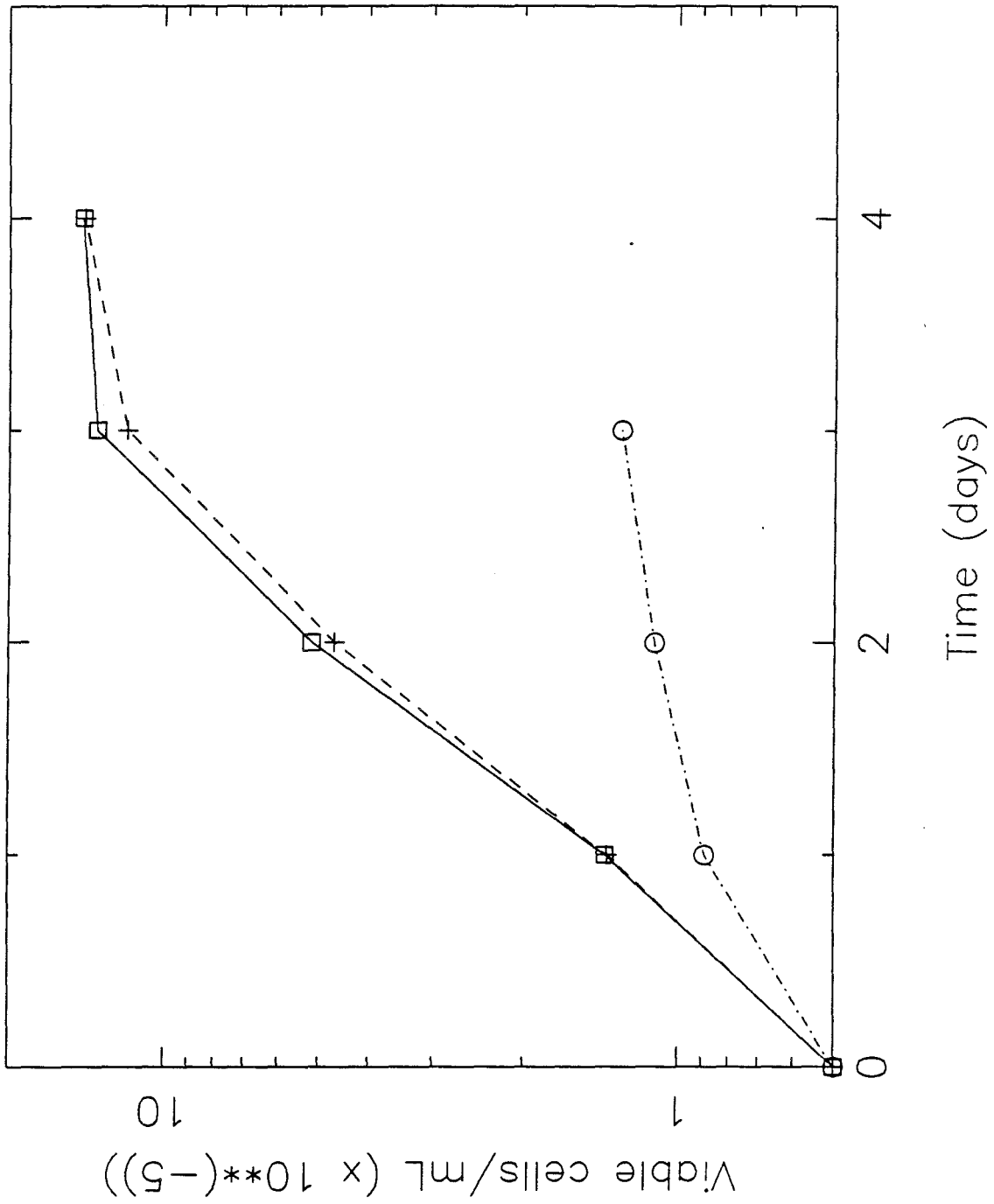

Figure 10B

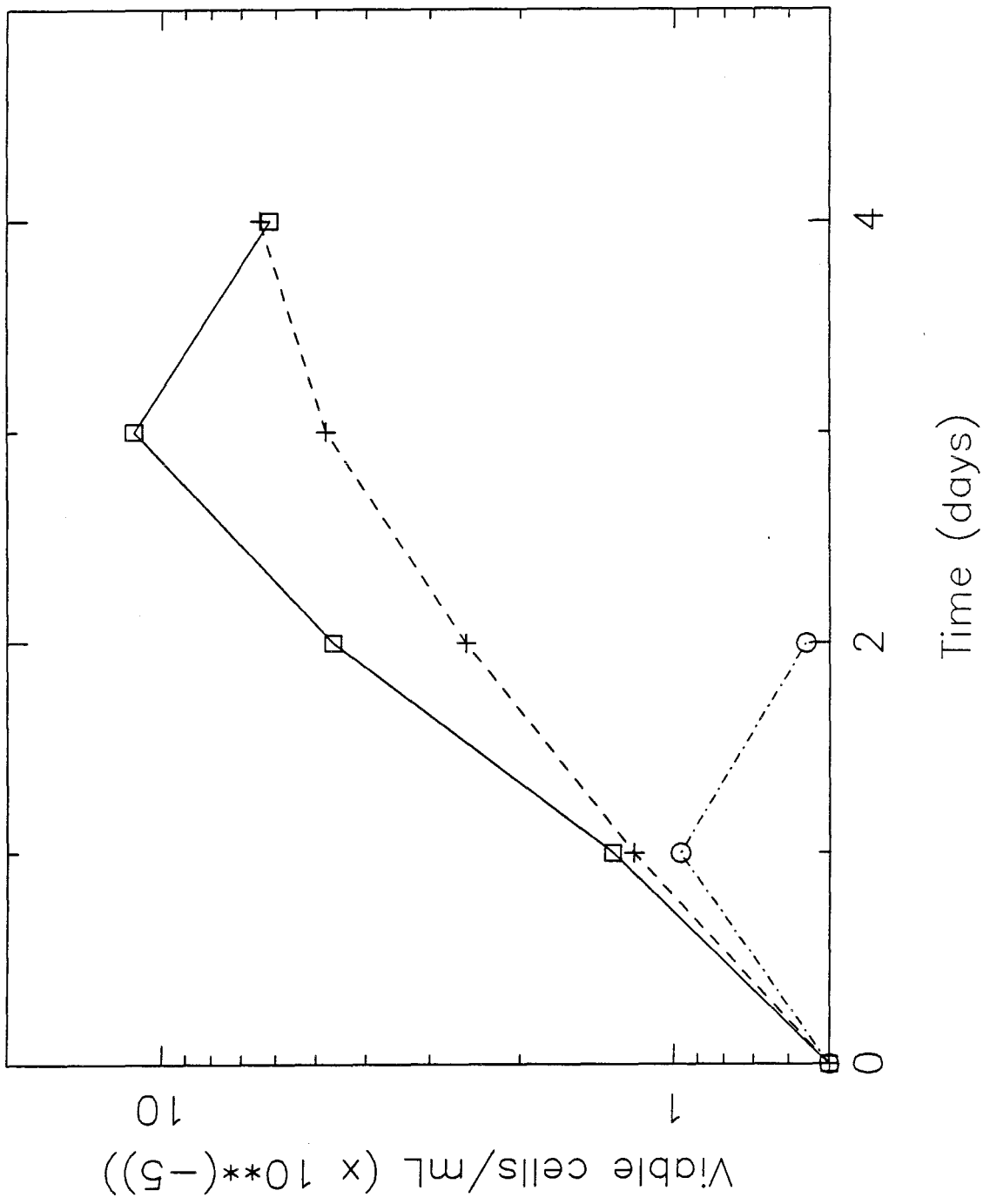

Figure 10C

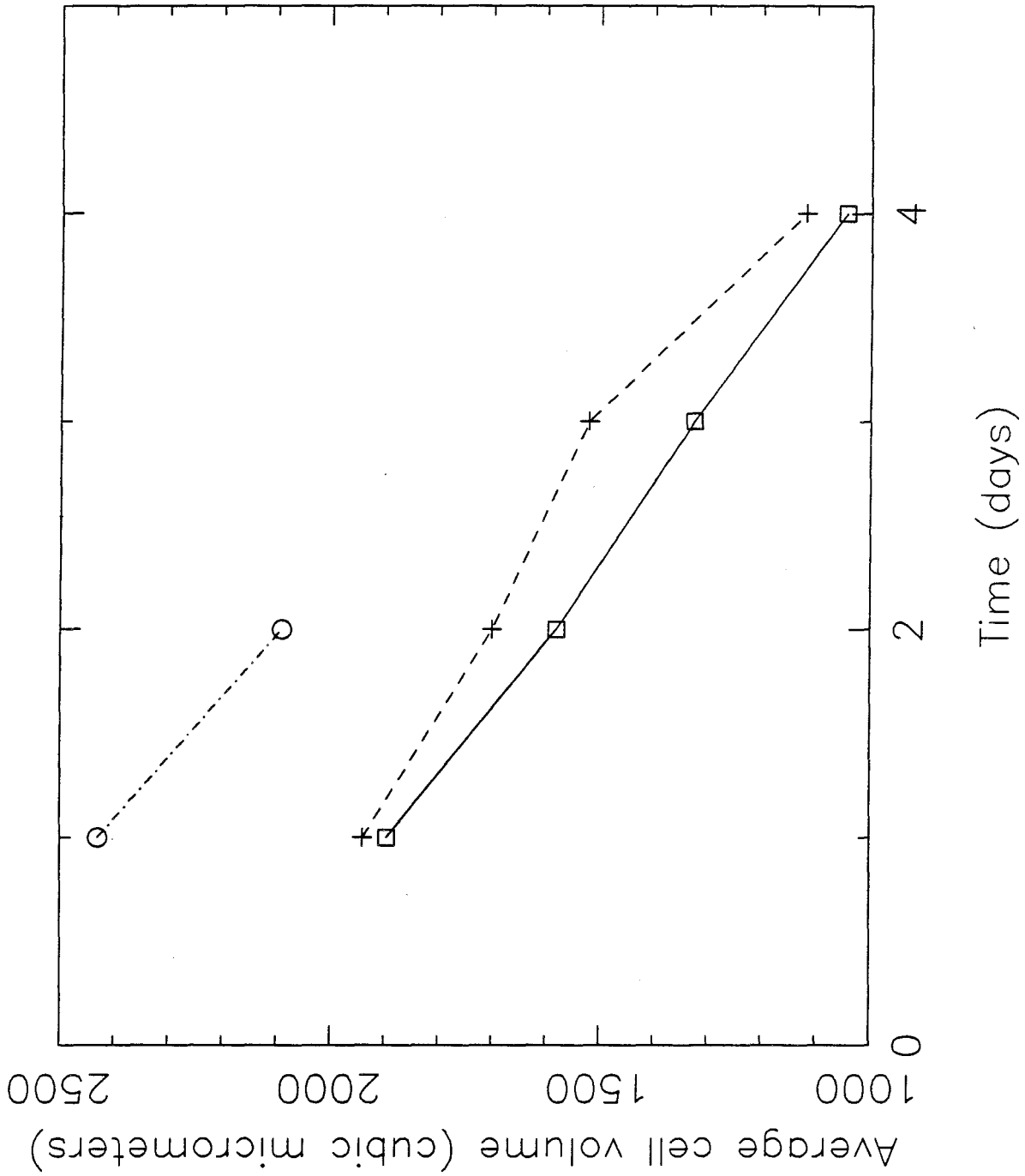
Average cell volume (cubic micrometers)
1000
1500
2000
2500
0
2
4
Time (days)

Figure 11

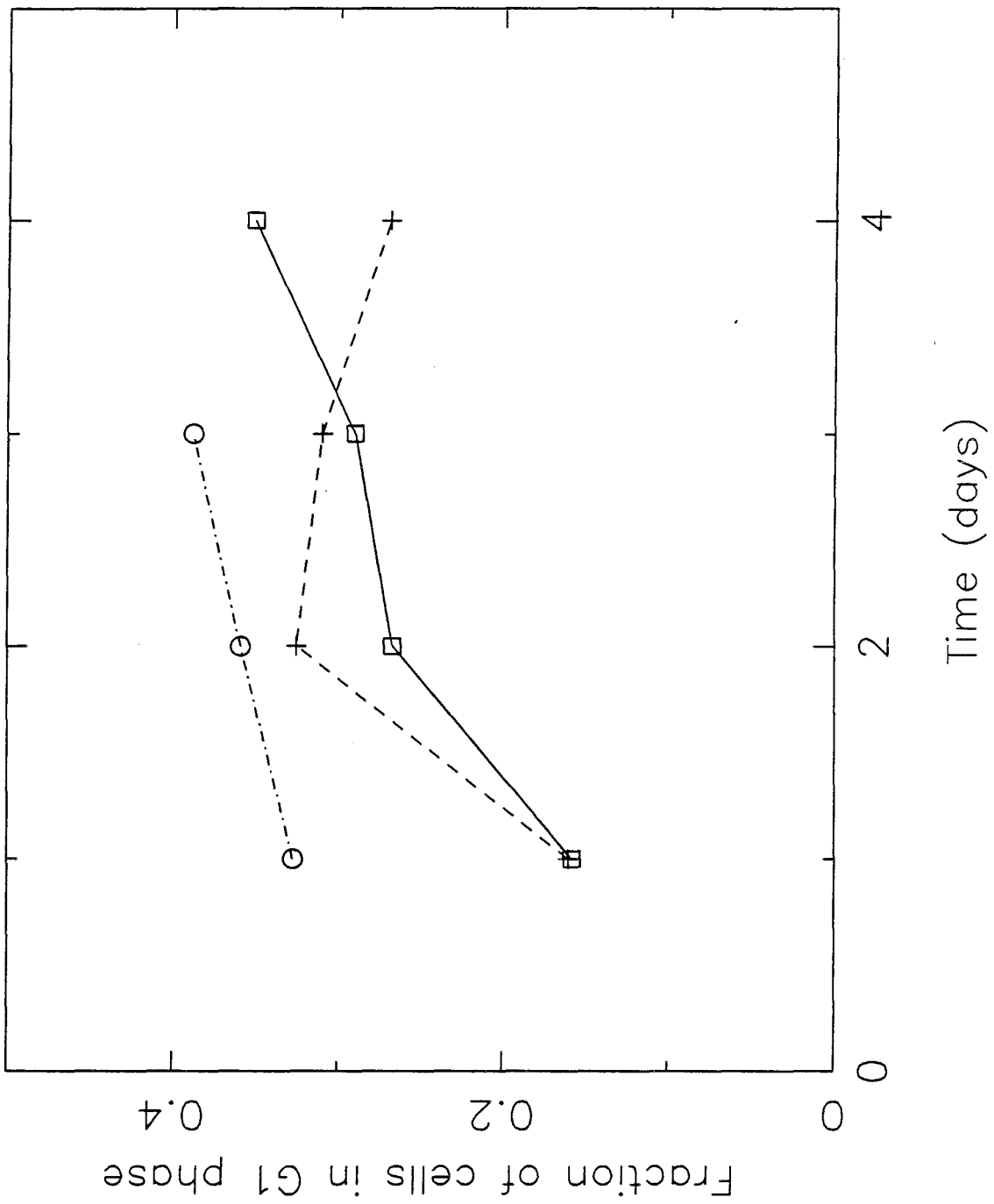

Figure 12A

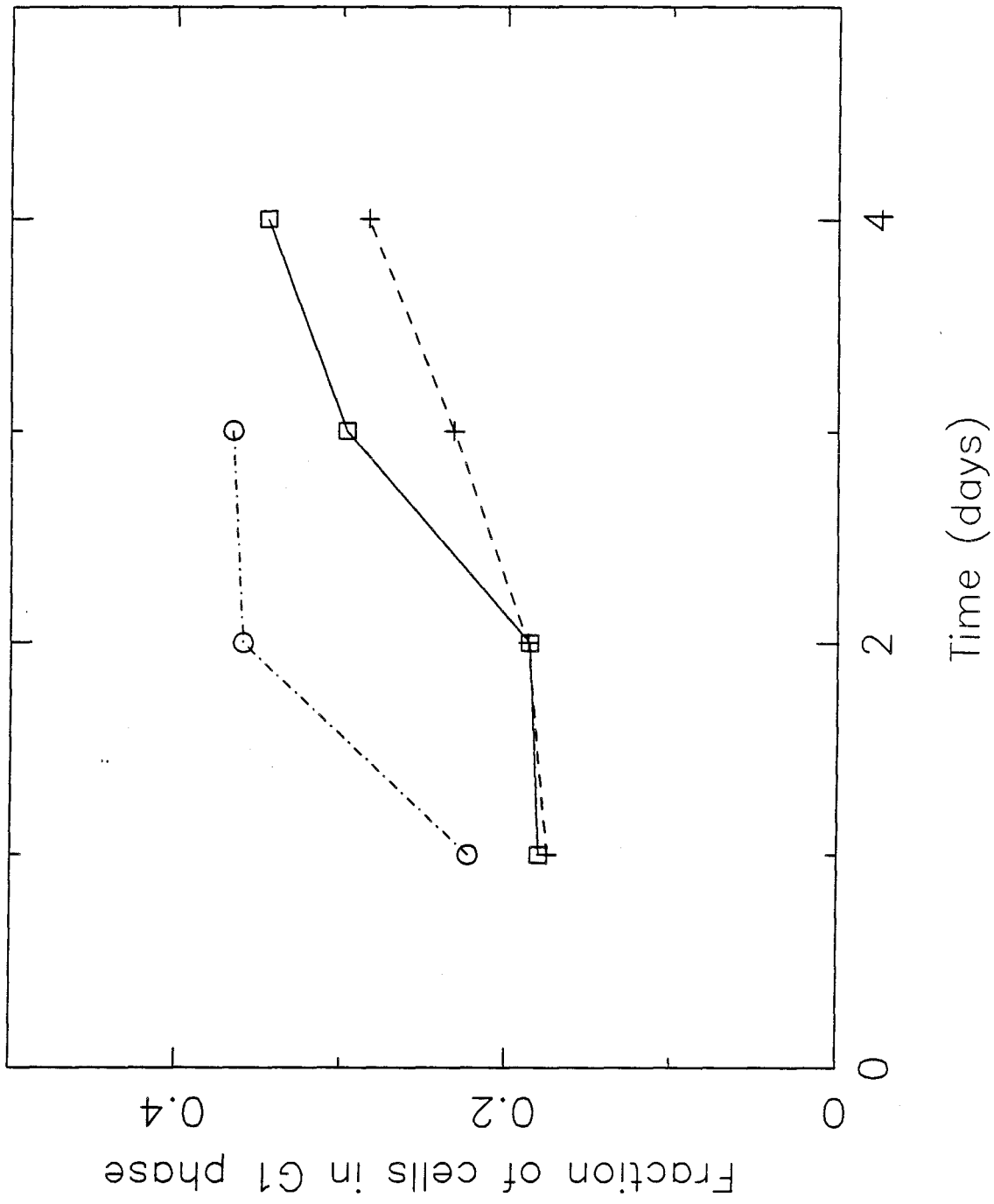

Figure 12B

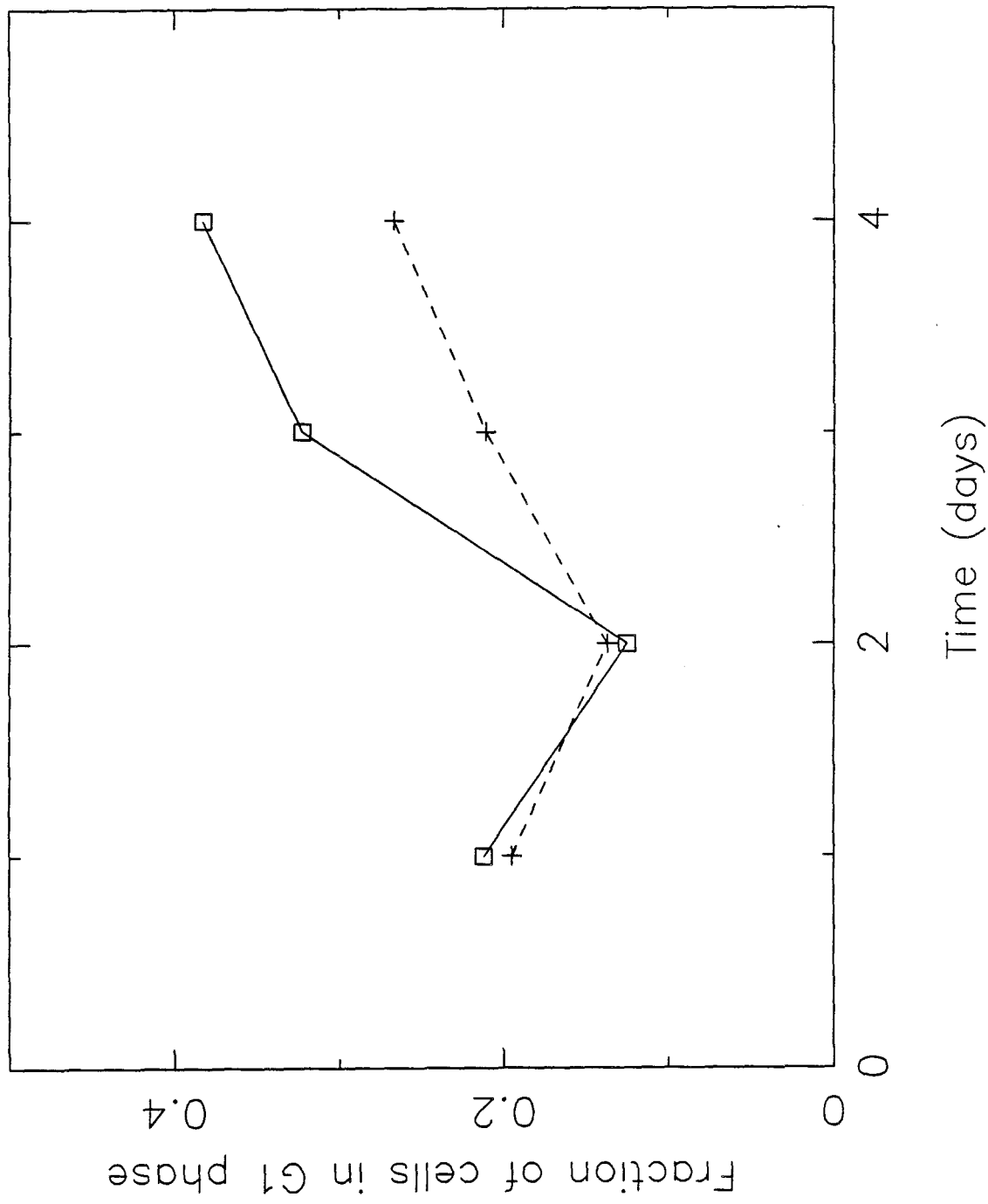

Figure 12C

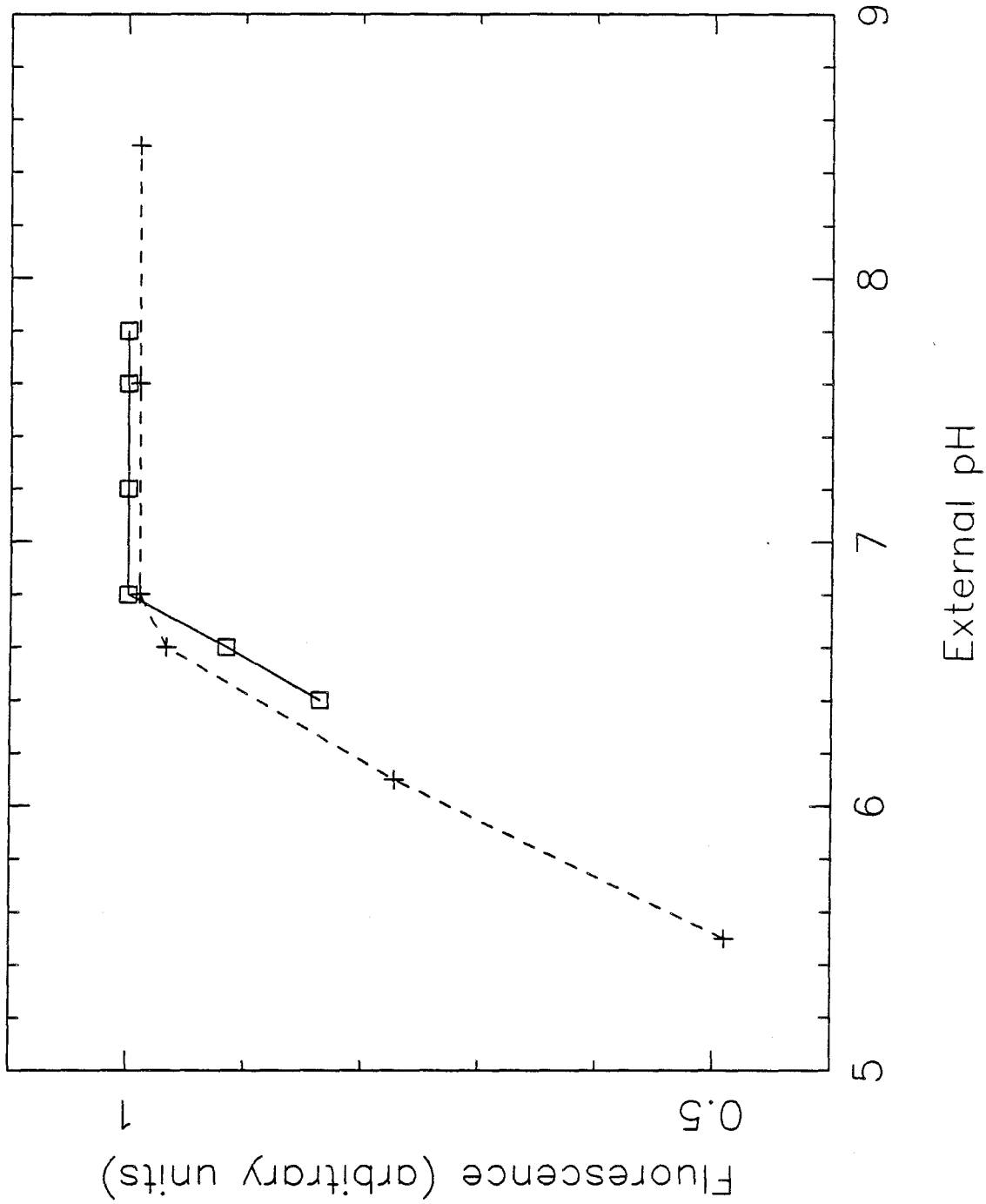

Figure 13

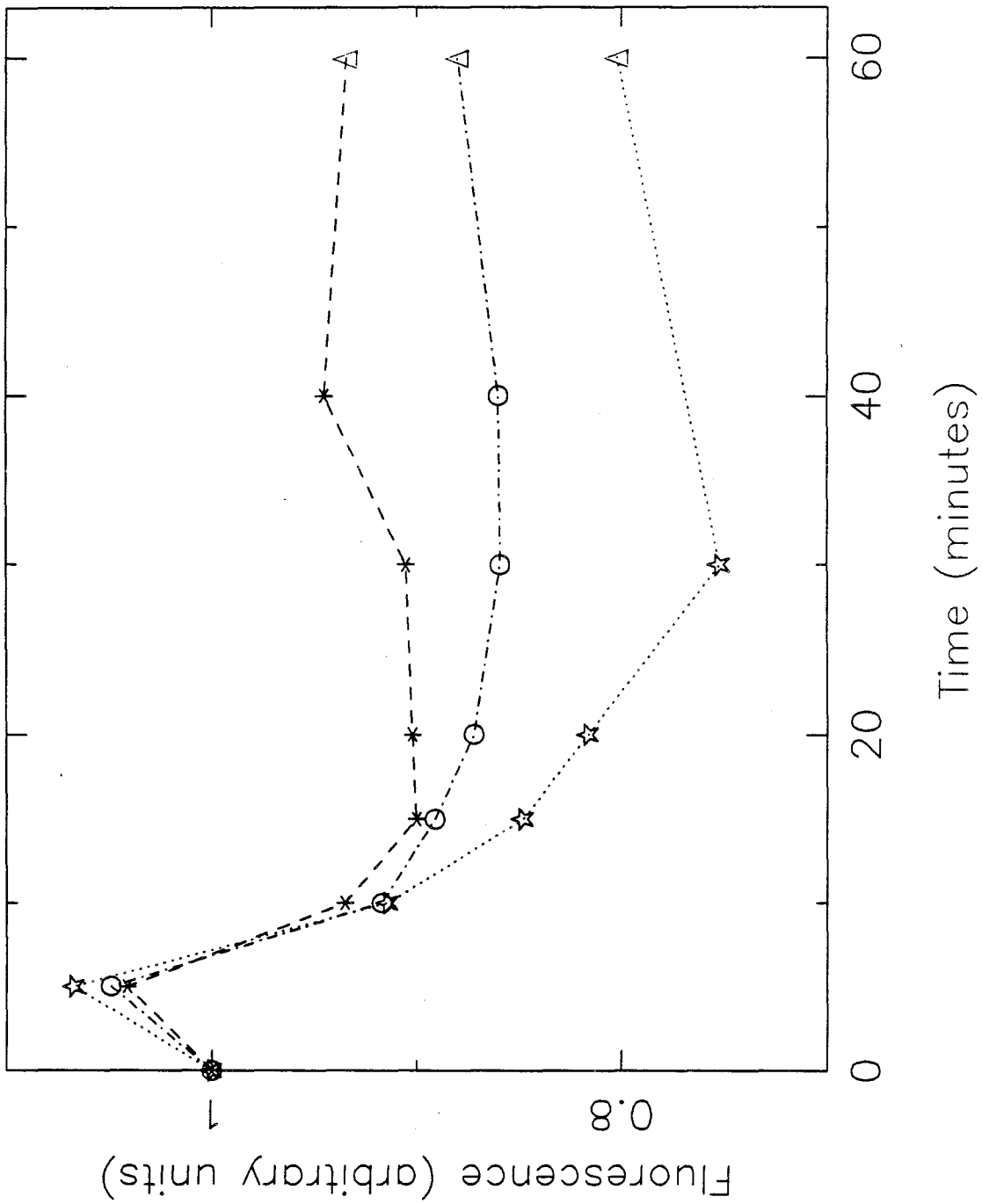

Figure 14

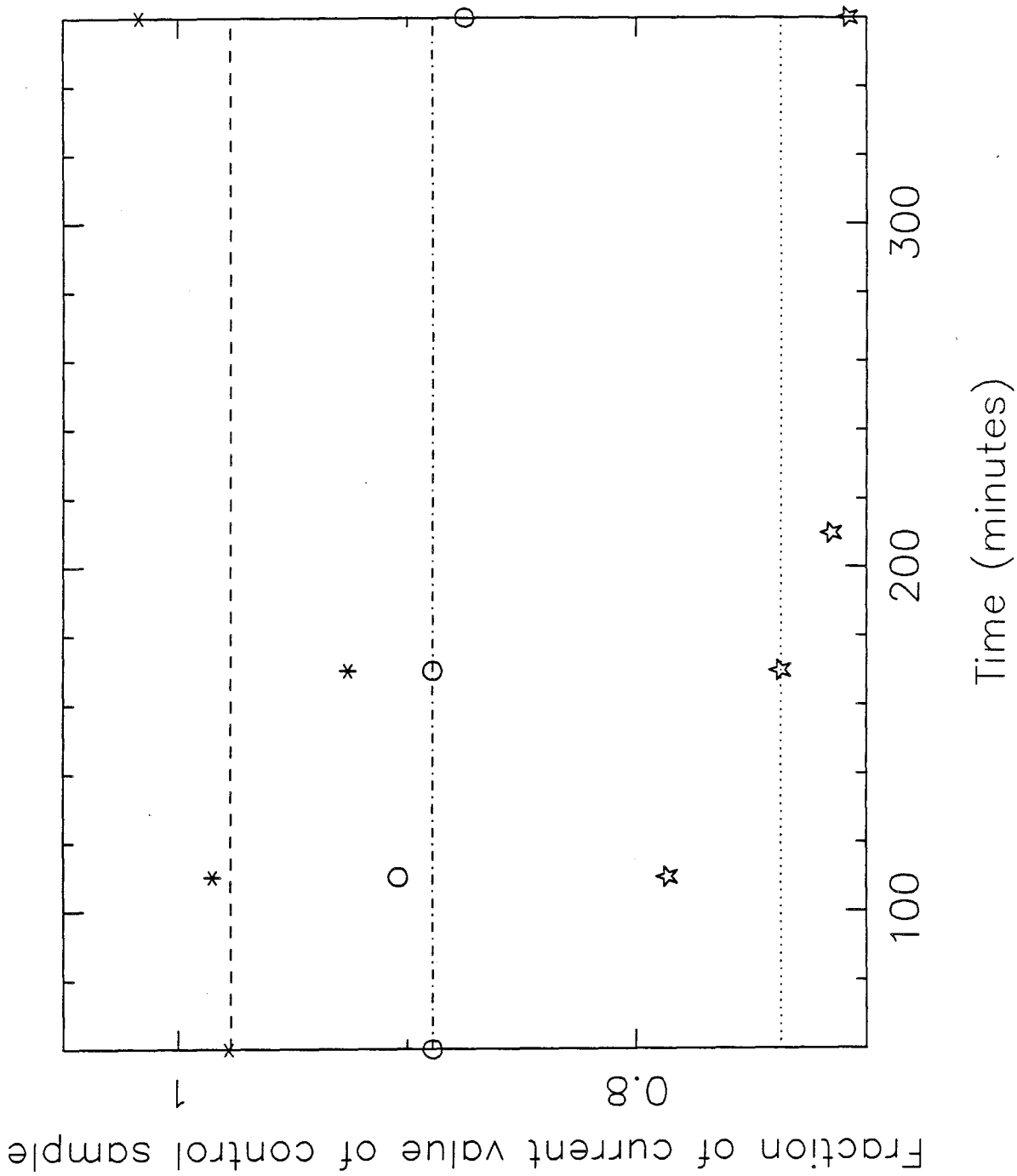
Fraction of current value of control sample
0.8
1
100
200
300
Time (minutes)

Figure 15A

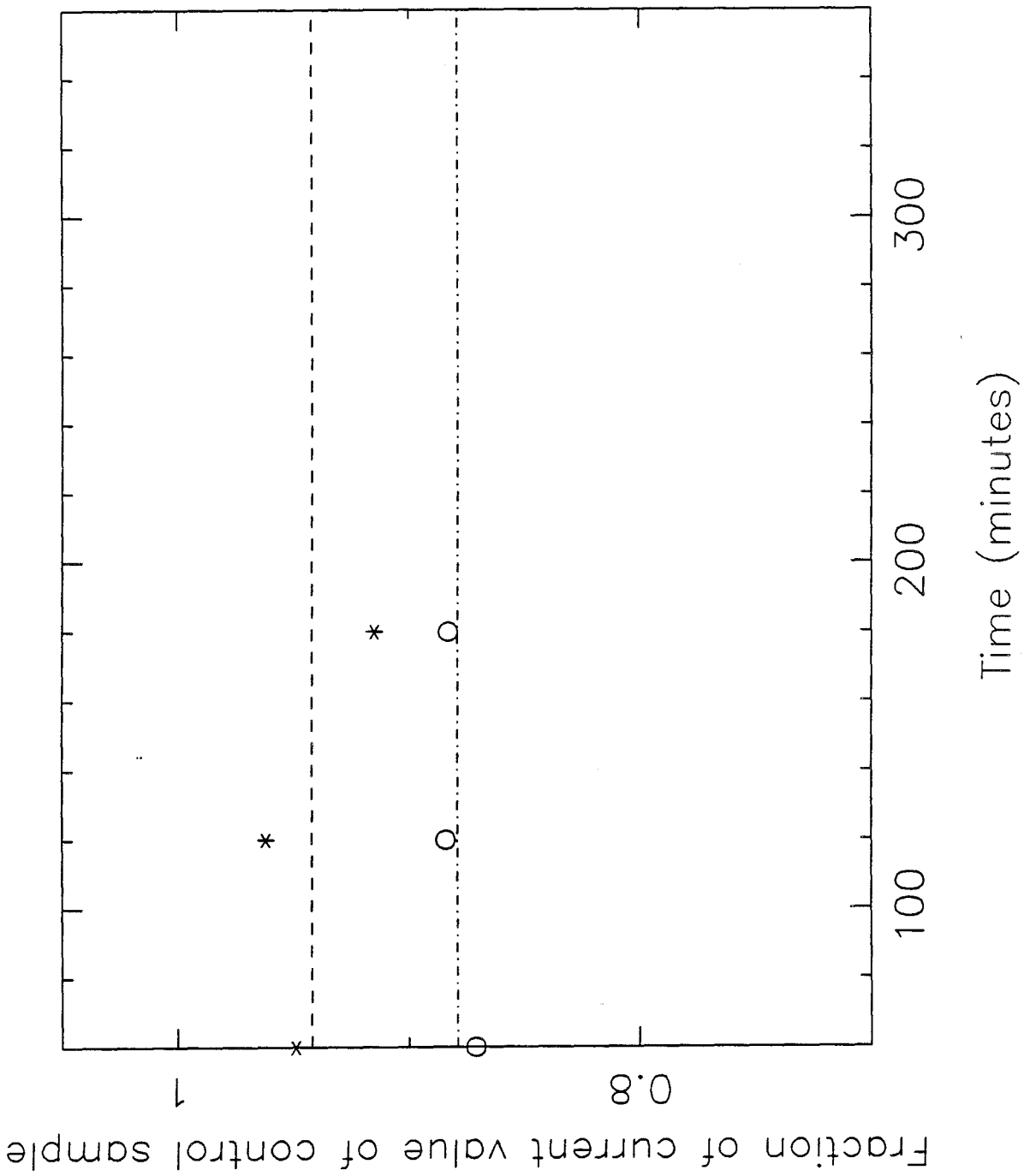
Fraction of current value of control sample
1
0.8
100
200
300
Time (minutes)

Figure 15B

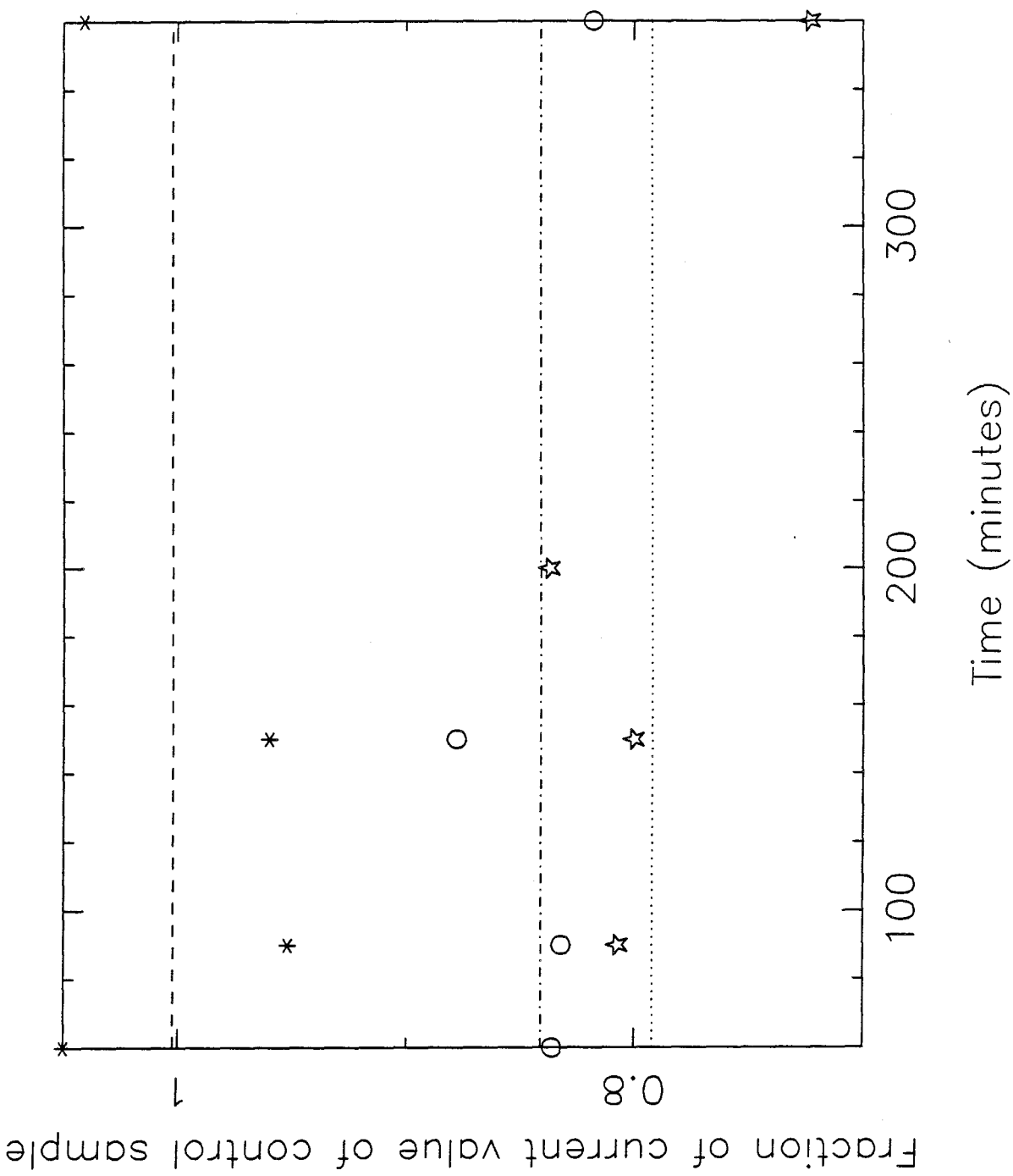
Fraction of current value of control sample
0.8
1
100
200
300
Time (minutes)

Figure 15C

CHAPTER 5.

Effect of Ammonium Ion on Hybridoma Cell Growth, Metabolism and Antibody Production in a Bioreactor

ABSTRACT

The effects of NH_4Cl addition on batch hybridoma cell growth at different external pH values (pH_e) were investigated in a bioreactor at constant pH and dissolved oxygen concentration and compared with previous results obtained in flasks in an incubator. In agreement with measurements in flasks, changes in pH_e over the range 6.8 to 7.6 had minor effects on growth, and 3 mM NH_4Cl had little effect on cell growth while 10 mM NH_4Cl caused a substantial growth inhibition. Measurements of the effects of pH_e and NH_4Cl concentration on cell metabolism gave similar results for cells grown in flasks in an incubator and in the bioreactor. Glucose consumption in batch growth decreases as pH_e decreases and as the NH_4Cl concentration increases. There is a correlation between the effects of different external pH values and NH_4Cl concentrations on glycolysis and growth and previous measurements of their effects on intracellular pH (pH_i). However, the cell yield on glucose (during the lag and exponential phases of growth) increases as pH_e decreases, but decreases as the NH_4Cl concentration increases. At all pH_e values, in the absence of NH_4Cl, the glutamine in the media is depleted at the time the maximum cell density is reached. Both pH_e decreases and NH_4Cl concentration increases lead to decreases in the cell yield on glutamine (during the lag and exponential phases of growth). Changes in pH_e and in the NH_4Cl concentration that cause growth inhibition have no effect on the specific antibody production rate for cells grown in flasks in an incubator or in the bioreactor.

Introduction

Previous work has indicated that ammonium ion is an important inhibitor of mammalian cell growth, including hybridoma cell growth [1-6]. The importance of studying the effects of NH_4^+ on cells results from the fact that glutamine has been found to be essential for mammalian cell growth [7] and the fact that NH_4^+ is a byproduct of glutamine metabolism. There are two possible mechanisms for growth inhibition by NH_4^+, as discussed in a previous paper [8]. The first mechanism involves the uptake of the weak base NH_3 into the lysosomes causing alkalinization [9-14], while the second mechanism involves the uptake of the weak acid NH_4^+ into the cytoplasm causing acidification [15]. Previous work had shown that a 0.2 unit decrease in pH_i is sufficient to inhibit growth [16-20]. The key difference between the first and second mechanisms of growth inhibition by NH_4^+ is that the first mechanism is expected to be pH_e-dependent since the concentration of NH_3, at a given NH_4Cl concentration, decreases as pH_e decreases. The second mechanism, however, should be pH_e-independent since the concentration of NH_4^+, at a given NH_4Cl concentration, is quite insensitive to pH_e in the range 6.8 to 7.6 (pK of NH_4^+ is 9.2). In a previous paper, the effects of NH_4Cl on growth and on pH_i were determined to see if there was any correlation between them. The pH_e dependence of the effects of NH_4Cl on growth and on pH_i was determined in order to evaluate the relative importance of the two possible mechanisms of growth inhibition by NH_4^+. Before looking at the effects of NH_4Cl at different pH_e values, the effects of pH_e alone were determined.

The effects of NH_4Cl on growth at different pH_e values were determined in long-term batch experiments (4 days) in flasks in an incubator at 37°C [8]. The

effects of NH_4Cl on pH_i at different pH_e values were determined in short-term experiments (6 hours or less) at 25°C, using a flow cytometric assay to measure the fluorescence of cells stained with a pH-sensitive indicator. The results of short-term experiments on NH_4Cl effects on pH_i could be compared with the results of long-term experiments on NH_4Cl effects on growth because the pH_i measurements indicated the rapid attainment of a steady-state. A correlation was found between the long-term effects of pH_e on growth at 37°C and the very short-term effects of pH_e on pH_i at 25°C. There was relatively little difference in cell growth at pH_e values 7.6, 7.2 and 6.8, whereas severe growth inhibition was observed at pH_e 6.6. pH_i was found to be constant over the pH_e range 6.8 to 7.6, and there was a 0.2 unit decrease in pH_i at pH_e 6.6. A correlation was also found between the long-term effects of NH_4Cl on growth at 37°C and the short-term effects of NH_4Cl on pH_i at 25°C. 3mM NH_4Cl has little effect on growth and on pH_i (0-0.1 unit decrease), while 10mM NH_4Cl causes a severe growth inhibition and decreases pH_i by 0.2-0.3 units. Previous work has shown that a pH_i decline of this magnitude is sufficient to inhibit growth. The same results are obtained at all three pH_e values tested, 6.8, 7.2 and 7.6, except that the toxicity of 10mM NH_4Cl is greater at pH_e 7.6. 10mM NH_4Cl leads to a substantial increase in the average cell volume at pH_e 7.6 but has little effect on the average cell volume at pH_e values 7.2 and 6.8. These results imply that the lysosomal (first) mechanism of growth inhibition by NH_4^+ is in effect at pH_e 7.6 but not at pH_e values 7.2 and 6.8 where the cytoplasmic (second) mechanism must be invoked to explain the results.

The purpose of this study is to determine the effects of NH_4Cl on hybridoma cell growth at different pH_e levels in a bioreactor with controlled pH and dissolved

oxygen concentration, in order to compare the results with those obtained in experiments in flasks in an incubator. The bioreactor experiments, in which pH is controlled, are necessary to complement the flask experiments due to the large pH_e decreases observed in flasks as a function of time. In addition, bioreactor experiments, in which oxygen supply is increased to meet cell needs such that dissolved oxygen is maintained at a constant value, will enable us to avoid the problem of possible oxygen limitation in flasks, which may compound the effects of other inhibitors of cell growth.

Literature data indicates that decreases in pH_i, such as those measured in the previous paper [8], severely inhibit glycolysis [21,22]. Therefore, it was decided to investigate whether inhibition of glycolysis occured under the conditions described in the previous paper, in which pH_i was depressed and batch growth was inhibited, and whether there was a correlation between glycolysis inhibition and growth inhibition. Previous work by other authors has indicated that cell growth is not dependent on glucose consumption, but that glutamine consumption is also important [23-29]. Therefore, it was decided to measure the effects of pH_e and NH_4Cl on glucose and glutamine consumption as well as the release of their major byproducts, lactate and NH_4^+, in batch growth. Data for cells grown in flasks in an incubator (as described in the previous paper [8]) and in the bioreactor at controlled pH and dissolved oxygen will be included.

The dependence of glycolysis on pH_i has been studied by several authors, as reviewed by Busa [21]. Busa noted that serum stimulates glycolysis in quiescent fibroblast cells and concomitantly causes an increase in the pH_i of these cells due to its activation of the Na^+/H^+ exchanger. Busa suggested that the 0.2 unit de-

crease in pH_i could be responsible for the increased glycolytic rate, based on *in vitro* measurements of the pH-dependence of the enzyme phosphofructokinase (a rate-controlling enzyme in the glycolytic pathway), which showed that a 0.2 unit pH decrease was sufficient to render the enzyme inactive. For the case of insulin stimulation of glycolysis in frog skeletal muscle, Moore [22] had previously established a clear cause-effect relationship between the pH_i increase caused by insulin (approximately 0.2 units) and the increase in glycolytic rate (approximately 50%). First, Moore showed that there was a correlation between the effects of insulin on the exchanger and its effects on glycolysis, namely that both effects were inhibited by amiloride and dependent on the external Na^+ concentration. Second, the glycolytic rate also increased when a 0.2 unit increase in pH_i was produced by a means other than adding insulin (by decreasing the CO_2 concentration from 5% to 2.5%).

To determine the consequences of the inhibition of glycolysis caused by decreases in pH_i on cell growth, cell glutamine consumption must be considered. Previous research on glycolysis and glutaminolysis in cultured cells [23-29] has shown the following: glutamine can substitute for glucose as an energy source in the absence of glucose, implying that cell growth is not dependent on glycolysis. Even in the presence of glucose, cultured cells derive a considerable amount of energy from glutamine. For example, Zielke [23] showed that HDF cells can grow in the absence of glucose provided that nucleotide precursors are supplied, implying that glucose is essential for its anabolic role only. Under these circumstances, the percent of cell energy obtained from glutamine increased from 33 to 98%. Zielke determined that the addition of glucose inhibited glutamine oxidation. Similarly, Scheffler [24] demonstrated that CHO cells normally derive 40% of their energy from glutamine. Reitzer

[25] found that the substitution of fructose for glucose in the media of HeLa cells led to a drastic reduction in the sugar consumption with an increase in the percent of cell energy obtained from glutamine from 65 to 100%. Although this decrease in sugar consumption led to a reduction in the level of glycolytic intermediates, there were no changes in the levels of ATP or of TCA cycle intermediates, indicating that the latter were independent of the rate of sugar consumption. Glacken's 1986 paper [26] confirmed Reitzer's results for FS-4 cells; the substitution of galactose for glucose led to a seven-fold decrease in the sugar consumption and lactate production rates. There was an increase in the oxygen uptake rate of the cells but no change in the glutamine consumption rate. The percent of cell energy derived from respiration increased from 33 to 97%. Miller's work on hybridoma cells [27-29] indicated that, as the glucose concentration increased, the glutamine consumption decreased and vice versa. The ratio of glucose consumption to glutamine consumption was proportional to their concentration in the feed over a wide range of values.

The assumptions that glucose is converted to lactate and that respiration is proportional to glutamine consumption are supported by the following data. Zielke [23] and Scheffler [24] have shown that the rate of glucose oxidation is very low in HDF and CHO cells, respectively. Reitzer [25] found that, in HeLa cells, 80% of glucose is converted to lactate and less than 5% enters the TCA cycle; while 13% of glutamine is converted to lactate, 35% is oxidized to CO_2 and 18-25% is incorporated into macromolecules.

The stoichiometry of NH_4^+ production from glutamine depends on the enzymes used to convert glutamine to glutamate and glutamate to 2-oxoglutarate. Glutaminase is the enzyme most commonly used for the first step, yielding 1 mole NH_4^+

per mole glutamine, but the distribution between the enzymes glutamate dehydrogenase and glutamate aminotransferase in the second step is more variable [7], such that between 1 and 2 moles of NH_4^+ are released per mole of glutamine. Glacken 1986 [26], Miller 1987 [28], and Himes 1988 [30] all determined that the stoichiometry of NH_4^+ production from glutamine remained approximately constant in spite of large changes in the glutamine consumption rate (due to changes in the glutamine concentration) for MDCK cells, hybridoma cells and BHK cells, respectively. The invariable stoichiometric coefficients were 1, 0.5, and 1.55, respectively.

MATERIALS AND METHODS

Cell line

A hybridoma cell line (ATCC TIB 131), which produces monoclonal antibody against all forms of intermediate filaments, was chosen.

Growth assay

The cells were grown in Dulbecco's modified Eagle's basal medium (DMEM), high glucose option (4.5 g/L glucose) (Irvine Scientific, Irvine, California), with 10% defined horse serum (HyClone, Logan, Utah) and antibiotics (100 units penicillin/mL and 50 μg streptomycin/mL) (Irvine Scientific, Irvine, California), in an incubator kept at 37°C and 10%CO_2. To determine the effect of pH_e on growth, the cells were resuspended in the same medium containing different bicarbonate concentrations, to which 20mM buffer were added (20 mL/L from a 1M stock), as described in the previous paper [8]. The pH of the 1M buffer stock solutions was adjusted to give the desired pH when added to the medium at a 20mM concentration. Control experiments were performed to show that variations in the $NaHCO_3$ concentration over the range 4.4mM to 44mM had no effect on cell growth. It was shown that cells grown at the same pH_e but at different bicarbonate concentrations had the same batch growth curves, proving that pH_e not $NaHCO_3$ concentration was the controlling factor. 3 or 10 mM NH_4Cl were added to the flasks as required.

The medium used for cell growth in the bioreactor was the same as that in flask experiments. The bioreactor was a 1L water jacketed model from LH fermentation. The stirring speed was maintained at 80 rpm and gas was supplied to the headspace. The pH and DO were controlled by varying the composition of the inlet gas stream. Nitrogen was fed continuously (to keep the vessel under positive

pressure) at a low rate, leading to the stripping of both oxygen and carbon dioxide from the medium. This was compensated for by intermittent addition of air and CO_2 (solenoid valves were opened), such that the pH and DO remained within a small deviation from their setpoints at all times to prevent excessive evaporation. The total gas flowrate was monitored and manually controlled. No base addition was used to maintain the pH value, which remained constant throughout each batch run except on the last day, at which time the batch run was terminated because the viable cell concentration had begun to decline.

Determination of glucose, lactate, glutamine and NH_4^+ concentrations in the culture supernatants

Glucose, lactate and NH_4^+ concentrations in the culture supernatants were determined by means of enzymatic assays (Sigma kits numbers 510, 826 and 170, respectively), in which the changes in optical density were measured and compared with those of standard solutions using a spectrophotometer. Glutamine was measured by treating the supernatant with glutaminase (Sigma number G8880) in 0.1M sodium acetate buffer at pH 4.9 at 37°C for sufficient time such that the reaction went to completion, releasing 1 mole NH_4^+/mole glutamine (as verified by tests with standard solutions). The NH_4^+ concentration in the treated supernatant was then compared with that in the untreated supernatant, diluted in a similar way, using the above enzymatic assay.

Determination of antibody concentrations in the culture supernatants

The antibody concentration was determined by ELISA as described in a previous paper [31].

RESULTS

Effects on cell growth in the bioreactor

Effects of pH_e

Figure 1 shows the viable cell concentration as a function of time for cells grown in the bioreactor at different pH_e levels, as described in the Materials and Methods. The pH and dissolved oxygen concentration were controlled by means of changes in the relative flowrates of O_2, CO_2, and N_2 in the gas feed to the bioreactor headspace. The cells were grown at different $NaHCO_3$ concentrations as described in the Materials and Methods, after it was found that the excessive gassing of the head space required to obtain a pH_e of 6.8 at 25mM $NaHCO_3$ caused cell death. (Similarly, sparging below the liquid surface was not used, because it inhibited cell growth.) Figure 1 demonstrates that the rate of cell growth does not vary substantially over the pH_e range 6.8 to 7.6 although the maximum cell density is lower at pH_e 6.8.

Effects of NH_4Cl

Figures 2A, 2B, and 2C show the viable cell concentration as a function of time for cells grown in the bioreactor at different NH_4Cl concentrations (as described in the Materials and Methods) for pH_e values 6.8, 7.2, and 7.6 respectively. Figure 2A demonstrates that, at pH_e 6.8, after a 36-hour lag phase, growth at 3mM NH_4Cl is similar to that at 0mM NH_4Cl. Similarly, Figure 2C indicates that, at pH_e 7.6, 3mM NH_4Cl does not greatly alter the maximum cell density attained. However, Figure 2B shows that, at pH_e 7.2, 10mM NH_4Cl severely inhibits growth causing an 85% reduction in the maximum cell density attained. After reaching their maximum

cell density, the cells enter a long stationary phase in which the percent cell viability decreases.

Presentation of data on cell metabolism

The data from batch bioreactor runs and from batch growth in flasks in an incubator are presented in the following way. First, the time trajectories of glucose, lactate, glutamine and NH_4^+ concentrations are plotted. Then, the following parameters are presented in tabular form:

$$\Delta\text{glucose} = \begin{pmatrix}\text{total change in the glucose concentration} \\ \text{during the lag and exponential phases of batch growth}\end{pmatrix}$$

and Δlactate, Δglutamine, and ΔNH_4^+, defined in a similar way, and

$$\Delta\text{cells} = \begin{pmatrix}\text{total increase in the viable cell concentration} \\ \text{during the lag and exponential phases of batch growth}\end{pmatrix}$$

These total changes are confined to the lag and exponential phase of growth because the intention is to see to what extent growth is dependent on glucose and glutamine consumption. During stationary phase, no cell growth occurs. To further illustrate the relationship between growth and glutamine or glucose consumption, the following ratios are tabulated:

$$\frac{\Delta\text{cells}}{\Delta\text{glucose}} = \text{cell yield on glucose}$$

$$= \begin{pmatrix}\text{ratio of the total cells produced to the total glucose consumed} \\ \text{during the lag and exponential phases of batch growth}\end{pmatrix}$$

and Δcells/Δglutamine, defined in a similar way. Finally, an approximate value of the stoichiometry of byproduct production to substrate consumption is obtained from the following ratios:

$$\frac{\Delta\text{lactate}}{\Delta\text{glucose}} = \begin{pmatrix}\text{ratio of the total lactate produced to the total glucose consumed} \\ \text{during the lag and exponential phases of batch growth}\end{pmatrix}$$

and $\Delta NH_4^+/\Delta$glutamine, defined in a similar way.

The data on the effects of pH_e and NH_4Cl on glucose consumption and lactate production is presented in Tables 1 and 2, for cells grown in the bioreactor or in flasks in an incubator, respectively. Table 3 contains the data on the effects of pH_e and NH_4Cl on glutamine consumption and NH_4^+ production for cells grown in the bioreactor.

Effects on glucose consumption and lactate production

Results from batch bioreactor runs are complemented by results from experiments in flasks in an incubator.

Effect of pH_e

In Figures 3 and 4, the glucose and lactate concentrations (in g/L for easier comparison) are presented as a function of time for cells grown at different pH_e values in the bioreactor and in flasks in an incubator, respectively. Tables 1 and 2 indicate that, as pH_e decreases, cell growth, glucose consumption, lactate production and the stoichiometry of lactate production to glucose consumption all decrease. However, the cell yield on glucose increases as pH_e decreases.

Effect of NH_4Cl

The time trajectories of the glucose and lactate concentrations for cells grown at different NH_4Cl concentrations, at pH_e values 6.8, 7.2, and 7.6, are shown in Figures 5A, 5B, and 5C, respectively, for cells grown in the bioreactor and in Figures 6A, 6B, and 6C, respectively, for cells grown in flasks in an incubator. From Tables 1 and 2, the addition of NH_4Cl has the same negative effect on Δcells, Δglucose, and Δlactate as a decrease in pH_e. However, in this case, the cell yield on glucose

decreased. The effects of NH_4Cl on the stoichiometry of lactate production to glucose consumption differ depending on whether cells are grown in the bioreactor or in flasks in an incubator. Table 1 shows that the ratio of the total lactate produced to the total glucose consumed increases as the NH_4Cl concentration increases, while, in Table 2, this parameter decreases as the NH_4Cl concentration increases.

Effects on glutamine consumption and ammonium ion production in the bioreactor

The results for the effects of pH_e and NH_4Cl on glutamine consumption and NH_4^+ production for batch growth of cells in flasks in an incubator were similar to those for batch growth of cells in the bioreactor. Therefore, only data from bioreactor experiments will be included in this section.

Effect of pH_e

Figure 7 illustrates the effects of pH_e on glutamine and NH_4^+ concentrations (in mM for easier comparison) as a function of time for cells grown in the bioreactor at different pH_e values. It is clear from Table 3 that glutamine consumption, NH_4^+ production, and the stoichiometry of NH_4^+ production to glutamine consumption all remain constant as pH_e decreases, even though cell growth decreases. Therefore, the cell yield on glutamine decreases as pH_e decreases.

Effect of NH_4Cl

The time trajectories of the glutamine and NH_4^+ concentrations for cells grown in the bioreactor at different NH_4Cl concentrations are shown in Figures 8A, 8B, and 8C, for pH_e values 6.8, 7.2, and 7.6, respectively. The addition of NH_4Cl leads to a decrease in the glutamine consumption and NH_4^+ production, coinciding with

the decrease in cell growth (Table 3). However, the cell yield on glutamine actually decreases as the NH_4Cl concentration increases, in agreement with the effects of pH_e decreases. As the NH_4Cl concentration increases, the stoichiometry of NH_4^+ production to glutamine consumption decreases.

Effects of pH_e and NH_4Cl on antibody production in the bioreactor

The antibody concentration in the supernatant of the cells was plotted against the integral viable cells, and the specific antibody production rate was obtained from the slope of the best fit straight line to this data, as described in a previous paper [31]. The values of the specific antibody production rate are listed in Table 4. All of the best fit lines had correlation coefficients greater than 0.99 and intercept values close to 0. However, the precision of the ELISA assay was determined to be $^+30\%$, based on plate-to-plate variations. This suggests that the differences in specific antibody production rates in the table are not significant since they are within assay error. Hence, it appears from Table 4 that there are no effects of pH_e or NH_4Cl on the specific antibody production rate.

DISCUSSION

Comparison of the effects on pH_e and NH_4Cl on batch growth in flasks and in the bioreactor

The same critical pH_e (6.6) and critical NH_4Cl concentration (10mM) for severe growth inhibition were found for batch growth in flasks in an incubator and for batch growth in the bioreactor at controlled pH and dissolved oxygen concentration. This implies that oxygen limitation did not influence the results obtained in the flask experiments. The 36-hour lag phase in the bioreactor at pH_e 6.8 in the presence of 3mM NH_4Cl suggests that cells are adapting to the conditions, as observed by Miller for hybridoma cells grown in continuous culture [1]. In a previous paper [8], our results for growth inhibition due to NH_4Cl were compared with those of other authors [1-6]. Briefly, previous work showed that 2-4mM NH_4Cl are required for growth inhibition, while 5-8mM NH_4Cl are required for cell death, depending on the cell line.

Correlation between the effects of pH_e and NH_4Cl on glucose consumption and on cell growth

Previous work on the effects of pH_e and NH_4Cl on glucose consumption include Miller's studies of the effects of these two parameters on hybridoma cells in continuous culture [32,1]. Miller [32] found that a pH_e decrease from 7.2 to 6.8 led to a large decrease in the glucose consumption rate while a pH_e increase from 7.2 to 7.7 led to a substantial increase. The pH_e decrease from 7.2 to 6.8 caused severe growth inhibition and eventual cell death, while the pH_e increase from 7.2 to 7.7 had no effect on cell growth. Table 5 shows the percent glycolysis inhibition (inhibition of

glucose consumption) and percent growth inhibition observed at pH_e values 6.8 and 6.6 relative to values at pH_e 7.2. Clearly, there is a correlation between the effects of pH_e decreases on glycolysis and on growth. In contrast with Miller's results, cell growth continues at pH_e 6.8. In agreement with Miller's results, at pH_e 7.6, glucose consumption is stimulated with no effect on growth.

Miller [1] found that a step change in the NH_4Cl concentration from 3.2 to 8mM had no effect on the steady-state rates of glucose consumption and growth, once the cells had adapted to the new conditions, a process that required 5 days. Table 5 shows the percent glycolysis inhibition and percent growth inhibition upon addition of 3 and 10mM NH_4Cl at pH_e 7.2. Again, the effects of NH_4Cl on glucose consumption and on growth are correlated, since, at pH_e 7.2, 3mM NH_4Cl has little effect on either whereas 10mM NH_4Cl causes a substantial inhibition of both. The addition of 10mM NH_4Cl at pH_e 7.2 inhibits glucose consumption to approximately the same extent as a pH_e decrease from 7.2 to 6.6. However, Table 5 indicates that decreases in pH_e inhibit growth less than they inhibit glycolysis, whereas increases in NH_4Cl concentration inhibit growth more than they inhibit glycolysis. This is also evident in the values for cell yield on glucose in Tables 1 and 2. Whereas this ratio increases when pH_e is decreased, this ratio decreases when the NH_4Cl concentration is increased.

Correlation between the effects of pH_e and NH_4Cl on glycolysis and growth and their effects on pH_i

Measurements of the effects of pH_e and NH_4Cl on pH_i from the previous paper [8] (summarized in the introduction) are included in Table 5 for comparison, because Moore's results [22] showed that pH_i is a controlling factor in glycolytic

rates. Table 5 indicates that there is a correlation between the effects of NH_4Cl on pH_i, as measured in 6-hour experiments (in which pH_i was observed to reach an approximate steady-state value), and the effects of NH_4Cl on glucose consumption. However, in the case of pH_e, the correlation between measured effects on pH_i and on glucose consumption is poorer. This is probably because the measurements of the effects of pH_e on pH_i were very short-term (1 hour or less), and the steady-state value of pH_i as a function of pH_e was not determined. The glycolysis inhibition at pH_e 6.8 (Table 5) suggests that a decrease in pH_e from 7.2 to 6.8 leads to a decrease in pH_i in the long-term, and that the magnitude of this pH_i decrease is likely to be less than 0.2 units, since *in vitro* measurements imply that a pH_i decrease of 0.2 units is sufficient to completely deactivate phosphofructokinase. At pH_e 6.6, glycolysis is completely inhibited suggesting a pH_i decrease of 0.2 units or greater, in agreement with experimental results.

Significance of increases in the stoichiometry of lactate production to glucose consumption

Miller's experiments on the effects of pH_e and NH_4Cl on hybridoma cells in continuous culture [32,1] showed that the stoichiometry of lactate production to glucose consumption did not vary as a function of these two parameters. However, we observed the ratio of the total lactate produced to the total glucose consumed to increase as a function of both pH_e decreases and NH_4Cl concentration increases for cells grown in the bioreactor. (For cells grown in flasks in an incubator, increases in the stoichiometry of lactate production to glucose consumption occur as pH_e is decreased but not as the NH_4Cl concentration is increased.) The reason that decreases in glucose consumption did not result in proportional decreases in lactate

production is that lactate is a product of glutamine metabolism also, as pointed out by Zielke and Reitzer [23,25]. Due to the substitution of glutamine for glucose as an energy source, as will be discussed below, as lactate production from glucose falls off, lactate production from glutamine increases.

Lack of correlation between the effects of pH_e and NH_4Cl on growth and on glutamine consumption

Previous work on the effects of pH_e and NH_4Cl concentration on glutamine consumption and NH_4^+ production include Miller's studies of the effects of these two parameters on hybridoma cells in continuous culture [32,1], and a paper by Glacken on the effects of NH_4Cl concentration of the metabolism of MDCK cells [26]. Miller [32] found that a pH_e decrease from 7.2 to 6.8 stimulated the rate of glutamine consumption on a per cell basis. Similarly, Table 3 indicates that the cell yield on glutamine decreases as pH_e decreases. This result, combined with the increase in the cell yield on glucose as pH_e decreases (seen in Tables 1 and 2), suggests that glutamine is substituted for glucose as an energy source, in agreement with the studies referred to in the introduction [23-29]. This substitution enables cells to continue to grow under conditions where glycolysis is inhibited due to pH_i decreases. The reason that the total glutamine consumed does not increase as pH_e decreases, as observed by Miller, is that, in this case, glutamine is depleted (in batch culture). The point at which glutamine depletion occurs coincides with the time at which the maximum cell concentration is reached at the start of stationary phase implying that glutamine may be limiting cell growth.

Miller's study [1] of the effects of a step change in the NH_4Cl concentration on the steady-state metabolism of hybridoma cells in continuous culture, in which cell

growth was unchanged, and Glacken's study [26] of MDCK cells, an NH_4^+-resistant cell line which showed little effect of NH_4Cl addition on growth, both indicated that increases in the NH_4Cl concentration had no effect on glutamine consumption. Unlike the behavior observed when pH_e is decreased, the addition of NH_4Cl to hybridoma cells in batch culture led to decreases in the total glutamine consumed in the lag and exponential phases of batch culture. Similar to the results obtained when pH_e is decreased, the addition of NH_4Cl caused a decrease in the cell yield on glutamine, implying that glutamine is being used as an energy source when glucose consumption is inhibited. However, since glutamine is not depleted when the cell concentration reaches its maximum value in the presence of NH_4Cl, this means that glutamine cannot be limiting cell growth in this case. Since both the cell yield on glucose and the cell yield on glutamine decrease upon NH_4Cl addition, in contrast to the results of a pH_e decrease (implying that the consumption of both substrates per unit increase in cell concentration increases), this suggests that different mechanisms are involved in growth inhibition by pH_e decrease and by NH_4Cl addition. The first mechanism outlined in the previous paper [8], lysosomal alkalinization, must be involved in growth inhibition by NH_4^+ as well as the second mechanism, cytoplasmic acidification, which is responsible for growth inhibition by pH_e decreases.

Significance of decreases in the stoichiometry of NH_4^+ production to glutamine consumption

Changes in pH_e were found to have no effect on the stoichiometry of NH_4^+ production to glutamine consumption, in agreement with Miller's results [32] for hybridoma cells in continuous culture. At all pH_e values, in the absence of NH_4Cl,

the ratio of NH_4^+ production to glutamine consumption is close to 1, in agreement with Glacken's results for MDCK cells [26]. This implies that the activity of glutamate dehydrogenase is small relative to that of the glutamate aminotransferases. The addition of NH_4Cl led to a decrease in the ratio of the total NH_4^+ produced to the total glutamine consumed, in agreement with Miller's results [1] for hybridoma cells in continuous culture. This implies that there is a decrease in the flux through glutamate dehydrogenase and an increase in the flux through glutamate aminotransferase, probably due to NH_4^+ feedback inhibition of the former enzyme [7]. This switching between pathways from glutamate to 2-oxoglutarate was proposed by Miller [1], and confirmed by measurements of alanine, the product of glutamate aminotransferase. However, Glacken did not observe any change in the stoichiometry of NH_4^+ production to glutamine consumption in his investigation of MDCK cells [26].

Lack of correlation between effects of pH_e and NH_4Cl on growth and on antibody production

Decreases in pH_e and increase in NH_4Cl concentration, which cause substantial growth inhibition, have no effect on the specific antibody production rate. This underlines the fact that antibody production is not growth related. It also implies that neither cytoplasmic acidification nor lysosomal alkalinization inhibit antibody production (secretion).

Acknowlegements: This research was supported by the National Science Foundation. Anne McQueen was supported in part by a Natural Sciences and Engineering Research Council of Canada (NSERC) fellowship.

REFERENCES

1. Miller, W.M., C.R. Wilke, and H.W. Blanch, *Bioprocess Eng.*, **3**, 113 (1988).

2. Glacken, M.W., E. Adema, and A.J. Sinskey, *Biotech. Bioeng.*, **32**, 491 (1988).

3. Thorpe, J.S., A.D. Murdin, P.G. Sanders, and R.E. Spier, presented at it The 194th National Meeting of the American Chemical Society, New Orleans, Louisiana (1987).

4. Reuveny, S., D. Velez, J.D. Macmillan, and L. Miller, *J. Immunol. Methods*, **86**, 53 (1986).

5. Iio, M., A. Moriyama, and H. Murakami, in *Growth and Differentiation of Cells in a Defined Environment*, H. Murakami, I. Yamane, D.W. Barnes, J.P. Mather, I. Hayashi, and G.H. Sato, eds., Springer, p. 437 (1985).

6. Butler, M., and R.E. Spier, *J. Biotechnology*, **1**, 187 (1984).

7. McKeehan, W.L., in *Carbohydrate Metabolism in Cultured Cells*, M. J. Morgan, ed., Plenum Press, p. 111 (1986).

8. McQueen, A., and J.E. Bailey, *Bioprocess Eng.*, in press (1989).

9. Poole, B., and S. Ohkuma, *J. Cell Biol.*, **90**, 665 (1981).

10. Van Leuven, F., J.-J. Cassiman, and H. Van Den Berghe, *Cell*, **20**, 37 (1980).

11. Tietze, C., P. Schlesinger, and P. Stahl, *Biochem. Biophys. Res. Commun.*, **93**, 1 (1980).

12. King, A.C., L. Hernaez-Davis, and P. Cuatrecasas, *PNAS U.S.A.*, **77**, 3283 (1980).

13. King, A.C., L. Hernaez-Davis, and P. Cuatrecasas, *PNAS U.S.A.*, **78**, 717 (1981).

14. Cain, C.C., and R.F. Murphy, *J. Cell Physiol.*, **129**, 65 (1986).

15. Boron, W.F., and P. DeWeer, *J. Gen. Physiol.*, **67**, 91 (1976).

16. Taylor, I.W., and P.J. Hodson, *J. Cell Physiol.*, **121**, 517 (1984).

17. Musgrove, E., M. Seaman, and D. Hedley, *Exp. Cell Res.*, **172**, 65 (1987).

18. L'Allemain, G., S. Paris, and J. Pouyssegur, *J. Biol. Chem.*, **259**, 5809 (1984).

19. Pouyssegur, J., A. Franchi, G. L'Allemain, and S. Paris, *FEBS Lett.*, **190**, 115 (1985).

20. Gerson, D.F., in *Intracellular pH: Its Measurement, Regulation, and Utilization in Cellular Functions*, R. Nuccitelli and D.W. Deamer, eds., Alan R. Liss, p. 375 (1982).

21. Busa, W. B., in $Na^+/H^+ - exchange$, *Intracellular pH, and Cell Function*, P.S. Aronson and W.F. Boron, eds., Academic Press, p. 291 (1986).

22. Moore, R.D., M.L. Fidelman, J.C. Hansen, and J.N. Otis, in *Intracellular pH: Its Measurement, Regulation, and Utilization in Cellular Functions*, R. Nuccitelli and D.W. Deamer, eds., Alan R. Liss, p. 385 (1982).

23. Zielke, H.R., C.M. Sumbilla, C.L. Zielke, J.T. Tildon, and P.T. Ozand, in *Glutamine Metabolism in Mammalian Tissues*, D. Haussinger and H. Sies, eds., Springer, p. 247 (1984).

24. Donnelly, M., and I.E. Scheffler, *J. Cell Physiol.*, **89**, 39 (1976).

25. Reitzer, L.J., B.M. Wice, and D. Kennell, *J. Biol. Chem.*, **254**, 2669 (1979).

26. Glacken, M.W., R.J. Fleischaker, and A.J. Sinskey, *Biotech. Bioeng.*, **28**, 1376 (1986).

27. Miller, W.M., C.R. Wilke, and H.W. Blanch, *Biotech. Bioeng.*, **33**, 477 (1989).

28. Miller, W.M., C.R. Wilke, and H.W. Blanch, *Biotech. Bioeng.*, **33**, 487 (1989).

29. Miller, W.M., C.R. Wilke, and H.W. Blanch, presented at *The 196th National Meeting of the American Chemical Society*, Los Angeles, California (1988).

30. Himes, V.B., and W.-S. Hu, presented at *The 196th National Meeting of the American Chemical Society*, Los Angeles, California (1988).

31. Wittrup, K.D., E. Meilhoc, and J.E. Bailey, *Biotech. Bioeng.*, in press (1988).

32. Miller, W.M., H.W. Blanch, and C.R. Wilke, *Biotech. Bioeng.*, **32**, 947 (1988).

Table 1: Glucose consumption and lactate production as a function of pH_e and NH_4Cl concentration (total changes during the lag and exponential phases of batch bioreactor runs).

pH_e	NH_4Cl conc. mM	Δcells cells/mL $\times 10^{-5}$	Δglucose g/L	Δlactate g/L	Δcells/ Δglucose (cells/mL $\times 10^{-5}$)/ (g/L)	Δlactate/ Δglucose (g/L)/(g/L)
6.8	0	9.37	1.16	1.10	8.08	0.948
6.8	3	5.72	0.79	1.03	7.24	1.30
7.2	0	16.8	3.31	1.90	5.08	0.574
7.2	10	1.79	0.86	1.26	2.08	1.47
7.6	0	18.4	4.02	2.52	4.58	0.627
7.6	3	8.34	3.77	2.87	2.21	0.761

Table 2: Glucose consumption and lactate production as a function of pH_e and NH_4Cl concentration (total changes during the lag and exponential phases of batch growth in flasks in the incubator).

pH_e	NH_4Cl conc. mM	Δcells cells/mL $\times 10^{-5}$	Δglucose g/L	Δlactate g/L	Δcells/ Δglucose (cells/mL $\times 10^{-5}$)/ (g/L)	Δlactate/ Δglucose (g/L)/(g/L)
6.6	0	2.50	0.0	0.305	–	–
6.8	0	7.46	0.68	0.527	11.0	1.47
6.8	3	5.43	0.24	0.913	22.6	3.80
6.8	10	1.37	0.54	0.205	2.54	0.380
7.2	0	12.1	1.17	1.66	10.3	1.42
7.2	3	10.4	1.36	1.46	7.65	1.08
7.2	10	0.40	0.31	0.267	1.29	0.861
7.6	0	10.0	1.94	1.32	5.15	0.681
7.6	3	5.24	2.40	1.32	2.18	0.550

Table 3: Glutamine consumption and ammonium ion production as a function of pH_e and NH_4Cl concentration (total changes during the lag and exponential phases of batch bioreactor runs).

pH_e	NH_4Cl conc. mM	Δcells cells/mL $\times 10^{-5}$	Δglutamine mM	ΔNH_4^+ mM	Δcells/ Δglutamine (cells/mL $\times 10^{-5}$)/ (mM)	ΔNH_4^+/ Δglutamine (mM)/(mM)
6.8	0	9.37	4.38	4.94	2.14	1.13
6.8	3	5.72	2.68	2.07	2.13	0.772
7.2	0	16.8	3.84	4.79	4.38	1.25
7.2	10	1.79	2.03	1.38	0.882	0.680
7.6	0	18.4	3.85	4.18	4.78	1.06
7.6	3	8.34	3.84	3.63	2.17	0.896

Table 4: Specific antibody production rates as a function of pH_e and NH_4Cl for cells grown in the bioreactor ($\mu g/10^6$ cells/day).

	mM NH_4Cl		
pH_e	0	3	10
6.8	3.24	2.54	–
7.2	3.22	–	3.10
7.6	2.28	3.34	–

Table 5: Correlation between the effects of pH_e and NH_4Cl on glycolysis and growth, for cells grown in the bioreactor (B) or in flasks in an incubator (F), and their effects on pH_i.

pH_e	NH_4Cl conc. mM	ΔpH_i measured	Experiment type	Percent glycolysis inhibition	Percent growth inhibition
7.2	0	0.0	B	0	0
			F	0	0
6.8	0	0.0	B	65	44
			F	42	38
6.6	0	-0.2	F	100	79
7.2	3	-0-0.1	F	-16	14
7.2	10	-0.2-0.3	B	74	89
			F	74	97

Figure 1: Effect of pH_e on cell growth in the bioreactor

The concentration of viable cells is plotted as a function of time for cells grown in the bioreactor (as described in the Materials and Methods) at pH_e values 7.6 (solid line), 7.2 (dashed line), or 6.8 (dot-dashed line).

Figure 2: Effect of NH_4Cl on cell growth in the bioreactor

The concentration of viable cells is plotted as a function of time for cells grown in the bioreactor (as described in the Materials and Methods), in the presence of 0 mM (solid lines), 3 mM (dashed lines) or 10 mM (dot-dashed lines) NH_4Cl, at pH_e values 6.8 (Fig. 2A), 7.2 (Fig. 2B), and 7.6 (Fig. 2C).

Figure 3: Effect of pH_e on glucose consumption and lactate production for cells grown in the bioreactor

The glucose and lactate concentrations (measured as described in the Materials and Methods) are plotted as a function of time for cells grown in the bioreactor (as shown in Fig. 1), at pH_e values 7.6 (solid line), 7.2 (dashed line), or 6.8 (dot-dashed line).

Figure 4: Effect of pH_e on glucose consumption and lactate production for cells grown in flasks in an incubator

The glucose and lactate concentrations (measured as described in the Materials and Methods) are plotted as a function of time for cells grown in flasks in an incubator (as shown in a previous paper [8]) at pH_e values 7.6 (solid line), 7.2 (dashed line), or 6.8 (dot-dashed line).

Figure 5: Effect of NH_4Cl on glucose consumption and lactate production for cells grown in the bioreactor

The glucose and lactate concentrations (measured as described in the Materials and Methods) are plotted as a function of time for cells grown in the bioreactor (as shown in Fig. 2) in the presence of 0 mM (solid lines), 3 mM (dashed lines) or 10 mM (dot-dashed lines) NH_4Cl, at pH_e values 6.8 (Fig. 5A), 7.2 (Fig. 5B), and 7.6 (Fig. 5C).

Figure 6: Effect of NH_4Cl on glucose consumption and lactate production for cells grown in flasks in an incubator

The glucose and lactate concentrations (measured as described in the Materials and Methods) are plotted as a function of time for cells grown in flasks in an incubator (as shown in a previous paper [8]) in the presence of 0 mM (solid lines), 3 mM (dashed lines) or 10 mM (dot-dashed lines) NH_4Cl, at pH_e values 6.8 (Fig. 6A), 7.2 (Fig. 6B), and 7.6 (Fig. 6C).

Figure 7: Effect of pH_e on glutamine consumption and NH_4^+ production for cells grown in the bioreactor

The glutamine and NH_4^+ concentrations (measured as described in the Materials and Methods) are plotted as a function of time for cells grown in the bioreactor (as shown in Figure 1) at pH_e values 7.6 (solid line), 7.2 (dashed line), or 6.8 (dot-dashed line).

Figure 8: Effect of NH_4Cl on glutamine consumption and NH_4^+ production for cells grown in the bioreactor

The glutamine and NH_4^+ concentrations (measured as described in the Materials and Methods) are plotted as a function of time for cells grown in the bioreactor (as shown in Figure 2) in the presence of 0 mM (solid lines), 3 mM (dashed lines), or 10 mM (dot-dashed lines) NH_4Cl, at pH_e values 6.8 (Fig. 8A), 7.2 (Fig. 8B), or 7.6 (Fig. 8C).

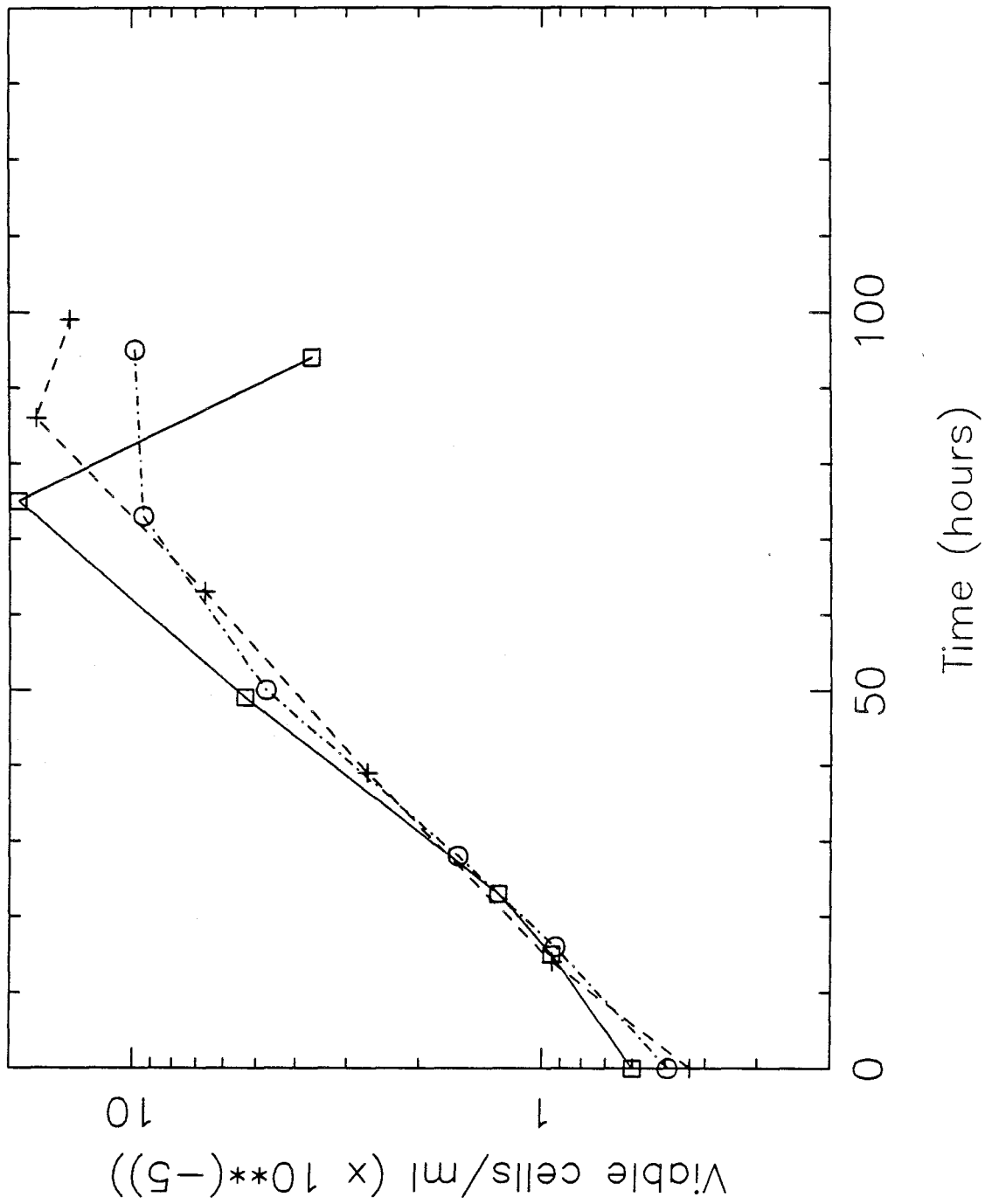

Figure 1

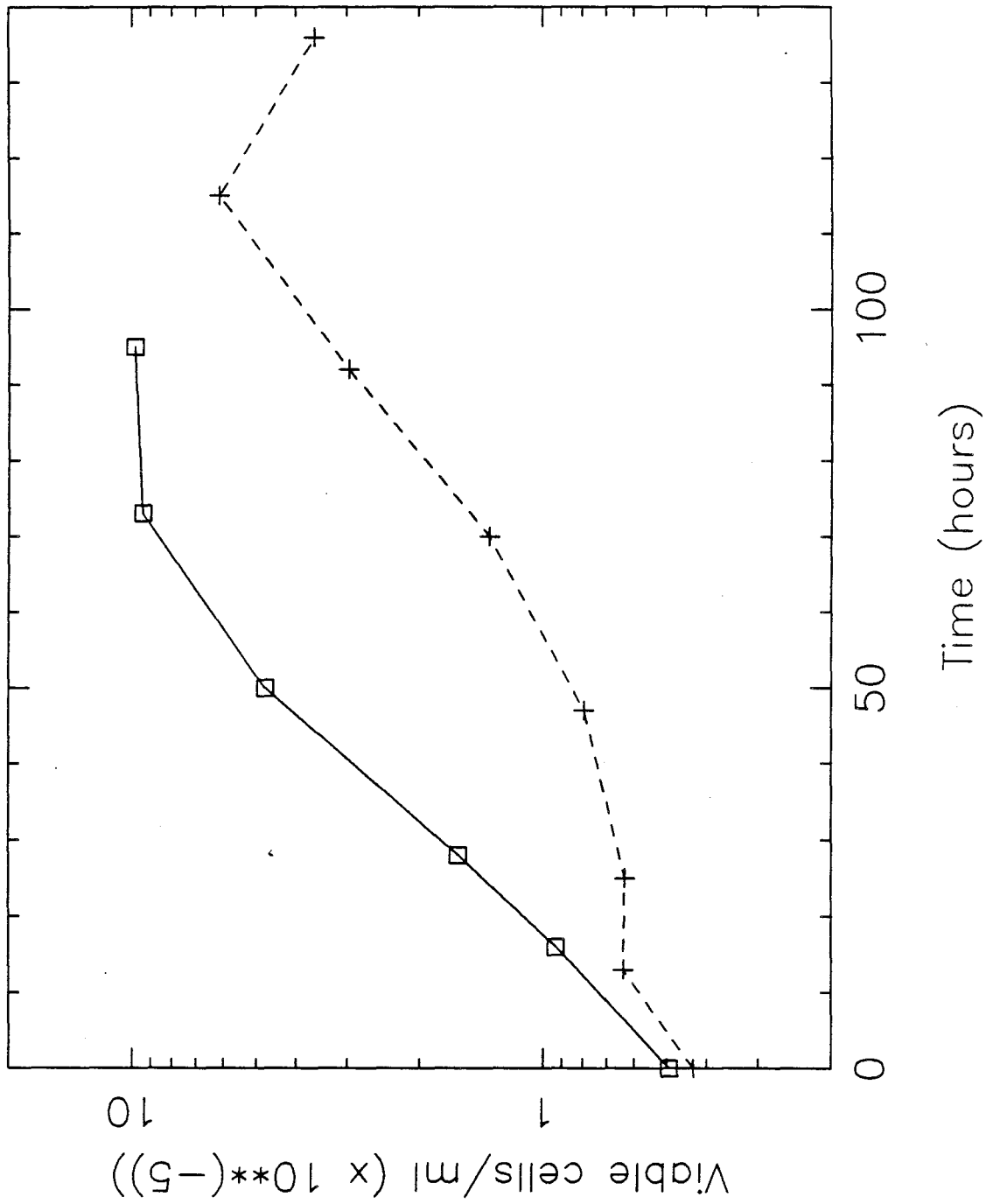

Figure 2A

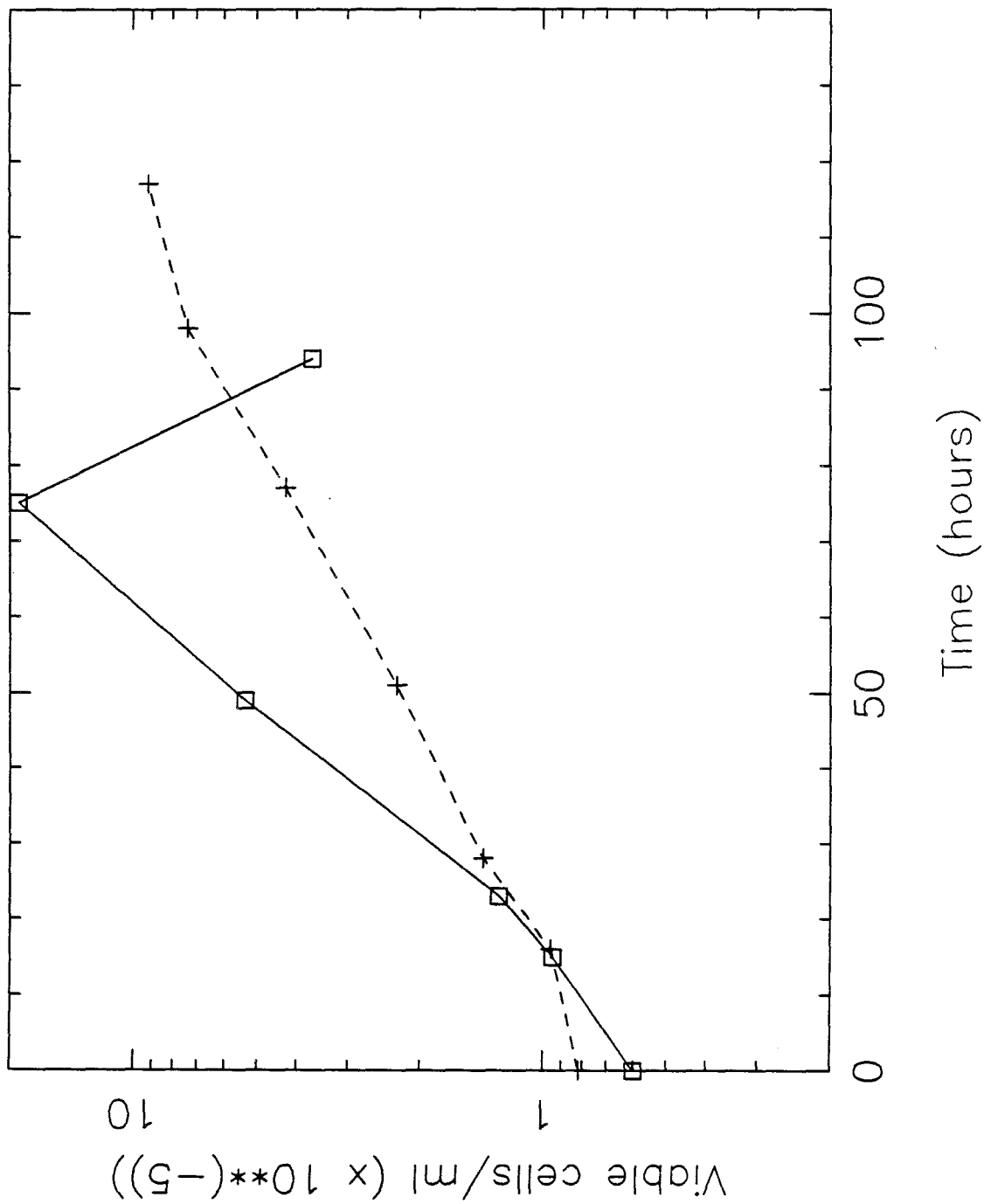

Figure 2B

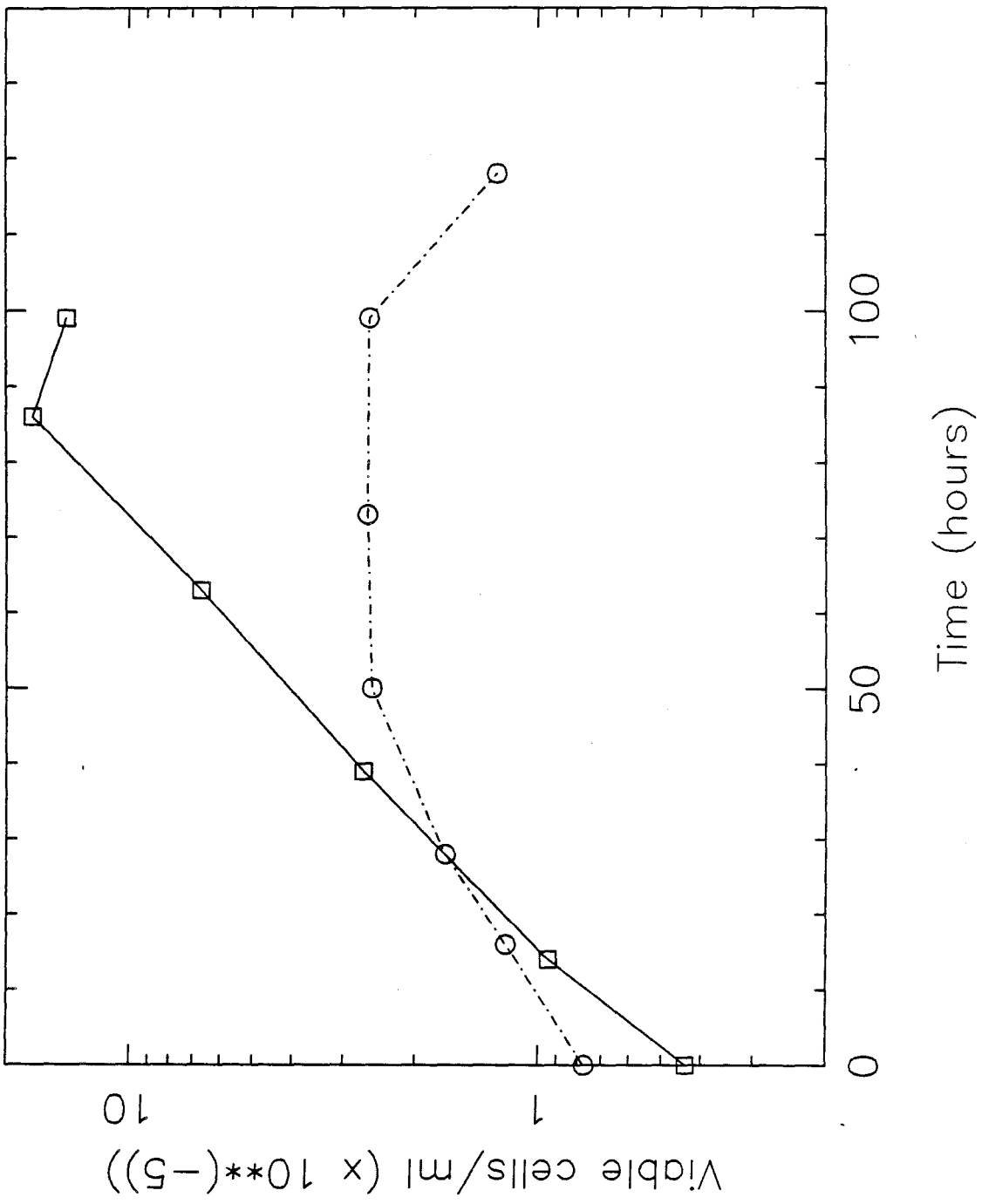

Figure 2C

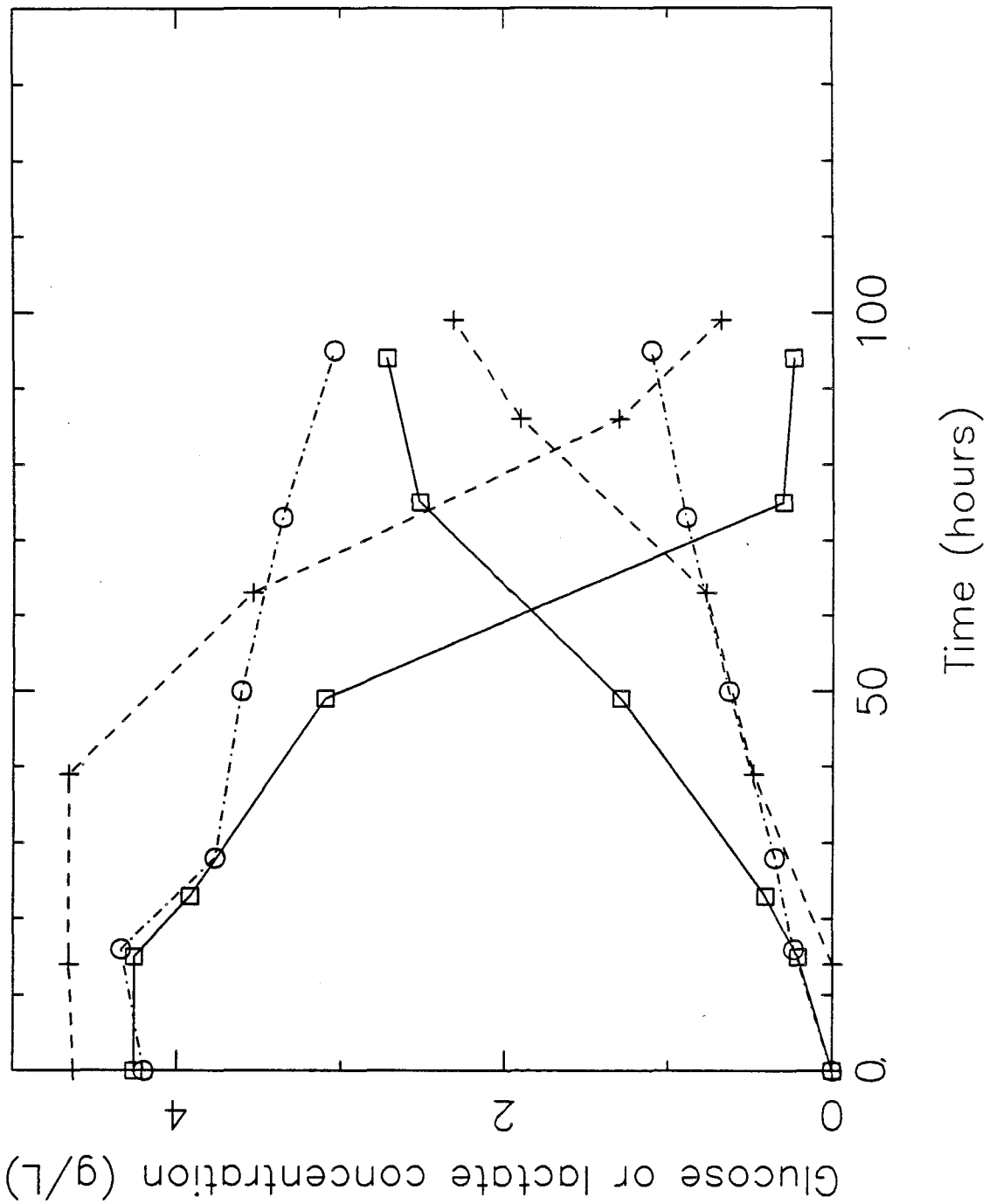

Figure 3

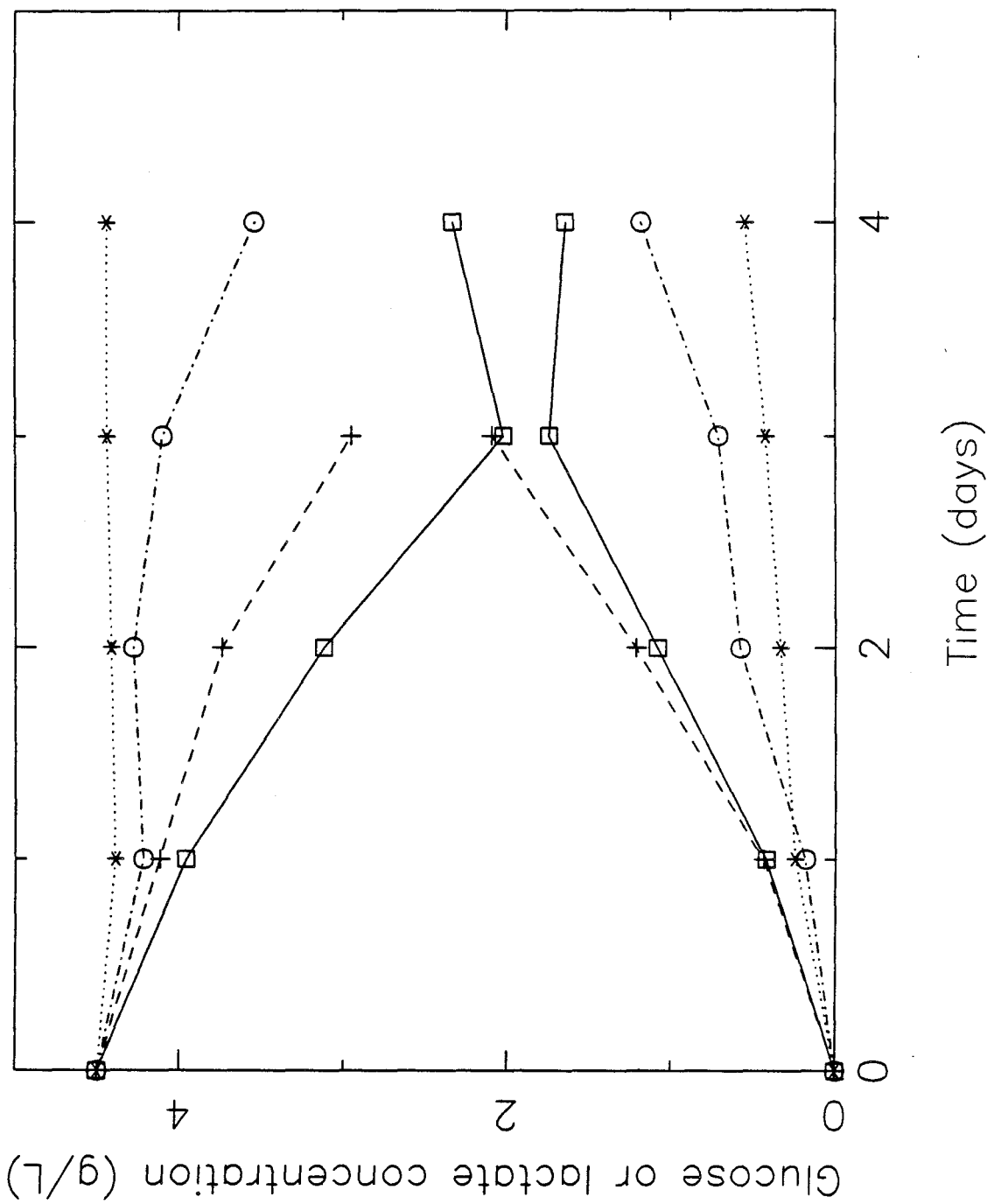

Figure 4

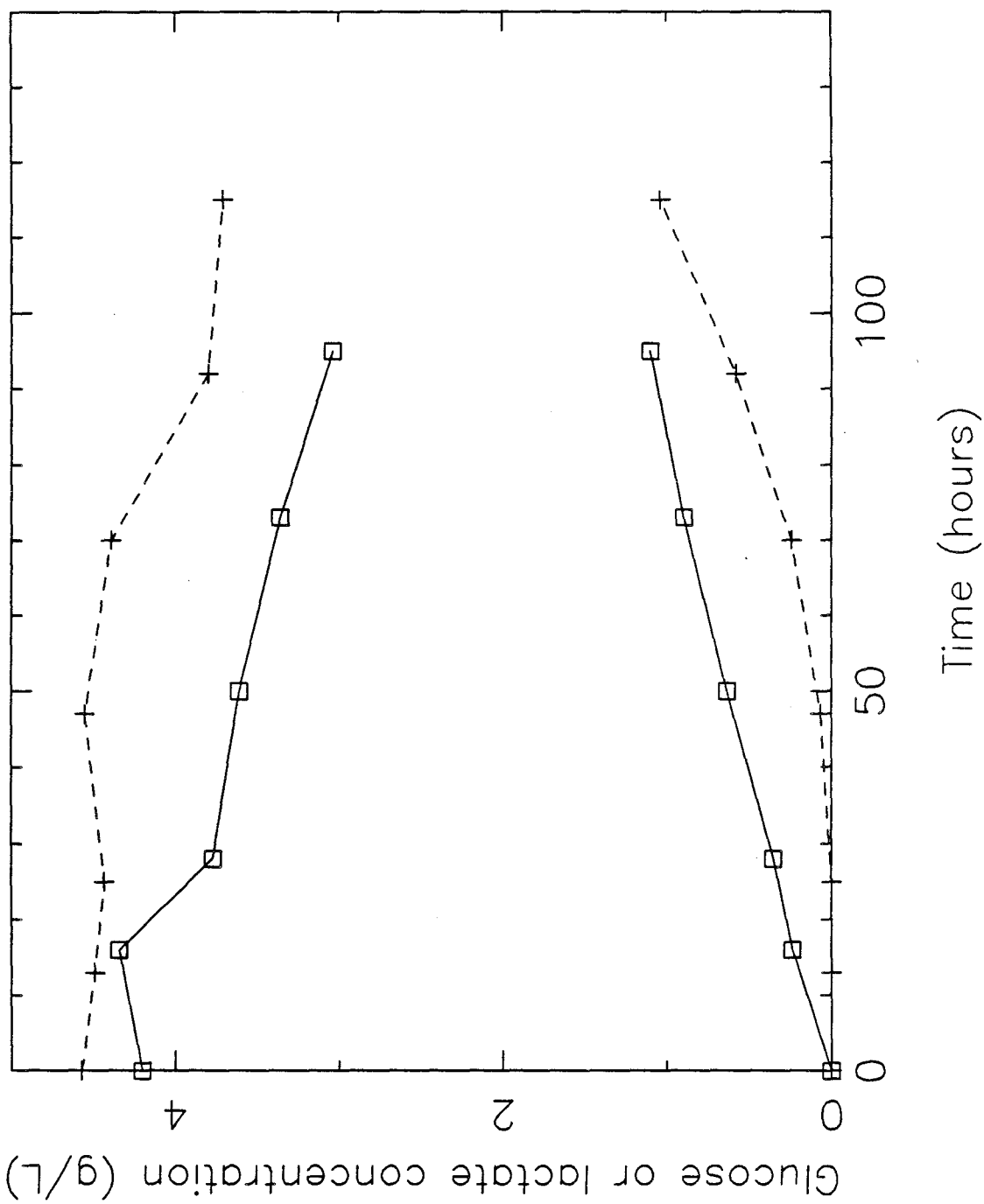

Figure 5A

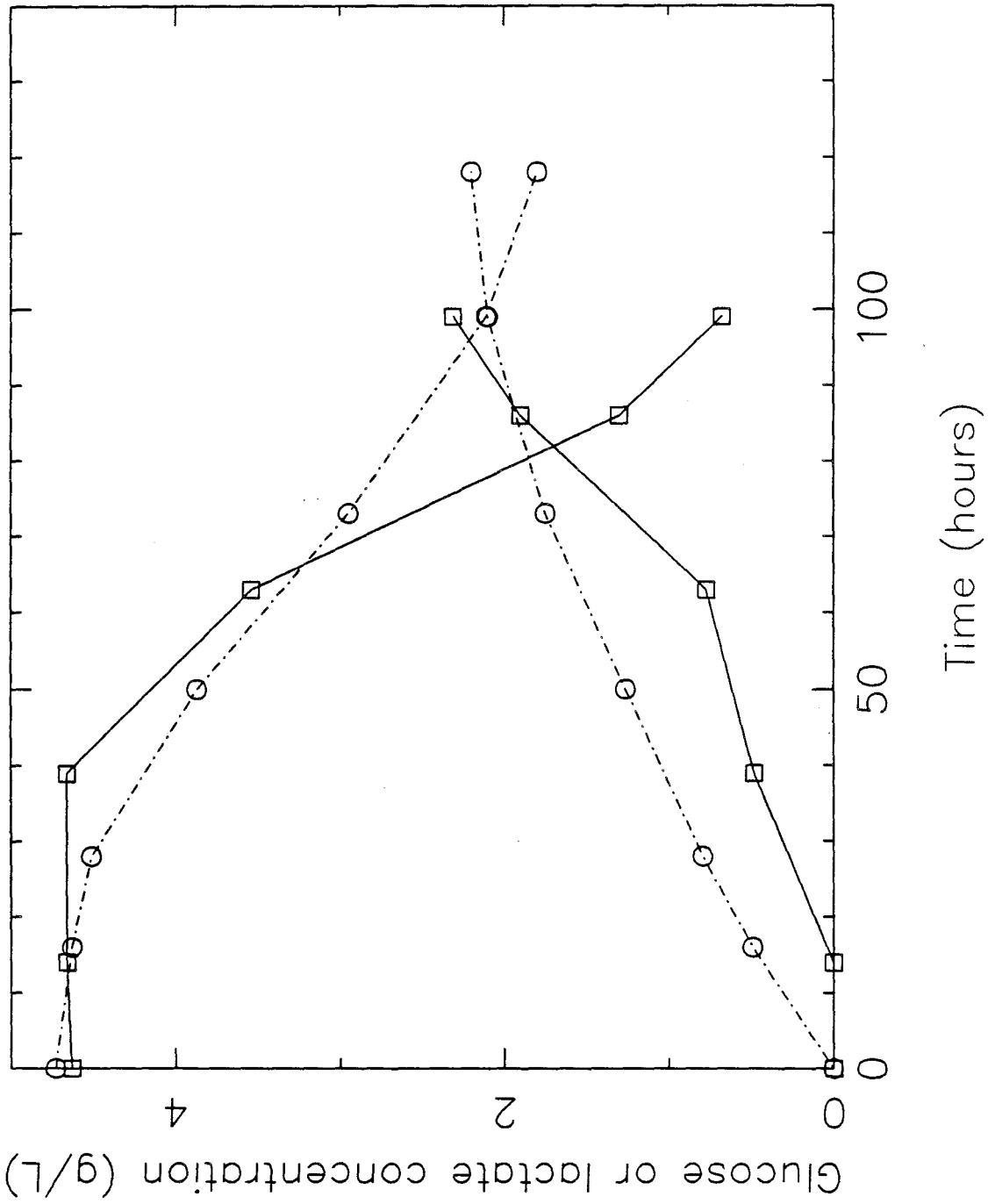

Figure 5B

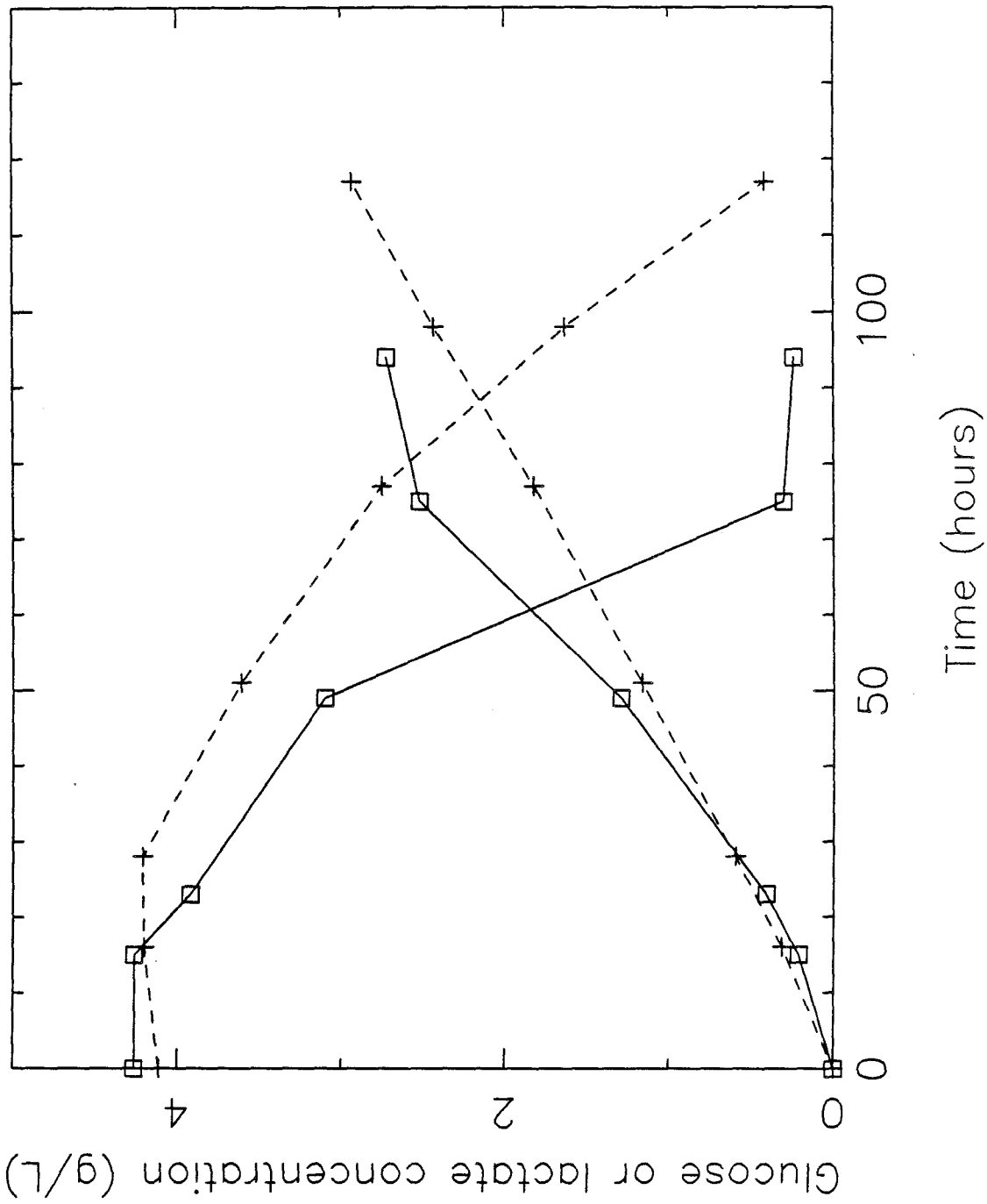

Figure 5C

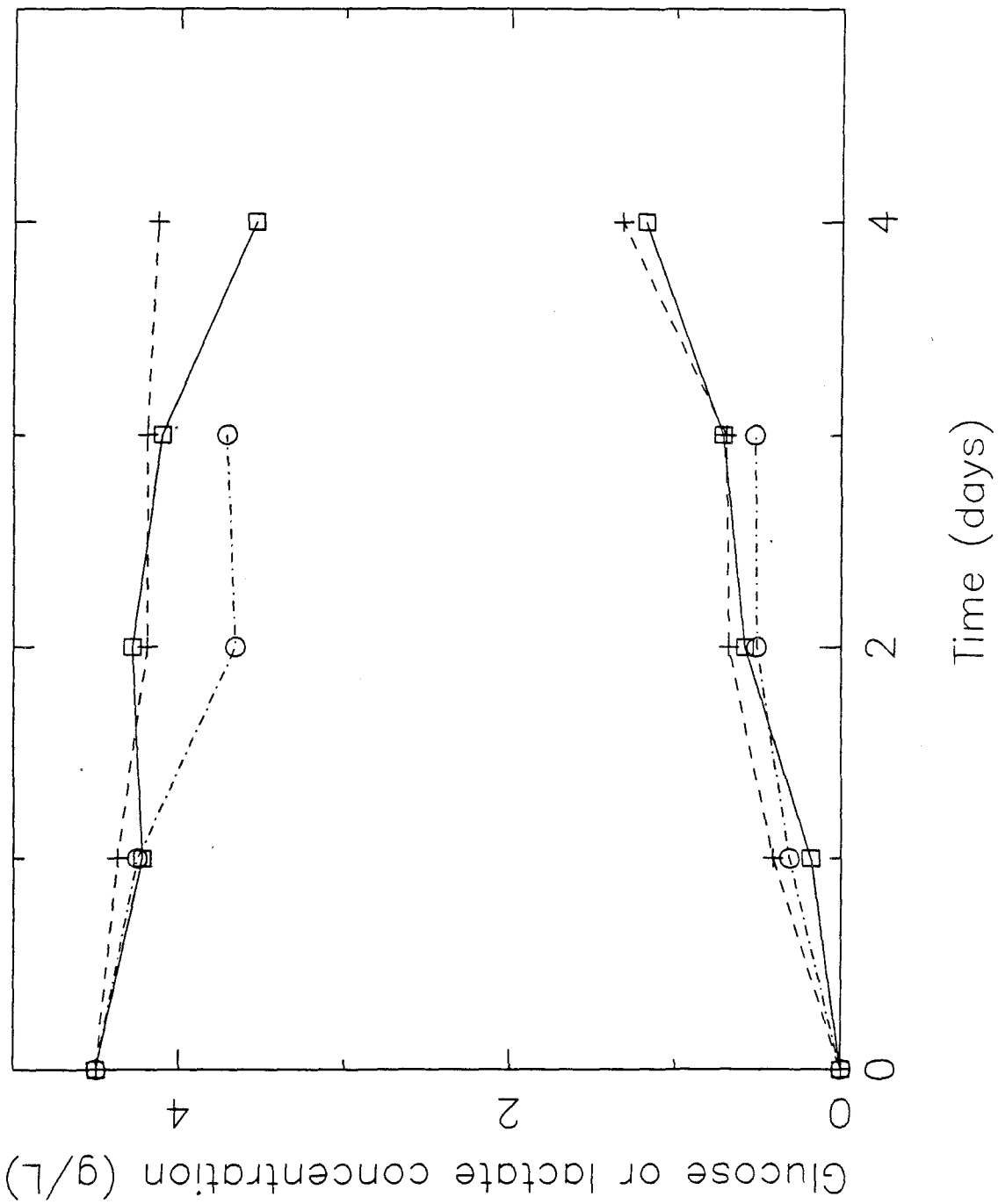

Figure 6A

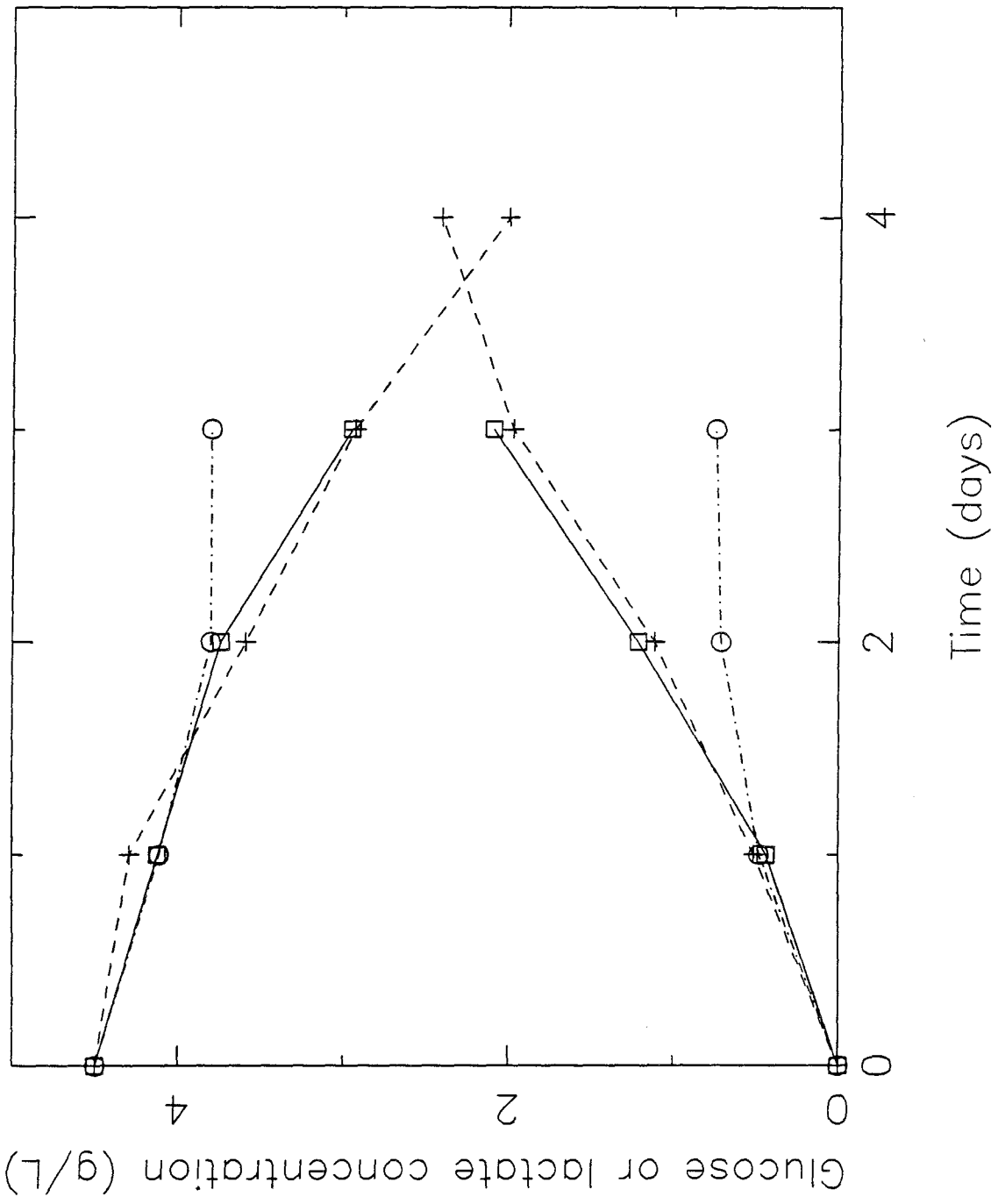

Figure 6B

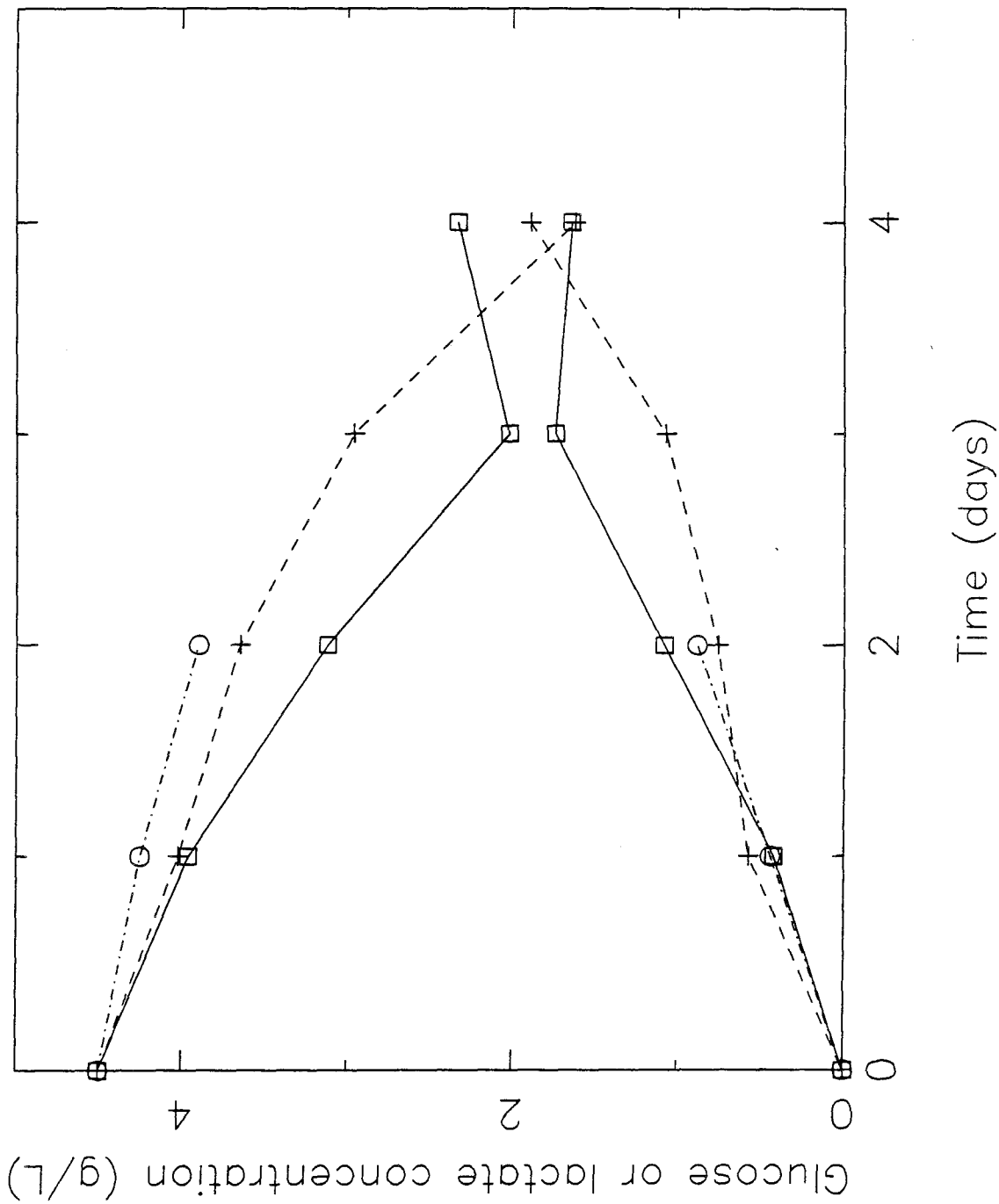

Figure 6C

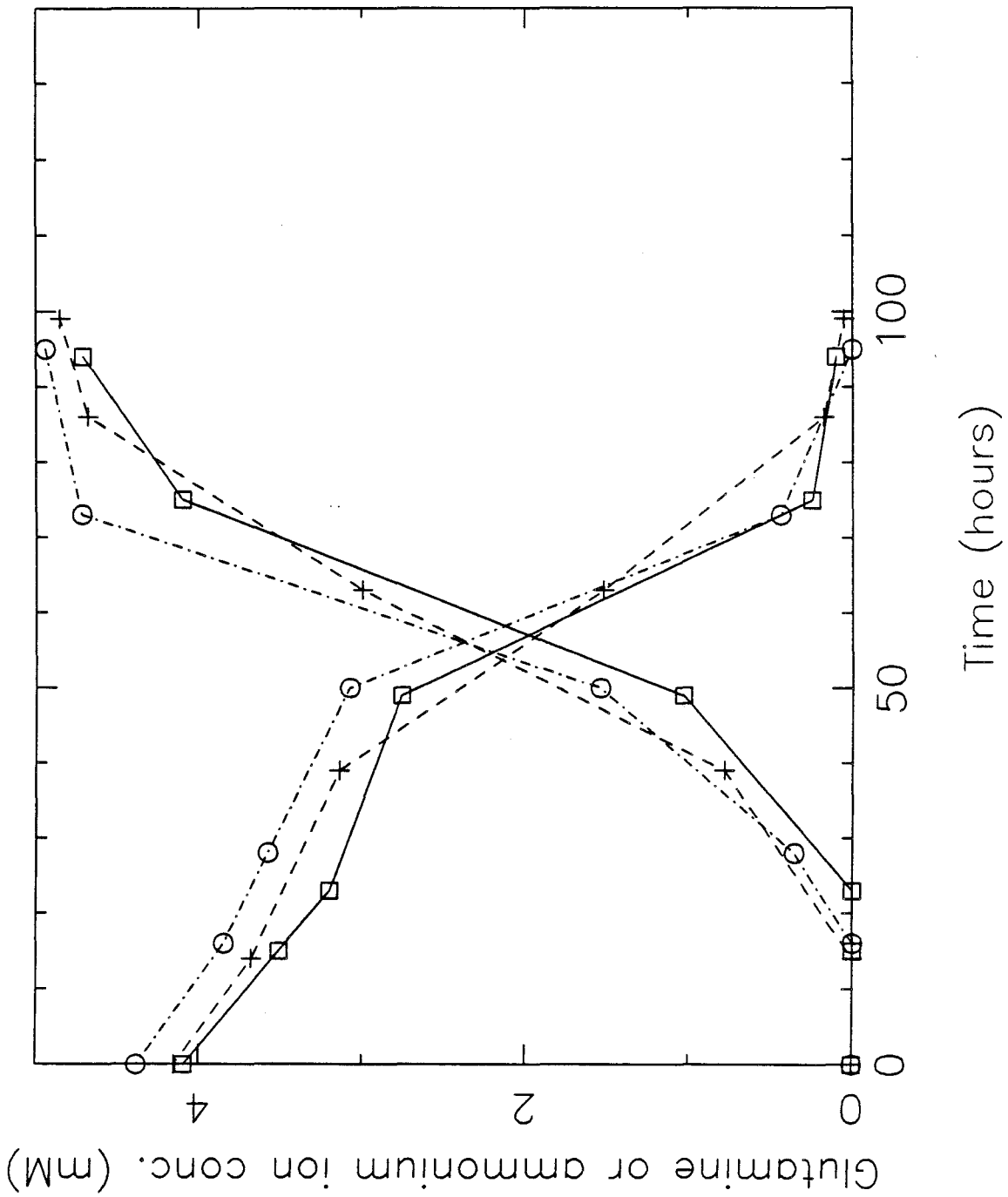

Figure 7

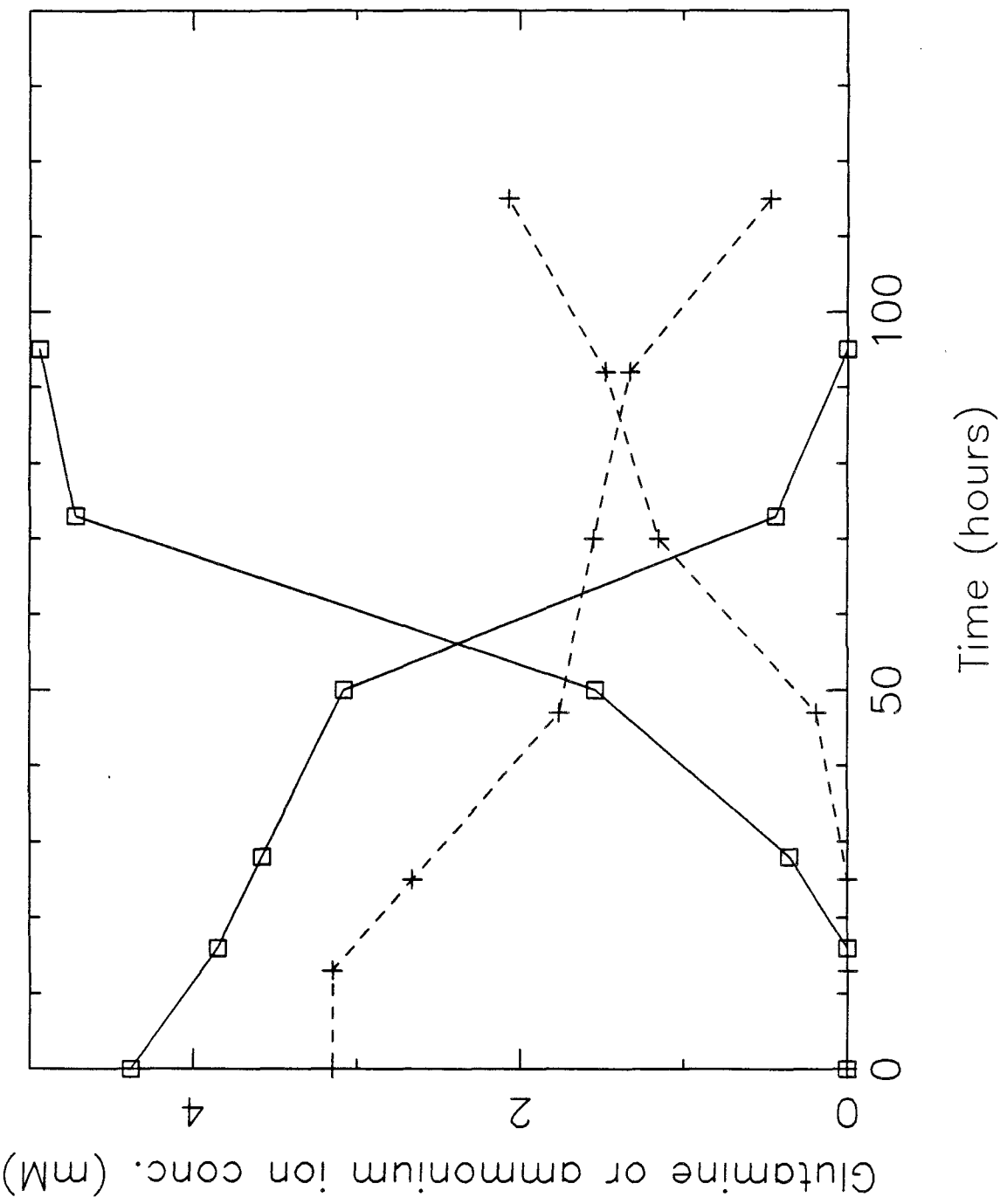

Figure 8A

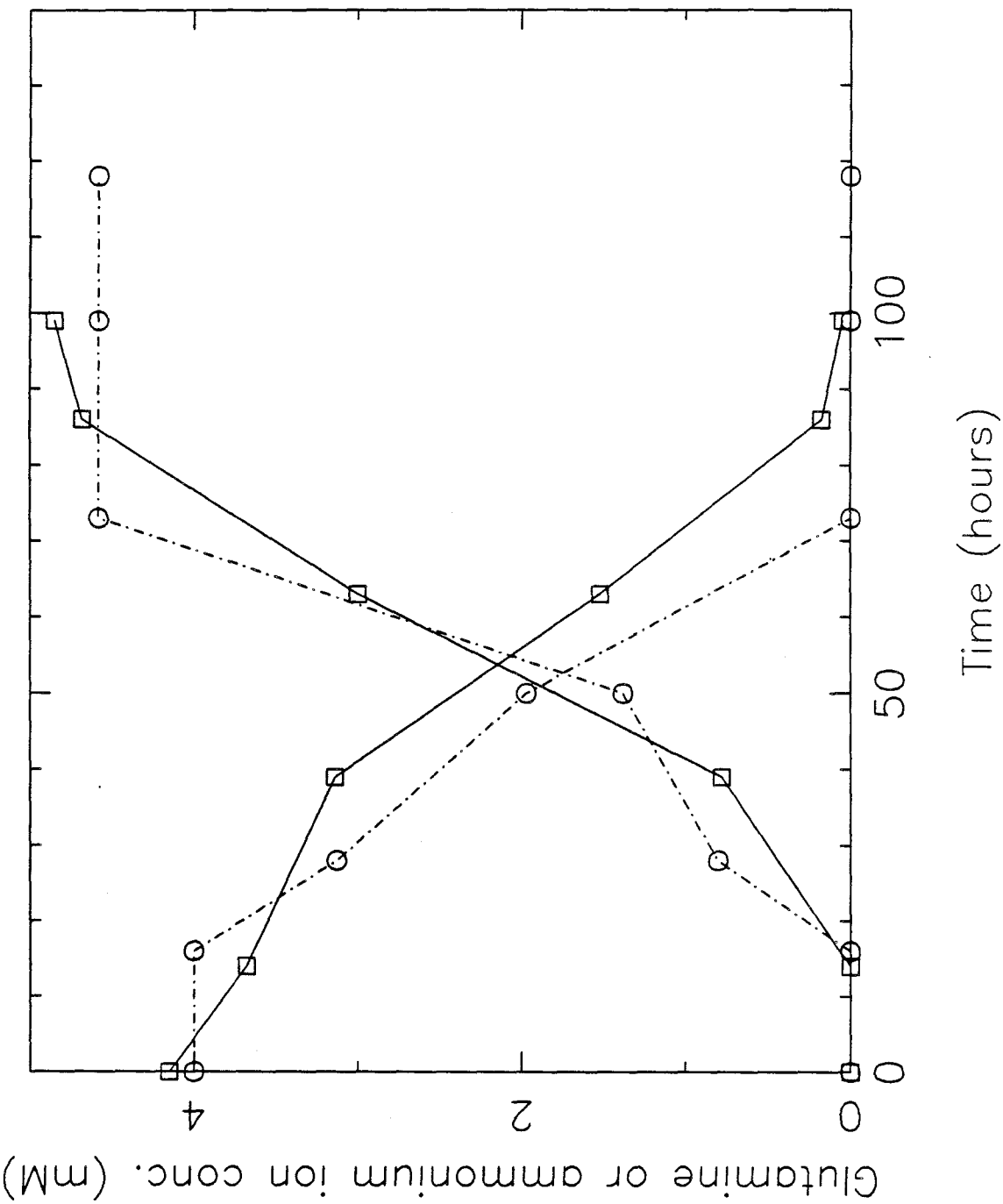

Figure 8B

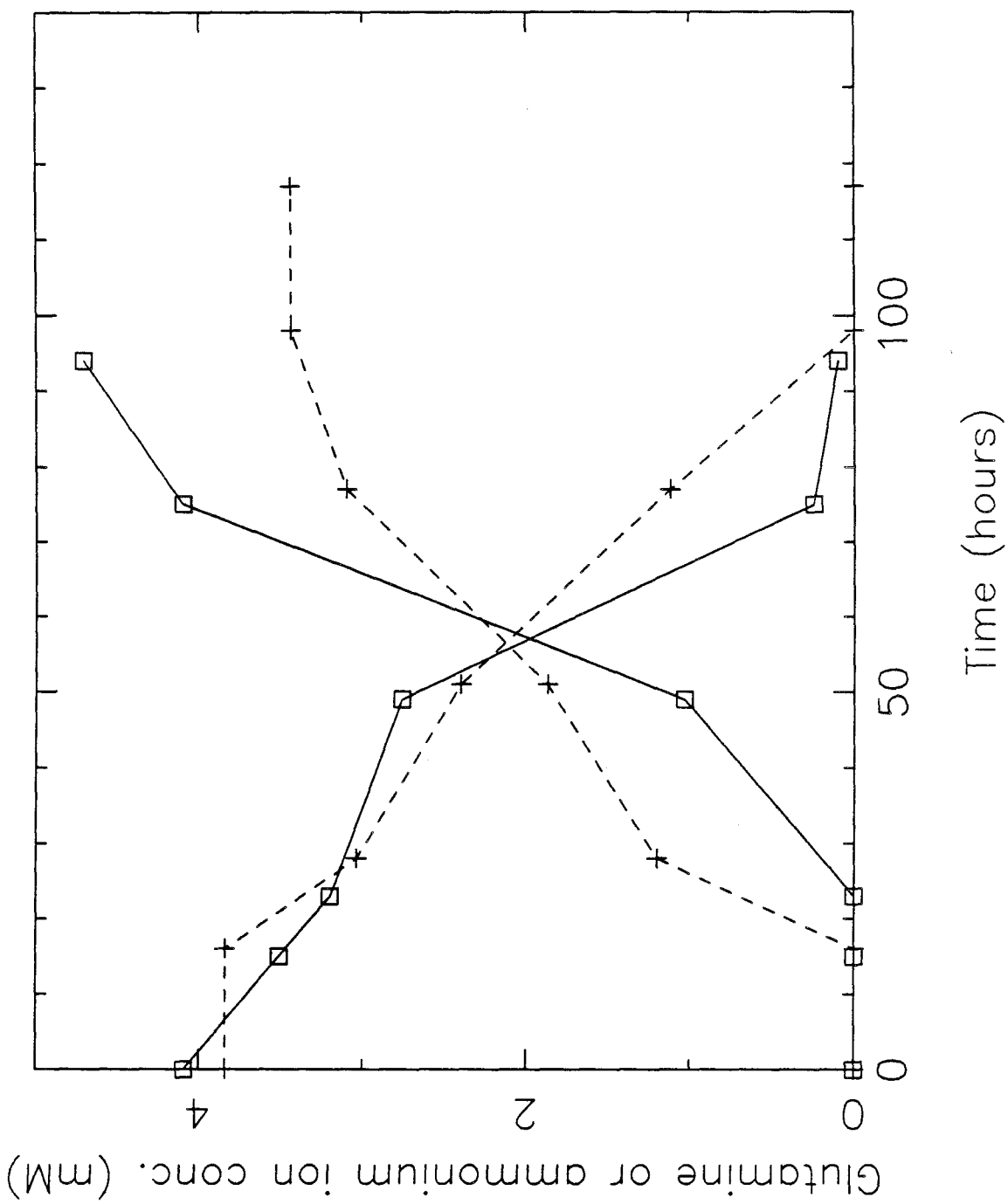

Figure 8C

CHAPTER 6.

Mathematical Modeling of the Effects of Ammonium Ion on Intracellular pH

ABSTRACT

A mathematical model for the effects of NH_4Cl addition on intracellular pH (pH_i) is presented, which includes a detailed description of the properties of the Na^+/H^+-exchanger. The effect of parameter variations on model results is investigated. The model is used to calculate the steady-state value of pH_i as a function of the NH_4Cl concentration, employing parameter values taken from the literature except for the cell permeability to NH_4^+, which is obtained by fitting simulation results to experimental data obtained previously for the steady-state value of pH_i in the presence of 10 mM NH_4Cl. The cell permeability to NH_4^+ is found to be 3.5×10^{-7} cm/s, which is on the order of typical cell permeability to K^+. Using this single fitted parameter, the model is able to reproduce the salient features of the experimental results for the changes in pH_i upon NH_4Cl addition: the transient characteristics, the dependence on the NH_4Cl concentration and the lack of dependence on the external pH value.

Introduction

Previous work has indicated that ammonium ion is an important inhibitor of mammalian cell growth, including hybridoma cell growth [1-6]. The importance of studying the effects of NH_4^+ on cells results from the fact that glutamine has been found to be essential for mammalian cell growth [7] and the fact that NH_4^+ is a byproduct of glutamine metabolism. There are two possible mechanisms for growth inhibition by NH_4^+, as discussed in a previous paper [8]. The first mechanism involves the uptake of the weak base NH_3 into the lysosomes causing alkalinization [9-14], while the second mechanism involves the uptake of the weak acid NH_4^+ into the cytoplasm causing acidification [15]. Previous work on the effects of pH_e on growth and on pH_i had shown that a 0.2 unit decrease in pH_i is sufficient to inhibit growth [16-21].

Boron and DeWeer [15] observed that NH_4Cl caused a rapid increase in the pH_i of squid giant axon cells followed by a slow decrease, which they explained by leakage of NH_4^+ into the cell. Boron and DeWeer's results suggest the possibility that a net cytoplasmic acidification may occur but they did not determine the steady-state value of pH_i after long-term continuous exposure to NH_4Cl.

In a previous paper [8], the effects of NH_4Cl addition on pH_i were measured at different pH_e values by staining the cells with a fluorescent pH indicator and monitoring their fluorescence as a function of time on the flow cytometer. Upon addition of NH_4Cl, there was a brief cytoplasmic alkalinization followed by a rapid acidification. Both the extent of the initial alkalinization and the magnitude of the ultimate acidification increase with the NH_4Cl concentration. pH_i levels off within 20-40 minutes of NH_4Cl addition. This pH_i value remains constant for 6 hours,

suggesting that it has reached steady-state. The new, lower steady-state pH_i values indicate decreases of 0.0-0.1 units at 3 mM NH_4Cl, 0.2-0.3 units at 10 mM NH_4Cl and 0.5-0.7 units at 30 mM NH_4Cl. 3 mM NH_4Cl had little effect on cell growth, while 10 mM NH_4Cl caused a substantial growth inhibition, indicating a correlation between the effects of NH_4Cl on growth and on pH_i. The magnitude of the pH_i decrease required to cause severe growth inhibition (0.2 units) is in agreement with literature data [16-21].

To explain how leakage of NH_4^+ into the cell can lead to a permanent (steady-state) cytoplasmic acidification, as observed in the experimental measurements, we proposed the following mechanism for NH_4^+ effects on pH_i. The mechanism that we propose is similar to that of Boron and DeWeer [15]. However, the nature of the competing H^+ fluxes that will determine the final steady-state value of pH_i is clarified.

The addition of NH_4Cl to a cell suspension is hypothesized to set off the following chain of events:

-NH_4Cl dissociates into NH_4^+ and Cl^- and NH_4^+ partially dissociates into NH_3 and H^+.

-NH_3 rapidly permeates the cell membrane and reassociates in the cytoplasm, causing an intracellular alkalinization.

-NH_4^+ slowly permeates the cell membrane, driven in by the membrane potential as well as the concentration gradient, and partially dissociates in the cytoplasm, causing intracellular acidification.

-When pH_i falls below its original steady-state value, the H^+ pump is activated and H^+ ions are pumped out of the cell to counteract the intracellular acidification

caused by NH_4^+.

-NH_4^+ creates a persistent acid load on the cells because it sets up a proton shuttle into the cell, in which NH_4^+ entry is balanced by NH_3 exit.

-This additional acid load upsets the previous equilibrium between H^+ production and entry and H^+ consumption and exit. pH_i reaches a new, lower steady-state value, at which the net rate of H^+ entry due to NH_4^+ leakage into the cell is exactly balanced by the increased rate of H^+ exit due to active transport.

Previously, Boron and DeWeer [15] had derived equations for the time rates of change of the total base concentration inside the cell and the intracellular pH, which included terms for the fluxes of NH_3 and NH_4^+ into and out of the cell and a rough mathematical description of the H^+ pump. They solved these equations numerically and showed that the rate of intracellular acidification is primarily dependent on the permeability of the cell to NH_4^+, which is expected to be cell-line dependent. However, they did not calculate the steady-state value of pH_i in the presence of NH_4Cl. Their derivation is reproduced here, modified as follows: The behavior of the H^+ pump, which is now known to be the Na^+/H^+-exchanger whose properties have been studied extensively [22-24], is described in detail, including the dependence of the rate of the exchanger on pH_i and pH_e. Using this more accurate representation of the cell mechanism for recovery from an acid load, the steady-state value of pH_i in the presence of NH_4Cl is determined, and the simulation results are compared with experimental results using suitable parameter values taken from the literature, including the kinetic rate constant of the Na^+/H^+-exchanger. This comparison is used to determine the cell permeability to NH_4^+ required to cause a steady-state cytoplasmic acidification of the magnitude observed experimentally.

An analysis of the dependence of model results on the values of the parameters used is included. Studying the effects of parameter variations permits a better understanding of the role of each of the physical phenomena contributing to the pH_i decrease observed experimentally. In addition, by examining the sensitivity of the model to changes in the different parameters, it is possible to predict the consequences of changes in the cell line (affecting the permeability to NH_4^+) and in the conditions, for example $[Na^+]_e$ (affecting the membrane potential and the kinetic rate constant of the Na^+/H^+-exchanger).

DERIVATION

Scope of the numerical simulation

The objective of the numerical simulation is to determine, given the total base (NH_4Cl) added to the cells and the external pH value, the transient behavior and the final steady-state values of the total base concentration inside the cell and the intracellular pH, by deriving equations for the rates of change of these parameters with time and integrating them numerically.

$[TB]_e$=total base concentration outside the cell

$[TB]_i$=total base concentration inside the cell

$[TB]_e = [BH^+]_e + [B]_e$

$[TB]_i = [BH^+]_i + [B]_i$

B=neutral base=NH_3 and BH^+=protonated base=NH_4^+

$[H^+]_e$=free hydrogen ion concentration outside the cell

$pH_e = -\log_{10}[H^+]_e$

$[H^+]_i$=free hydrogen ion concentration inside the cell

$pH_i = -\log_{10}[H^+]_i$

The rates of change of $[TB]_i$ and $[H^+]_i$ with time, $d[TB]_i/dt$ and $d[H^+]_i/dt$, will be functions of the following physical phenomena, mentioned in the introduction:

-the passive fluxes of B (NH_3) and BH^+ (NH_4^+)

-the equilibrium between the species B and BH^+, governed by the acid dissociation constant:

$$K = \frac{[B]_i[H^+]_i}{[BH^+]_i} = \frac{[B]_e[H^+]_e}{[BH^+]_e} \qquad (1)$$

-the active transport of H^+ by the H^+ pump

-the intracellular buffering power

Derivation of equations for the rates of change of $[TB]_i$ and $[H^+]_i$ with time

Both material balance equations can be written in the form:

$$\begin{pmatrix}\text{rate of change of concentration}\\ \text{with time}\end{pmatrix} =$$

$$\frac{\text{cell area}}{\text{cell volume}} \times \left(\begin{pmatrix}\text{net fluxes in}\\ \text{per unit area}\end{pmatrix} - \begin{pmatrix}\text{net fluxes out}\\ \text{per unit area}\end{pmatrix}\right) +$$

$$\begin{pmatrix}\text{net production}\\ \text{per unit volume}\end{pmatrix} - \begin{pmatrix}\text{net consumption}\\ \text{per unit volume}\end{pmatrix} \qquad (2)$$

The equation for $d[TB]_i/dt$ must include the inward fluxes of B and BH^+. The following additional terms must be included in the equation for dQ_i/dt, where Q_i is the total hydrogen ion concentration (free and bound) inside the cell.

-net outward flux of H^+ due to the H^+ pump

-net inward flux of H^+ due to H^+ leakage into the cell

-net inward or outward flux of H^+ due to CO_2/HCO_3^- fluxes into and out of the cell

-production or consumption of H^+ by chemical reactions inside the cell (for example glycolysis, respiration and oxidative phosphorylation)

Defining α and $(1-\alpha)$ as follows:

$$\alpha = \frac{[BH^+]_i}{[TB]_i} = \frac{[H^+]_i}{K + [H^+]_i} \qquad (3a)$$

$$(1-\alpha) = \frac{[B]_i}{[TB]_i} = \frac{K}{K + [H^+]_i} \qquad (3b)$$

Then, at at any given time, the fraction of entering B that will associate to form BH^+, consuming a proton, is approximately equal to α, and the fraction of entering BH^+ that will dissociate to form B, releasing a proton, is approximately equal to $(1-\alpha)$. Therefore, the material balance equations can be written.

$$\frac{d[TB]_i}{dt} = \rho \times (M_B + M_{BH+}) \tag{4a}$$

$$\frac{dQ_i}{dt} = \rho \times (-\alpha M_B + (1-\alpha)M_{BH+} - M_{H+} + M_L + M_{CO_2/HCO_3^-}) + M_P - M_C \tag{4b}$$

where ρ=(cell area)/(cell volume), cm^{-1}

M_B=net inward flux of B, (moles cm)/(L s)

M_{BH+}=net inward flux of BH^+, (moles cm)/(L s)

M_{H+}=net outward flux of H^+ due to H^+ pump, (moles cm)/(L s)

M_L=net inward flux of H^+ due to H^+ leakage into the cell, (moles cm)/(L s)

M_{CO_2/HCO_3^-}=net inward flux of H^+ due to CO_2/HCO_3^- fluxes into and out of the cell, (moles cm)/(L s)

M_P=production of H^+ by chemical reactions inside the cell, moles/L

M_C=consumption of H^+ by chemical reactions inside the cell, moles/L

The purpose of this simulation is to determine specifically the initial effects of of NH_4Cl on pH_i, in terms of a deviation from the original steady-state value which occurs within 40 minutes of NH_4Cl addition, in order to compare the results with experimental measurements. Therefore, this equation was simplified as follows. In the absence of NH_4Cl, the equation for dQ_i/dt can be written:

$$\left(\frac{dQ_i}{dt}\right)^o = \rho \times (-M^o_{H+} + M^o_L + M^o_{CO_2/HCO_3^-}) + M^o_P - M^o_C \tag{5}$$

where all quantities with superscripts o are the original values of the variables prior to NH_4Cl addition. Since pH_i was originally at steady-state prior to NH_4Cl addition,

$$\left(\frac{dQ_i}{dt}\right)^{\circ} = 0 \tag{6}$$

Substituting this equation back into the expression for dQ_i/dt in the presence of NH_4Cl, we have:

$$\frac{dQ_i}{dt} = \rho \times (-\alpha M_B + (1-\alpha)M_{BH+} - (M_{H+} - M^{o}_{H+}) + (M_L - M^{o}_{L}) +$$

$$(M_{CO_2/HCO_3^-} - M^{o}_{CO_2/HCO_3^-})) + (M_P - M^{o}_{P}) - (M_C - M^{o}_{C})$$

In order to solve this equation using available data, as a first approximation, it will be assumed that changes in the terms M_L, M_{CO_2/HCO_3^-}, M_P and M_C upon NH_4Cl addition (due to the subsequent changes in pH_i or due to direct effects of NH_4Cl) are negligible compared to the other terms in the equation during the first 40 minutes after NH_4Cl addition. This is a reasonable assumption since it is likely that the time scale of changes in these terms upon NH_4Cl addition will be longer that 40 minutes. Therefore, we have:

$$\frac{dQ_i}{dt} = \rho \times (-\alpha M_B + (1-\alpha)M_{BH+} - (M_{H+} - M^{o}_{H+})) \tag{8}$$

In this equation, we have removed the physical phenomena that contribute to the original steady-state value of pH_i but not to the steady-state value attained rapidly upon NH_4Cl addition, in agreement with the purpose stated above.

To determine $[H^+]_i$, it is necessary to take into account multiple complex ion equilibria. As an approximation, the intracellular buffering power is used to relate

the rate of change of the total hydrogen ion concentration to the rate of change of the free hydrogen ion concentration.

$$\frac{dpH_i}{dt} = \frac{1}{\beta} \times \frac{dQ_i}{dt} \tag{9}$$

where β=the intracellular buffering power

$$\frac{d[H^+]_i}{dt} = \frac{-2.303[H^+]_i}{\beta} \times \frac{dQ_i}{dt} \tag{10}$$

Therefore:

$$\frac{d[H^+]_i}{dt} = \frac{-2.303[H^+]_i}{\beta} \times \rho \times (-\alpha M_B + (1-\alpha)M_{BH+} - (M_{H+} - M^o_{H+})) \tag{11}$$

Evaluation of M_B and M_{BH+} based on the concentration gradients and permeabilities of B and BH^+ and on the membrane potential

Using Fick's law governing the net passive fluxes of uncharged particles, we have:

$$M_B = P_B([B]_e - [B]_i) \tag{12}$$

where P_B= permeability of B (NH_3), cm/s

Using the constant field equation describing the net fluxes of charged particles, we have:

$$M_{BH+} = P_{BH+} \times (\frac{V_m F}{RT}) \times (\frac{[BH^+]_e - [BH^+]_i \epsilon}{\epsilon - 1}) \tag{13}$$

where P_{BH+}=permeability of BH^+ (NH_4^+), cm/s

V_m=membrane potential, volts

ϵ=exponent($V_m F/RT$), where

F=Faraday constant=96500 joules/(volt mole),

R=gas constant=8.314 joules/(mole K) and

T=temperature=298K.

Evaluation of M_{H+} based on the properties of the Na^+/H^+ exchanger

The primary pH_i-regulating system in mammalian cells is the Na^+/H^+ exchanger, which has the following properties [22]: The exchanger uses the Na^+ gradient ($[Na^+]_e > [Na^+]_i$) to drive H^+ out of the cell against its gradient ($[H^+]_e < [H^+]_i$). The activities of the Na^+/H^+ exchanger are closely coupled to those of the Na^+/K^+-ATPase, which pumps Na^+ out of the cell and K^+ into the cell, to maintain both the Na^+ gradient and the membrane potential. The exchanger becomes quiescent at a certain alkaline pH_i value due to the action of a second cytoplasmic H^+ binding site that allows the exchanger to be allosterically activated at acidic pH_i values.

The second cytoplasmic H^+ binding site gives the exchanger its distinctive pH_i dependence:

-At a given pH_i value, the exchanger becomes quiescent. This is the setpoint of the exchanger, which depends on several factors: pH_e, $[Na^+]_e$, and the presence or absence of growth factors.

-When pH_i falls below the setpoint, the rate of the exchanger increases linearly with pH_i until it reaches its maximum value.

-When pH_i rises above the setpoint, the exchanger remains quiescent. The cell must use secondary pH_i-regulating mechanisms to recover from an alkaline load [23]. These include the Cl^-/HCO_3^- exchanger, which exchanges external Cl^- for internal HCO_3^-, causing intracellular acidification.

Therefore, an expression for M_{H+} based on the behavior of the Na^+/H^+ exchanger is:

$$M_{H+} = \begin{cases} (M_{H+})_{max} \text{ for } pH_i \leq (pH_i)_{maxM_{H+}} \\ k_e((pH_i)_{setpt} - pH_i) \text{ for } (pH_i)_{maxM_{H+}} < pH_i < (pH_i)_{setpt} \\ 0 \text{ for } pH_i \geq (pH_i)_{setpt} \end{cases} \quad (14)$$

where k_e=exchanger kinetic rate constant, (moles cm)/(L s)

$(M_{H+})_{max}$=maximum value of the rate of the exchanger, (moles cm)/(L s)

$(pH_i)_{maxM_{H+}}$=value of pH_i at which M_{H+} attains its maximum value

$(pH_i)_{setpt}$=setpoint of the exchanger

Therefore,

$$M^o_{H+} = k_e((pH_i)_{setpt} - (pH_i)_{oss}) \quad (15)$$

assuming that $(pH_i)_{maxM_{H+}} < (pH_i)_{oss} < (pH_i)_{setpt}$, where $(pH_i)_{oss}$=original steady-state value of pH_i, and

$$(M_{H+} - M^o_{H+}) = k_e((pH_i)_{oss} - pH_i) \quad (16)$$

assuming that $(pH_i)_{maxM_{H+}} < pH_i < (pH_i)_{setpt}$ at all times.

Final versions of the equations for $d[TB]_i/dt$ and $d[H^+]_i/dt$

$$\frac{d[TB]_i}{dt} = \rho\left\{P_B\left([B]_e - (1-\alpha)[TB]_i\right) + P_{BH+}\frac{V_m F}{RT}\left(\frac{[BH^+]_e - \alpha[TB]_i\epsilon}{\epsilon - 1}\right)\right\} \quad (17a)$$

$$\frac{d[H^+]_i}{dt} = \frac{-2.303[H^+]_i\rho}{\beta}\left\{-\alpha P_B\left([B]_e - (1-\alpha)[TB]_i\right) + \right.$$

$$\left.(1-\alpha)P_{BH+}\frac{V_m F}{RT}\left(\frac{[BH^+]_e - \alpha[TB]_i\epsilon}{\epsilon - 1}\right)\right.$$

$$-k_e((pH_i)_{oss} - pH_i)\Big\} \tag{17b}$$

Steady-state equations for $[TB]_i$ and pH_i

At steady-state,

$$\frac{d[TB]_i}{dt} = 0 = \frac{d[H^+]_i}{dt} \tag{18}$$

From equations (4a) and (11), this implies that both of the following conditions must hold:

$$M_B + M_{BH+} = 0 \tag{19a}$$

$$-\alpha M_B + (1-\alpha)M_{BH+} - (M_{H+} - M^o_{H+}) = 0 \tag{19b}$$

implying that:

$$M_{BH+} = -M_B = (M_{H+} - M^o_{H+}) \tag{20}$$

Defining C as follows:

$$C = \frac{V_m F}{RT} \times \frac{1}{\epsilon - 1} \tag{21}$$

then the steady-state equations can be written as follows:

$$P_{BH+}C([BH^+]_e - \alpha[TB]_i\epsilon) = -P_B([B]_e - (1-\alpha)[TB]_i) \tag{22a}$$

$$P_{BH+}C([BH^+]_e - \alpha[TB]_i\epsilon) = k_e((pH_i)_{oss} - pH_i) \tag{22b}$$

Analytical solutions of steady-state equations for $[TB]_i$ and pH_i using reasonable approximations

The first approximations are based on $K << [H^+]_i$. This is a reasonable approximation since pK=9.2 and pH_i is in the physiological range (7.6 or below).

$$\alpha = \frac{[H^+]_i}{K + [H^+]_i} \simeq 1 \tag{23a}$$

$$(1-\alpha) = \frac{K}{K+[H^+]_i} \simeq \frac{K}{[H^+]_i} \qquad (23b)$$

Using these approximations, equations (22a) and (22b) can be rewritten as follows:

$$P_{BH^+}C([BH^+]_e - [TB]_i\epsilon) = -P_B([B]_e - (K/[H^+]_i)[TB]_i) \qquad (24a)$$

$$P_{BH^+}C([BH^+]_e - [TB]_i\epsilon) = k_e((pH_i)_{oss} - pH_i) \qquad (24b)$$

These equations can be solved explicitly for $[TB]_i$ and pH_i as follows:

$$[TB]_i = \frac{P_B[B]_e + P_{BH^+}C[BH^+]_e}{P_{BH^+}C\epsilon + P_B(K/[H^+]_i)} \qquad (25a)$$

$$pH_i = (pH_i)_{oss} - (P_{BH^+}C/k_e)([BH^+]_e - [TB]_i\epsilon) \qquad (25b)$$

The second approximation, which is necessary to solve the equations analytically, is based on $\epsilon << 1$. This approximation is valid because $\epsilon = \text{exponent}(V_mF/RT)$ and (V_mF/RT) is much less than zero. This second approximation implies that $[TB]_i\epsilon << [BH^+]_e$, such that the equation for the steady-state value of pH_i becomes:

$$pH_i \simeq (pH_i)_{oss} - (P_{BH^+}C/k_e)[BH^+]_e \qquad (26)$$

This equation can also be solved explicitly for P_{BH^+}:

$$P_{BH^+} \simeq \frac{((pH_i)_{oss} - pH_i)}{(C/k_e)[BH^+]_e} \qquad (27)$$

This relationship can be used to estimate the value of P_{BH^+}, which will give the best fit of the simulation results to the experimental data, as described in the section on the choice of parameter values to be used in the simulations. In practice, the following approximations (not necessary for an analytical solution) are also found to hold true for the parameter values used in the simulations: $P_{BH^+}C[BH^+]_e <<$

$P_B[B]_e$ and $P_{BH^+}C\epsilon << P_B(K/[H^+]_i)$. Using these approximations, the equation for the steady-state value of $[TB]_i$ becomes:

$$[TB]_i \simeq \frac{[B]_e[H^+]_i}{K} \tag{33}$$

Equation (28) can also be arrived at by using the definition of K and employing the following approximations, which are based on the high permeability of B (NH_3) and on the first approximation listed above ($\alpha \simeq 1$): $[B]_i \simeq [B]_e$ and $[TB]_i \simeq [BH^+]_i$.

COMPUTATIONAL RESULTS AND DISCUSSION

Choice of parameter values to be used in the simulations

ρ, the cell area-to-volume ratio, was evaluated based on Coulter counter measurements of cell area and volume. An average value of ρ for different pH_e values and NH_4Cl concentrations was chosen. β, the intracellular buffering power, P_B, the permeability of the neutral base NH_3, V_m, the membrane potential, and k_e, the Na^+/H^+ exchanger kinetic rate constant, were obtained from the literature. The parameters, the values chosen (for the simulations to be compared with experimental data) and the references used are presented in Table 1. However, since there exists some uncertainty in applying parameter values obtained from the literature, exploratory simulations were performed in which each of the parameters was varied in turn, to determine effects on the results, as discussed in the next section. Minimum and maximum values of the parameters to be used in the exploratory simulations were also based on data from the literature. They are also listed in Table 1, together with the references used.

The value of P_{BH+} for this cell line is not available in the literature, and little information was available for other cell lines. Instead, P_{BH+} was chosen as the single adjustable parameter, which was used to fit the results of the numerical simulation to the experimental data. The approximate value of P_{BH+} required to give a decrease in the steady-state value of pH_i of 0.3 units upon addition of 10mM NH_4Cl at pH_e 7.2 (experimental measurements gave values of 0.2 to 0.3 units under these conditions) was calculated (analytically) using the simplified steady-state equations, equations (26) and (28). Alternatively, the value of P_{BH+} could have been taken from the literature and k_e, the Na^+/H^+ exchanger kinetic rate

constant, could have been chosen as the single fitted parameter. However, more literature data is available on k_e than on P_{BH+}. The effects of varying P_{BH+} were determined in exploratory simulations, discussed in the next section, using the alternate values listed in Table 1. The use of a fitted parameter allows one to compensate for errors in the selection of the values of the remaining parameters taken from literature data.

Effect of variations in parameter values on transient and steady-state values of $[TB]_i$ and pH_i

Some of the benefits of studying the effects of parameter variations were stated in the introduction. A further advantage of studying these effects is that this will enable us to predict the consequences of errors in the selection of the parameter values for the simulations to be compared with experimental data. The simplified steady-state equations, equations (26) and (28), can be used to estimate parameter effects on the final steady-state values of $[TB]_i$ and pH_i. These estimates can be compared with the final steady-state values obtained from numerical simulations, which also supply the transient behavior. The final steady-state values of $[TB]_i$ and pH_i for different parameter values obtained from simulations on the base case, $[NH_4Cl]_e$=10mM, pH_e=7.2, are presented in Table 2. In addition, ΔpH_i, the deviation of the final steady-state value from the original steady-state value, is included in Table 2. ($\Delta pH_i = (pH_i)_{fss} - (pH_i)_{oss}$, where the subscript fss refers to final steady-state value.) $(pH_i)_{oss}$=7.6 was assumed (both as a starting value and to substitute into $(M_{H+} - M^o_{H+})$) based on experimental results on the absolute value of pH_i as a function of pH_e.

Effects of ρ and β

From the steady-state equations, equations (22a) and (22b), ρ, the cell surface area-to-volume ratio, and β, the intracellular buffering power, are not expected to have any effect on the final steady-state values of $[TB]_i$ and pH_i. This is evident in Figures 1 and 2 and Figures 3 and 4, in which the values of $[TB]_i$ and pH_i as a function of time for different values of ρ and β, respectively, are plotted. Since ρ and β have no effect on the final steady-state value of pH_i, errors in the selection of the parameter values chosen (for the simulation to be compared with experimental data), such as using an average value for ρ and applying a value of β determined for a different cell line, will have no effect on the value of ΔpH_i obtained from the simulation. The minimum and maximum values of ρ and β were chosen based on the references presented in Table 1. In Figures 1, 2, 3, and 4, the transient behavior of $[TB]_i$ and pH_i indicates that, as ρ increases, the time required to reach steady-state decreases, while, as β increases, the time required to reach steady-state increases.

Effects of V_m

From the simplified steady-state equations, equations (26) and (28), an increase in the magnitude of V_m, the membrane potential, will cause the final steady-state value of pH_i to decrease and that of $[TB]_i$ to increase since C increases as V_m increases. (In fact, since $\epsilon << 1$, $C = (V_m F/RT)/(\epsilon - 1) \simeq (-V_m F/RT)$, which is proportional to V_m.) This is evident in Figures 5 and 6, in which the values of $[TB]_i$ and pH_i as a function of time for different values of V_m are plotted, and in Table 2, in which the steady-state values of $[TB]_i$ and pH_i for different parameter values are given. The minimum and maximum values of V_m used were chosen based on references presented in Table 1. From Figures 5 and 6, changes in V_m had little effect on the transient behavior observed: the time to reach steady-state was

constant as a function of V_m. From Table 2, note that to obtain a 0.1 unit change in ΔpH_i a substantial error in the evaluation of V_m (30mV) is required.

Effects of k_e and P_{BH+}

From the simplified steady-state equations, equations (26) and (28), a decrease in k_e, the Na^+/H^+ exchanger kinetic rate constant, or an increase in P_{BH+}, the permeability of NH_4^+, will cause the final steady-state value of pH_i to decrease and that of $[TB]_i$ to increase. This is evident in Figures 7 and 8 and in Figures 9 and 10, in which the values of $[TB]_i$ and pH_i as a function of time for different values of k_e and P_{BH+}, respectively, are plotted, and in Table 2, in which the steady-state values of $[TB]_i$ and pH_i for different parameter values are given. The miniumum and maximum values of k_e used were chosen based on references presented in Table 1. Figures 7, 8, 9, and 10 indicate that the time required to reach steady-state increases as either k_e decreases or P_{BH+} increases. The minimum and maximum values of P_{BH+}, the single fitted parameter of the simulation (used to fit simulation results to experimental data, as explained in section 8)), were chosen to demonstrate the effect of orders of magnitude variation in this parameter (10^{-8} to10^{-6}). Note that $P_{BH+} = 10^{-8}$ gives simulation results similar to the experimental results of Boron and DeWeer [15] for squid giant axon cells, which are expected to be relatively impermeable to NH_4^+.

In the section on the choice of parameter values to be used in the simulations, it was indicated that the roles of the parameters k_e (obtained from the literature) and P_{BH+} (simulation-derived) can be interchanged. From equations (26) and (28), a two-fold increase in k_e is equivalent to a two-fold decrease in P_{BH+}. (In agreement with this result, running a simulation with k_e=0.0416 and $P_{BH+} = 1.75 \times 10^{-7}$ gave

the same results as running one with k_e=0.0832 and $P_{BH+} = 3.5 \times 10^{-7}$.) From Table 2, the results of the simulation are strongly dependent on the value of k_e chosen (which is based on literature data for a different cell line). However, since P_{BH+} is a fitted parameter and since changes in P_{BH+} are inversely proportional to changes in k_e, this implies that corrections in P_{BH+} will directly compensate for errors in the selection of the value of k_e.

Comparison of computer simulation results with experimental results

The effects of different NH_4Cl concentrations at constant pH_e and of different pH_e values at constant NH_4Cl concentration on $[B]_e$ and on $[BH^+]_e$ are shown in Table 3. These values are calculated using a pK value of 9.2 for NH_4^+ taken from the literature [12]. Simulation results for the effects of different NH_4Cl concentrations at constant pH_e (7.2) and the effects of different pH_e values at constant NH_4Cl concentration (10 mM) on the final steady-state values of $[TB]_i$ and pH_i are presented in Table 4. The values of the deviation of the final steady-state value of pH_i from the original steady-state value (ΔpH_i) are compared with experimental results in Table 4. Simulation results for the effects of different NH_4Cl concentrations at pH_e 7.2 on $[TB]_i$ and pH_i as a function of time are presented in Figures 11 and 12. Experimental results for the effects of different NH_4Cl concentrations on pH_i as a function of time at pH_e 7.2 are shown in Figure 13. These effects were found to be independent of pH_e over the range 6.8 to 7.6. Note that the variable actually measured experimentally was the deviation of pH_i from its original steady-state value in the absence of NH_4Cl (pH_i as a function of time of a treated sample was compared with that of a control sample at the same pH_e). Short-term measurements of the absolute value (by comparison with calibration samples) of pH_i as a

function of pH_e indicated that pH_i remained constant at 7.6 at pH_e values 6.8, 7.2, and 7.6. Therefore, the absolute pH_i values plotted in Figure 13 were obtained by subtracting from 7.6 the experimentally measured deviations of pH_i from its original steady-state value, and $(pH_i)_{oss}$ was assumed to be 7.6 (both as a starting value and in the equation for $(M_{H+} - M^{o}_{H+})$) in the simulations in Figures 11 and 12.

As described in the section on the choice of parameter values to be used in the simulations, the parameter P_{BH+} was used to fit the final steady-state value of pH_i, in the presence of 10 mM NH_4Cl at pH_e 7.2, obtained from the simulation (using the selected parameter values in Table 1, column 3) to the experimental final steady-state value. A comparison of Figures 12 and 13 indicates that the simulation, using the selected parameter values in Table 1 (column 3) including the simulation-derived value of the fitted parameter P_{BH+}, reproduces fairly well the transient characteristics of the experimental results: the initial increase in pH_i (whose magnitude increases with the NH_4Cl concentration), followed by the rapid decrease in pH_i (whose extent also increases with the NH_4Cl concentration), and the attainment of a new, lower steady-state within approximately 30 minutes (1800 seconds) of NH_4Cl addition. Table 4 shows that the simulation also reproduces fairly well the dependence of ΔpH_i, the deviation of the final steady-state value of pH_i from the original steady-state value in the absence of NH_4Cl, on the NH_4Cl concentration at constant pH_e.

Experimental results had shown that ΔpH_i did not vary as a function of pH_e. In order to use the simulation to evaluate the effect of pH_e on ΔpH_i at constant NH_4Cl concentration (10mM) (which affects $[B]_e$ and $[BH^+]_e$ as shown in Table 3), a value of $(pH_i)_{oss}$ as a function of pH_e must be assumed, both to use as an initial

value and to substitute into the equation for $(M_{H+} - M^{o}_{H+})$. Initially, $(pH_i)_{oss}$ was set equal to 7.6 at all 3 pH_e values tested; 6.8, 7.2 and 7.6, based on experimental measurements of the absolute value of pH_i as a function of pH_e, as described above. The values of $[TB]_i$ and pH_i as a function of time for different pH_e values are plotted in Figures 14 and 15. The final steady-state values of $[TB]_i$ and pH_i, together with ΔpH_i, are listed in Table 4. Table 4 indicates that ΔpH_i remains approximately constant as a function of pH_e, in agreement with experimental results.

CONCLUSIONS

The permeability of the hybridoma cell to NH_4^+ was found to be 3.5×10^{-7}, which is on the order of the K^+ permeability of a typical cell, in agreement with the predictions of Boron and DeWeer [15]. However, unlike the results of Boron and DeWeer's simulation, this $P_{NH_4^+}$ is sufficient to cause a rapid cytoplasmic acidification at steady-state, based on the behavior of the Na^+/H^+-exchanger and the other parameter values (taken from the literature) incorporated into the model.

The model, using $P_{NH_4^+}$ as the single fitted parameter, is consistent with the salient features of the experimental data: namely, the transient characteristics, the dependence on the NH_4Cl concentration and the lack of dependence on pH_e (provided $(pH_i)_{ss}$ is assumed to vary as a function of pH_e). This suggests that the following assumptions used in the model could be valid:

-The assumption that the changes upon NH_4Cl addition in the other flux terms and in the production and consumption terms in the material balance equation for H^+ are negligible compared to the terms which were retained, on the time scale of the effects of NH_4Cl on pH_i (40 minutes).

-The assumption that the Na^+/H^+-exchanger is the main pH_i controller of the cell (and that its characteristics do not vary greatly from cell line to cell line).

-The mechanism for NH_4Cl effects on pH_i, outlined in the introduction.

REFERENCES

1. Miller, W.M., C.R. Wilke, and H.W. Blanch, *Bioprocess Eng.*, **3**, 113 (1988).

2. Glacken, M.W., E. Adema, and A.J. Sinskey, *Biotech. Bioeng.*, **32**, 491 (1988).

3. Thorpe, J.S., A.D. Murdin, P.G. Sanders, and R.E. Spier, presented at it The 194th National Meeting of the American Chemical Society, New Orleans, Louisiana (1987).

4. Reuveny, S., D. Velez, J.D. Macmillan, and L. Miller, *J. Immunol. Methods*, **86**, 53 (1986).

5. Iio, M., A. Moriyama, and H. Murakami, in *Growth and Differentiation of Cells in a Defined Environment*, H. Murakami, I. Yamane, D.W. Barnes, J.P. Mather, I. Hayashi, and G.H. Sato, eds., Springer, p. 437 (1985).

6. Butler, M., and R.E. Spier, *J. Biotechnology*, **1**, 187 (1984).

7. McKeehan, W.L., in *Carbohydrate Metabolism in Cultured Cells*, M. J. Morgan, ed., Plenum Press, p. 111 (1986).

8. McQueen, A., and J.E. Bailey, *Bioprocess Eng.*, in press (1989).

9. Poole, B., and S. Ohkuma, *J. Cell Biol.*, **90**, 665 (1981).

10. Van Leuven, F., J.-J. Cassiman, and H. Van Den Berghe, *Cell*, **20**, 37 (1980).

11. Tietze, C., P. Schlesinger, and P. Stahl, *Biochem. Biophys. Res. Commun.*, **93**, 1 (1980).

12. King, A.C., L. Hernaez-Davis, and P. Cuatrecasas, *PNAS U.S.A.*, **77**, 3283 (1980).

13. King, A.C., L. Hernaez-Davis, and P. Cuatrecasas, *PNAS U.S.A.*, **78**, 717 (1981).

14. Cain, C.C., and R.F. Murphy, *J. Cell Physiol.*, **129**, 65 (1986).

15. Boron, W.F., and P. DeWeer, *J. Gen. Physiol.*, **67**, 91 (1976).

16. Taylor, I.W., and P.J. Hodson, *J. Cell Physiol.*, **121**, 517 (1984).

17. Musgrove, E., M. Seaman, and D. Hedley, *Exp. Cell Res.*, **172**, 65 (1987).

18. L'Allemain, G., S. Paris, and J. Pouyssegur, *J. Biol. Chem.*, **259**, 5809 (1984).

19. Pouyssegur, J., A. Franchi, G. L'Allemain, and S. Paris, *FEBS Lett.*, **190**, 115 (1985).

20. Gerson, D.F., in *Intracellular pH: Its Measurement, Regulation, and Utilization in Cellular Functions*, R. Nuccitelli and D.W. Deamer, eds., Alan R. Liss, p. 375 (1982).

21. Busa, W. B., in $Na^+/H^+ - exchange$, *Intracellular pH, and Cell Function*, P.S. Aronson and W.F. Boron, eds., Academic Press, p. 291 (1986).

22. Grinstein, S., and A. Rothstein, *J. Membrane Biol.*, **90**, 1 (1986).

23. Boron, W.F., *J. Membrane Biol.*, **72**, 1 (1983).

24. Grinstein, S., S. Cohen, and A. Rothstein, *J. Gen. Physiol.*, **83**, 341 (1984).

25. Roos, A., and W.F. Boron, *Physiol. Reviews*, **61**, 296 (1981).

26. Alberts, B., D. Bray, J. Lewis, M. Raff, K. Roberts and J.D. Watson, *Molecular Biology of the Cell*, Garland Publishing, p. 291 (1983).

Table 1: Parameter values used in the simulations.

Parameter		Value (units)	Reference	Min. value	Reference	Max. value	Reference
Cell area to volume ratio	ρ	4000 cm^{-1}	cell diameter 15μm	2000	cell diameter 30μm	6000	cell diameter 10μm
Intracellular buffering power	β	-25 mM	Grinstein [24] (rat thymic lymphocyte)	-18	Boron and Deweer [15] (squid giant axon)	-50	Roos and Boron [25] (rat brain)
Permeability of neutral base NH_3	P_B	0.01 cm/s	Boron and Deweer [15] (squid giant axon)	–	–	–	–
Membrane potential	V_m	-90 mV	Roos and Boron [25] (mammalian cells)	-60	Boron and Deweer [15] (squid giant axon)	-120	Alberts *et al* [26] (mammalian cells)
Na^+/H^+ exchanger kinetic rate constant	k_e	0.0416 μM cm/s	Grinstein [24] (rat thymic lymphocyte)	0.0208	Grinstein [24]	0.0832	Grinstein [24]
Permeability of protonated base NH_4^+	P_{BH+}	3.5×10^{-7} cm/s	Simulation (fitted parameter)	10^{-8}	–	10^{-6}	–

Table 2: Effect of variation in parameter values on the final steady-state values of $[TB]_i$ and pH_i (subscript fss), and on ΔpH_i, the deviation of the final steady-state value of pH_i from the original steady-state value, obtained from the simulation (symbols used for parameters are defined in Table 2). The NH_4Cl concentration added was 10 mM, pH_e was 7.2, and $(pH_i)_{oss}$ was 7.6. The values of the remaining parameters were taken from Table 1, column 3.

V_m mV	k_e μM cm/s	P_{BH+} cm/s	$([TB]_i)_{fss}$ mM	$(pH_i)_{fss}$	ΔpH_i
-60	0.0416	3.5×10^{-7}	6.49	7.40	-0.2
-90	0.0416	3.5×10^{-7}	8.03	7.31	-0.3
-120	0.0416	3.5×10^{-7}	10.0	7.21	-0.4
-90	0.0208	3.5×10^{-7}	15.2	7.03	-0.6
-90	0.0416	3.5×10^{-7}	8.03	7.31	-0.3
-90	0.0832	3.5×10^{-7}	5.76	7.45	-0.15
-90	0.0416	1.0×10^{-8}	3.86	7.62	0.0*
-90	0.0416	3.5×10^{-7}	8.03	7.31	-0.3
-90	0.0416	1.0×10^{-6}	25.6	6.81	-0.8

*From Figure 5, no steady-state is reached in this case.

Table 3: Values of the external concentrations of NH_3 and NH_4^+ as a function of the NH_4Cl concentration added and the pH_e value.

NH_4Cl conc. added mM	pH_e	$[NH_3]_e$ mM	$[NH_4^+]_e$ mM
10	7.6	0.25	9.75
10	7.2	0.10	9.90
10	6.8	0.04	9.96
3	7.2	0.03	2.97
10	7.2	0.10	9.90
30	7.2	0.30	29.7

Table 4: Effect of the NH_4Cl concentration added and the pH_e value on the final steady-state values of $[TB]_i$ and pH_i (subscript fss), and on ΔpH_i, the deviation of the final steady-state value of pH_i from the original steady-state value. Comparison of simulation results with experimental data. $(pH_i)_{oss}$ was 7.6. The parameter values were taken from Table 1, column 3.

NH_4Cl conc. added	pH_e	Simulation $([TB]_i)_{fss}$	Simulation $(pH_i)_{fss}$	Simulation ΔpH_i	Experimental ΔpH_i
3	7.2	1.51	7.51	-0.1	-0.0-0.1
10	7.2	8.03	7.31	-0.3	-0.2-0.3
30	7.2	75.2	6.81	-0.8	-0.5-0.7
10	7.6	19.2	7.30	-0.3	-0.2-0.3
10	7.2	8.03	7.31	-0.3	-0.2-0.3
10	6.8	3.32	7.32	-0.3	-0.2-0.3

Figure 1: Effect of cell surface area-to-volume ratio

The time trajectories of the total base concentration in the cell (Fig. 1A) or the intracellular pH (Fig. 1B), determined from the simulation, are plotted for different values of ρ, the cell surface area to volume ratio. ρ= 2000 (dashed lines), 4000 (solid lines), or 6000 (dot-dashed lines) cm^{-1}. All other parameter values are as in Table 1, column 3. The NH_4Cl concentration added was 10 mM and pH_e was 7.2.

Figure 2: Effect of intracellular buffering power

The time trajectories of the total base concentration inside the cell (Fig. 2A) or the intracellular pH (Fig. 2B), determined from the simulation, are plotted for different values of β, the intracellular buffering power. β= -18 (dashed lines), -25 (solid lines), or -50 (dot-dashed lines) mM. All other parameter values are as in Table 1, column 3. The NH_4Cl concentration added was 10 mM and pH_e was 7.2.

Figure 3: Effect of membrane potential

The time trajectories of the total base concentration inside the cell (Fig. 3A) or the intracellular pH (Fig. 3B), determined from the simulation, are plotted for different values of V_m, the membrane potential. V_m= -60 (dashed lines), -90 (solid lines), or -120 (dot-dashed lines) mV. All other parameter values are as in Table 1, column 3. The NH_4Cl concentration added was 10 mM and pH_e was 7.2.

Figure 4: Effect of Na^+/H^+ exchanger kinetic rate constant

The time trajectories of the total base concentration inside the cell (Fig. 4A) or the intracellular pH (Fig. 4B), determined from the simulation, are plotted for different values of k_e, the Na^+/H^+ exchanger kinetic rate constant. k_e= 0.0208 (dashed lines), 0.0416 (solid lines), or 0.0832 (dot-dashed lines) μM cm/s. All other

parameter values are as in Table 1, column 3. The NH_4Cl concentration added was 10 mM and pH_e was 7.2.

Figure 5: Effect of cell permeability to NH_4^+

The time trajectories of the total base concentration inside the cell (Fig. 5A) or the intracellular pH (Fig. 5B), determined from the simulation, are plotted for different values of $P_{NH_4^+}$, the cell permeability to NH_4^+. $P_{NH_4^+} = 10^{-8}$ (dashed lines), 3.5×10^{-7} (solid lines), or 10^{-6} (dot-dashed lines) cm/s. All other parameter values are as in Table 1, column 3. The NH_4Cl concentration added was 10 mM and pH_e was 7.2.

Figure 6: Effect of NH_4Cl concentration added at pH_e 7.2

The time trajectories of the total base concentration inside the cell (Fig. 6A) or the intracellular pH (Fig. 6B), determined from the simulation, are plotted for different values of the NH_4Cl concentration added at pH_e 7.2. The NH_4Cl concentration added was 3 (dashed lines), 10 (solid lines), or 30 (dot-dashed lines) mM. All parameter values are as in Table 1, column 3. The external concentrations of NH_3 and NH_4^+ at each NH_4Cl concentration are given in Table 3.

Figure 7: Experimental data on the effect of the NH_4Cl concentration added at pH_e 7.2

The deviation of pH_i from its original steady-state value upon NH_4Cl addition at pH_e 7.2 was measured as described in a previous paper [15]. These deviation values were subtracted from 7.6 and plotted as a function of time because short-term measurements of the effect of pH_e on the absolute value of pH_i indicated that the original steady-state value of pH_i was 7.6 at pH_e 7.2. The NH_4Cl concentrations added were 3 (dashed line), 10 (solid line), or 30 (dot-dashed line) mM.

Figure 8: Effect of external pH value at 10 mM NH_4Cl

The time trajectories of the total base concentration inside the cell (Fig. 8A) or the intracellular pH (Fig. 8B), determined from the simulation, are plotted for different values of the external pH value. pH_e= 7.6 (solid lines), 7.2 (dashed lines), or 6.8 (dot-dashed lines). The original steady-state value of pH_i was set equal to 7.6 at all pH_e values. All other parameter values are as in Table 1, column 3. The NH_4Cl concentration added was 10 mM. The external concentrations of NH_3 and NH_4^+ at each pH_e value are given in Table 3.

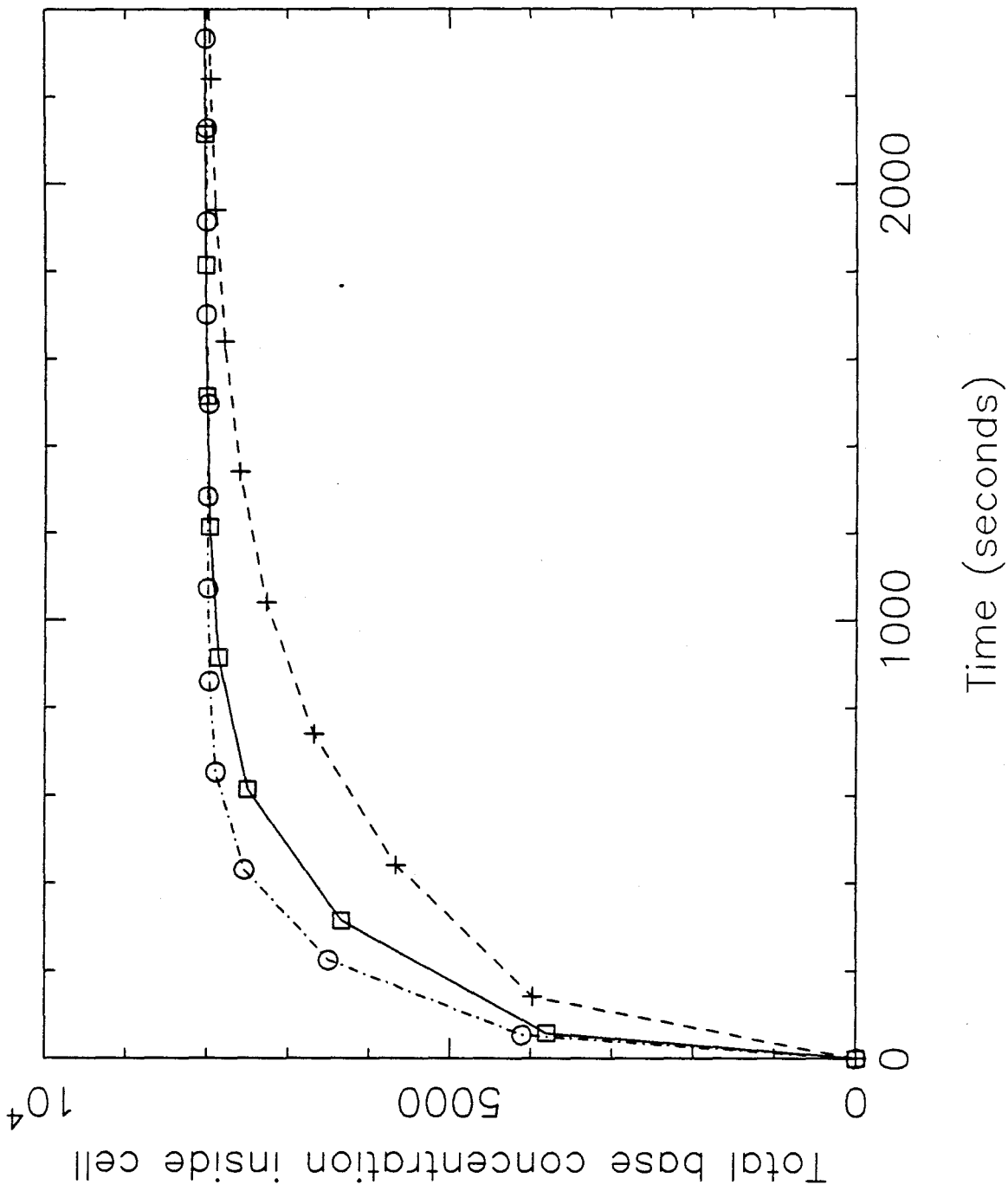
Total base concentration inside cell
10^4
5000
0
0
1000
2000
Time (seconds)

Figure 1A

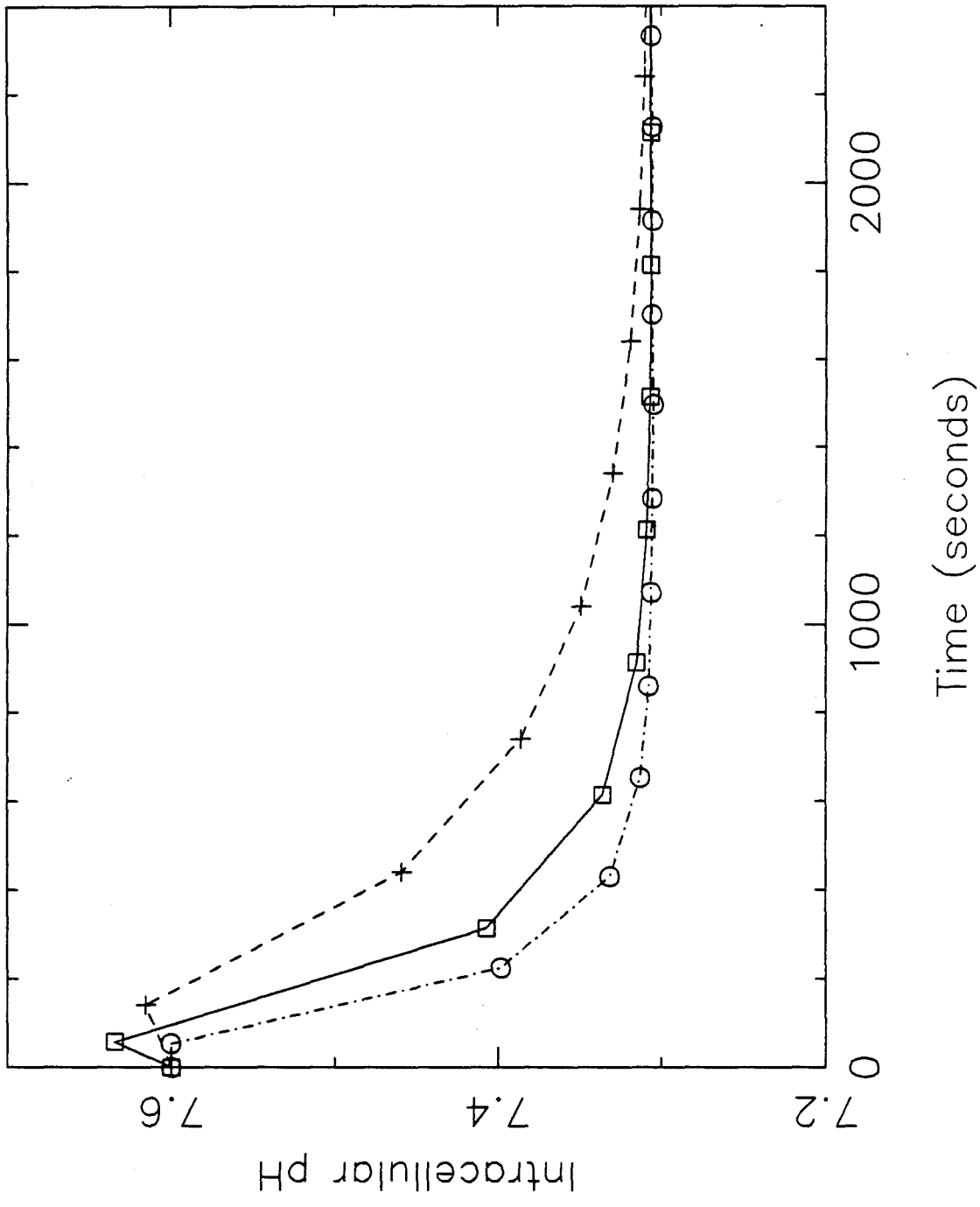

Figure 1B

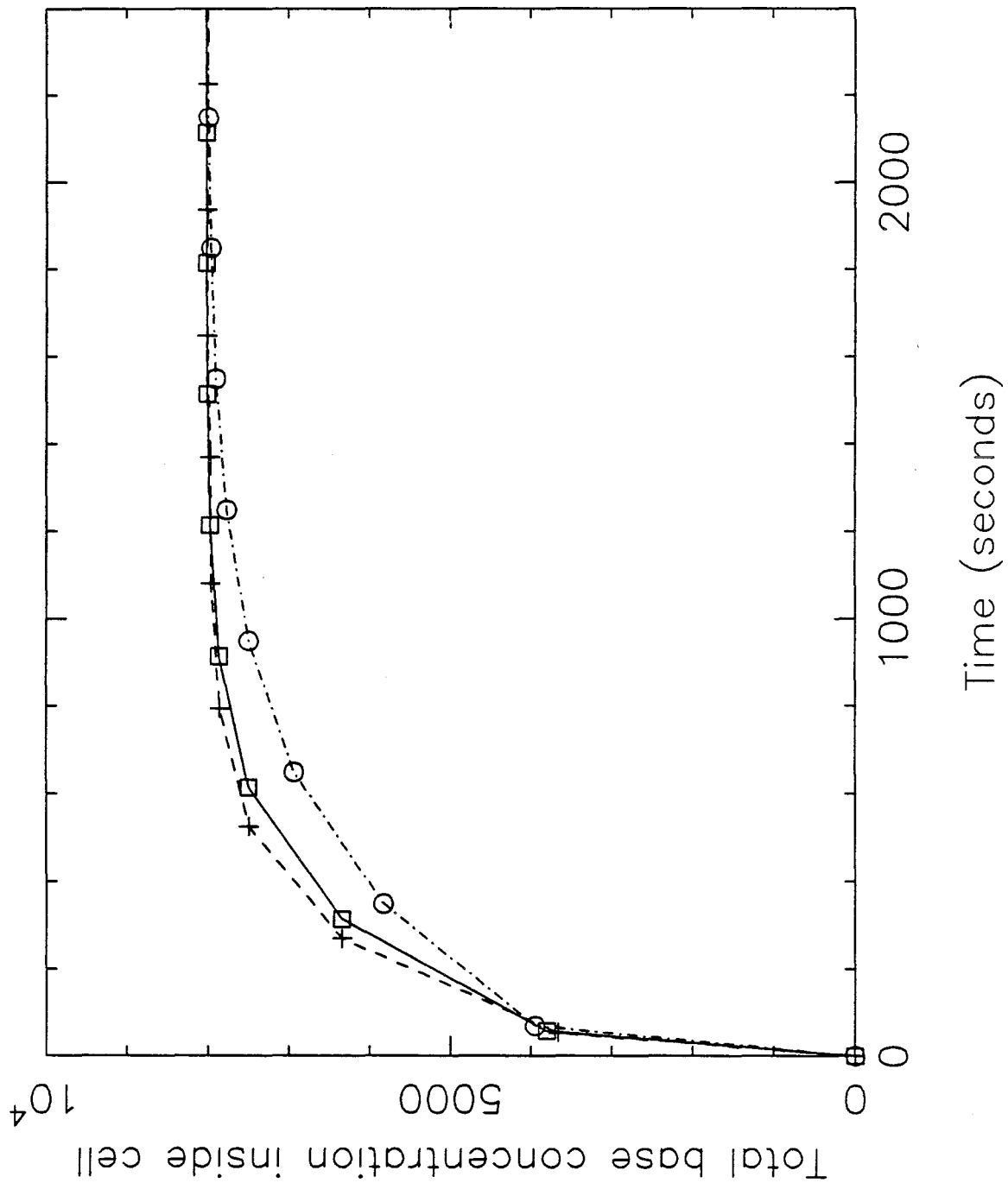
Total base concentration inside cell
0
5000
10^4
0
1000
2000
Time (seconds)

Figure 2A

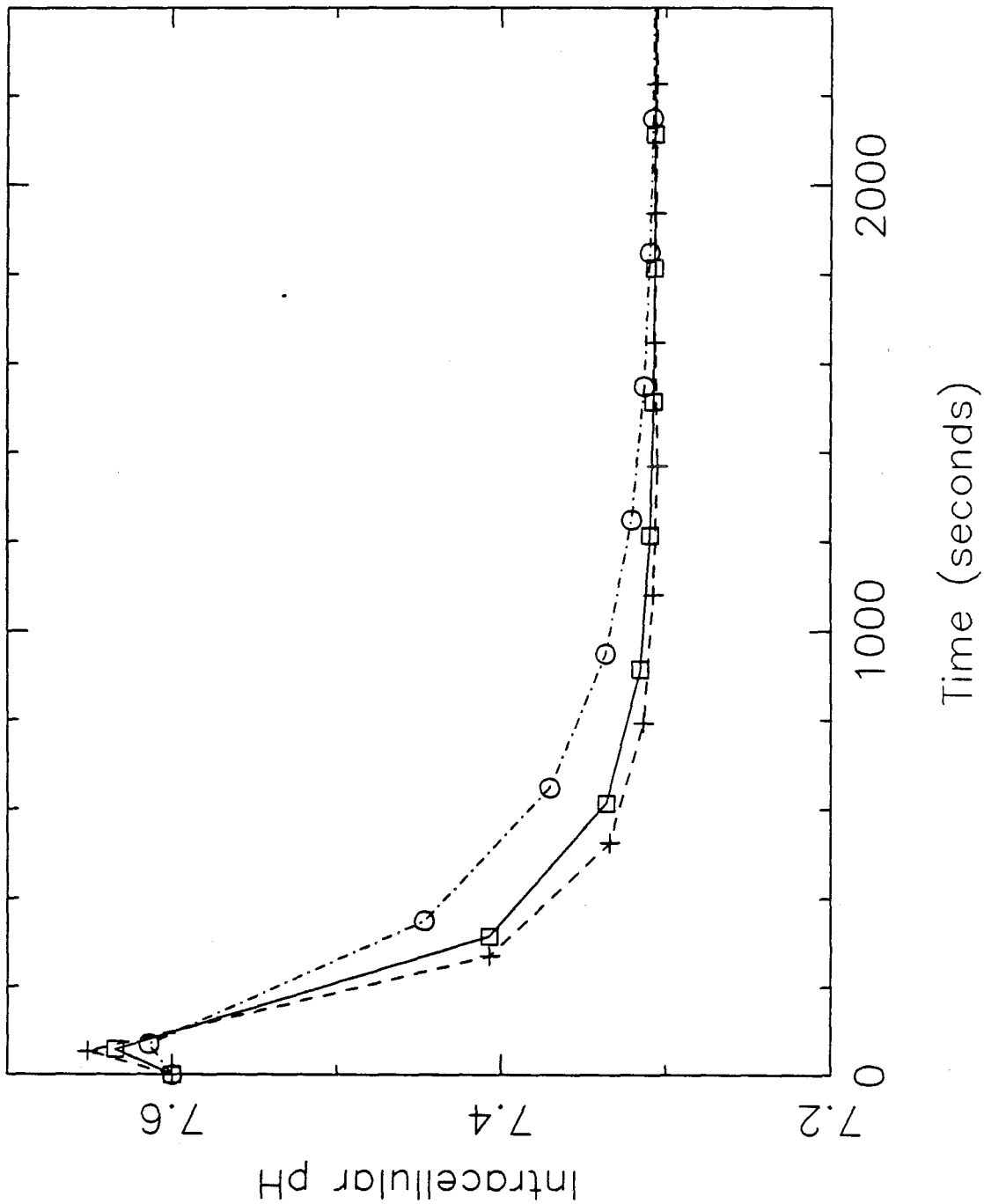

Figure 2B

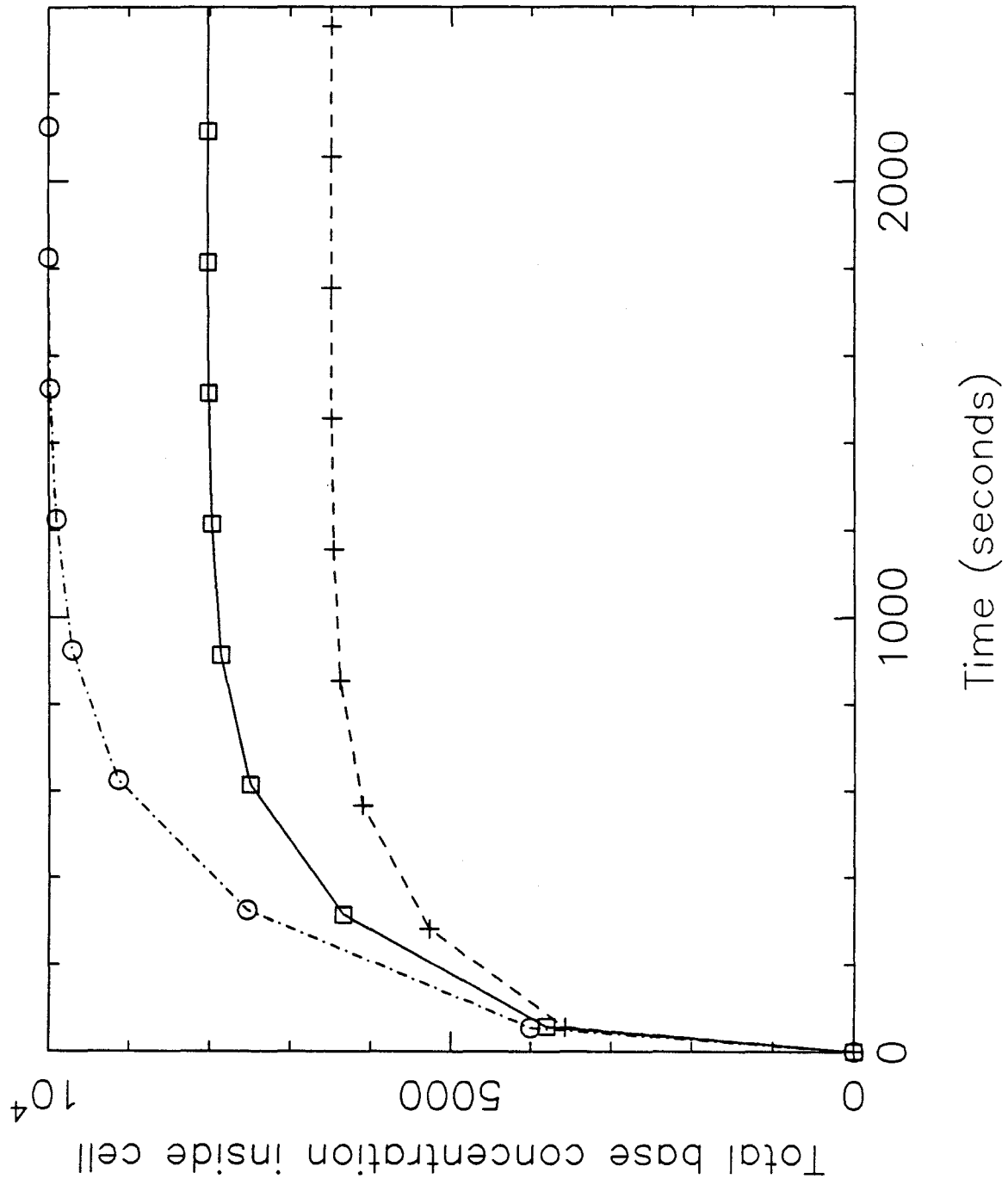
Total base concentration inside cell
10^4
5000
0
0
1000
2000
Time (seconds)

Figure 3A

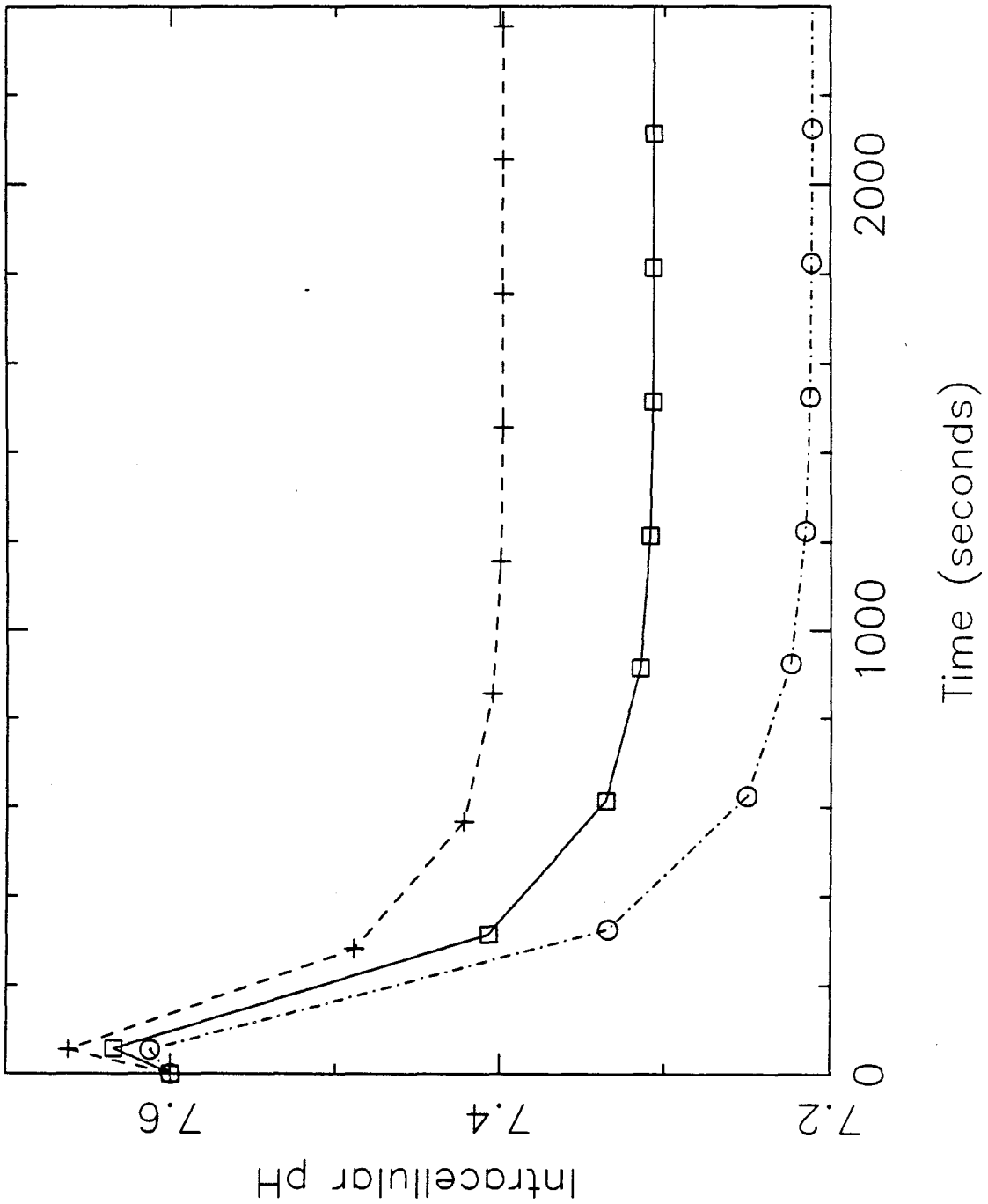

Figure 3B

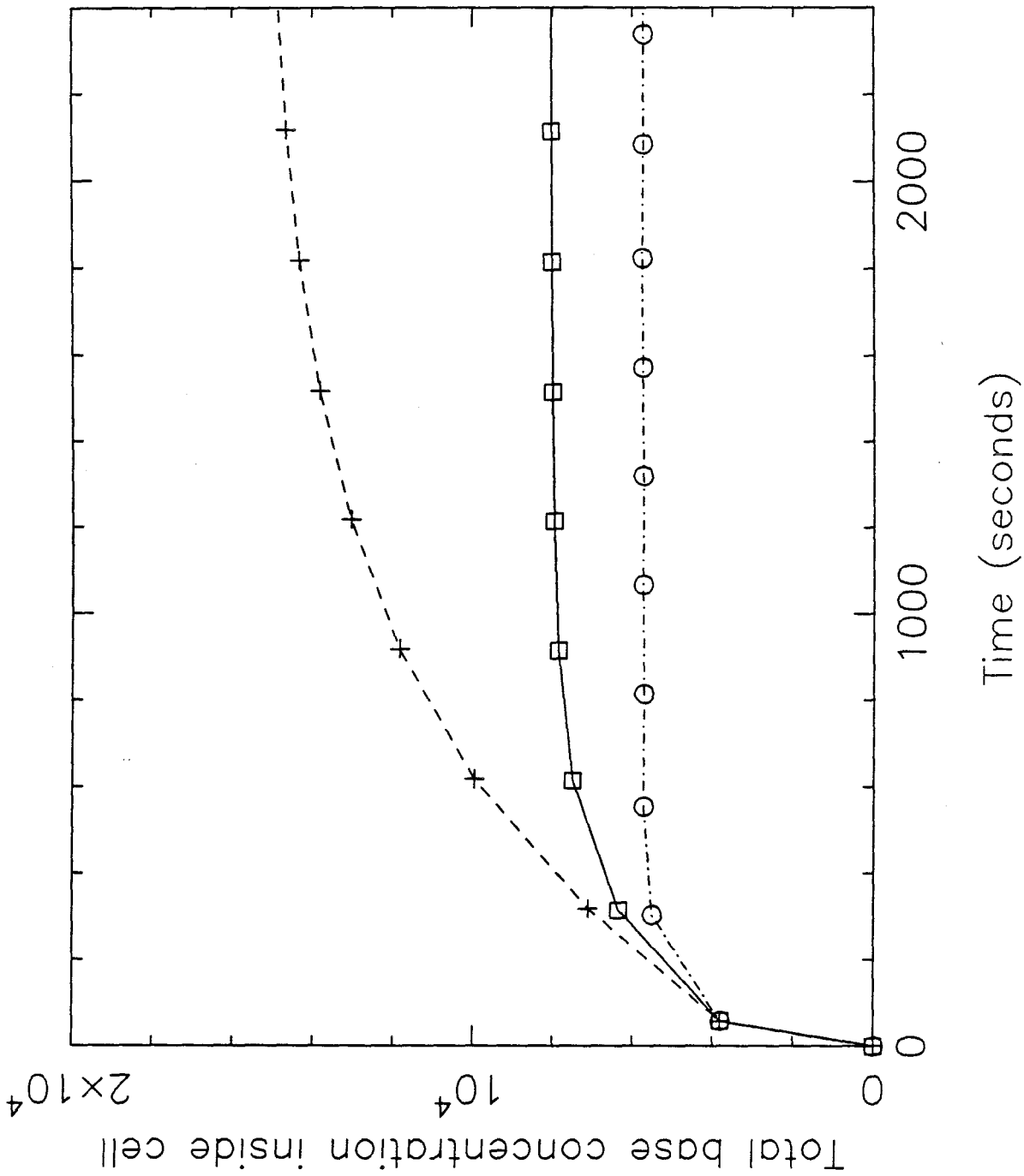
Total base concentration inside cell
0
10⁴
2×10⁴
0
1000
2000
Time (seconds)

Figure 4A

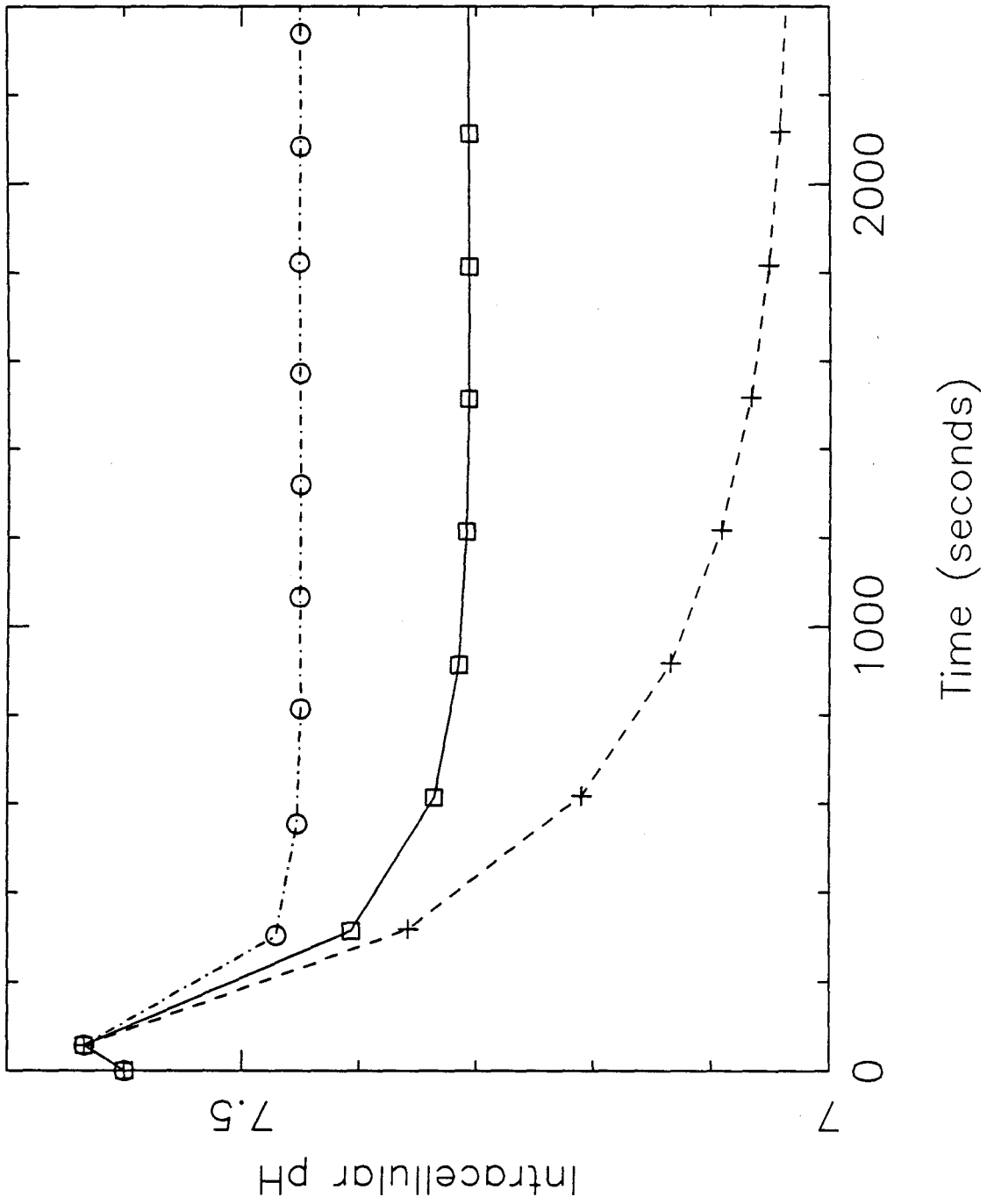

Figure 4B

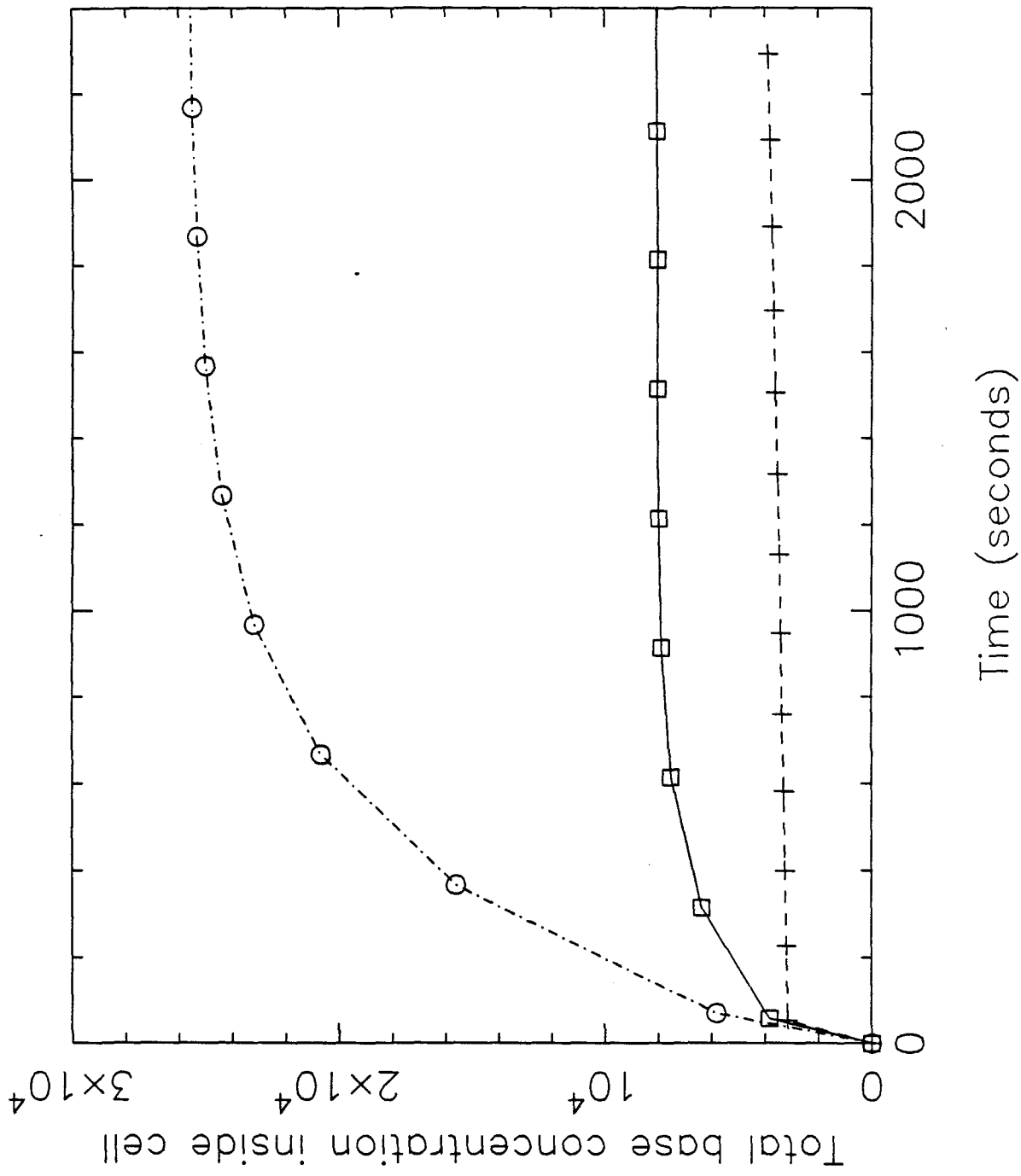
Total base concentration inside cell
0
10⁴
2×10⁴
3×10⁴
0
1000
2000
Time (seconds)

Figure 5A

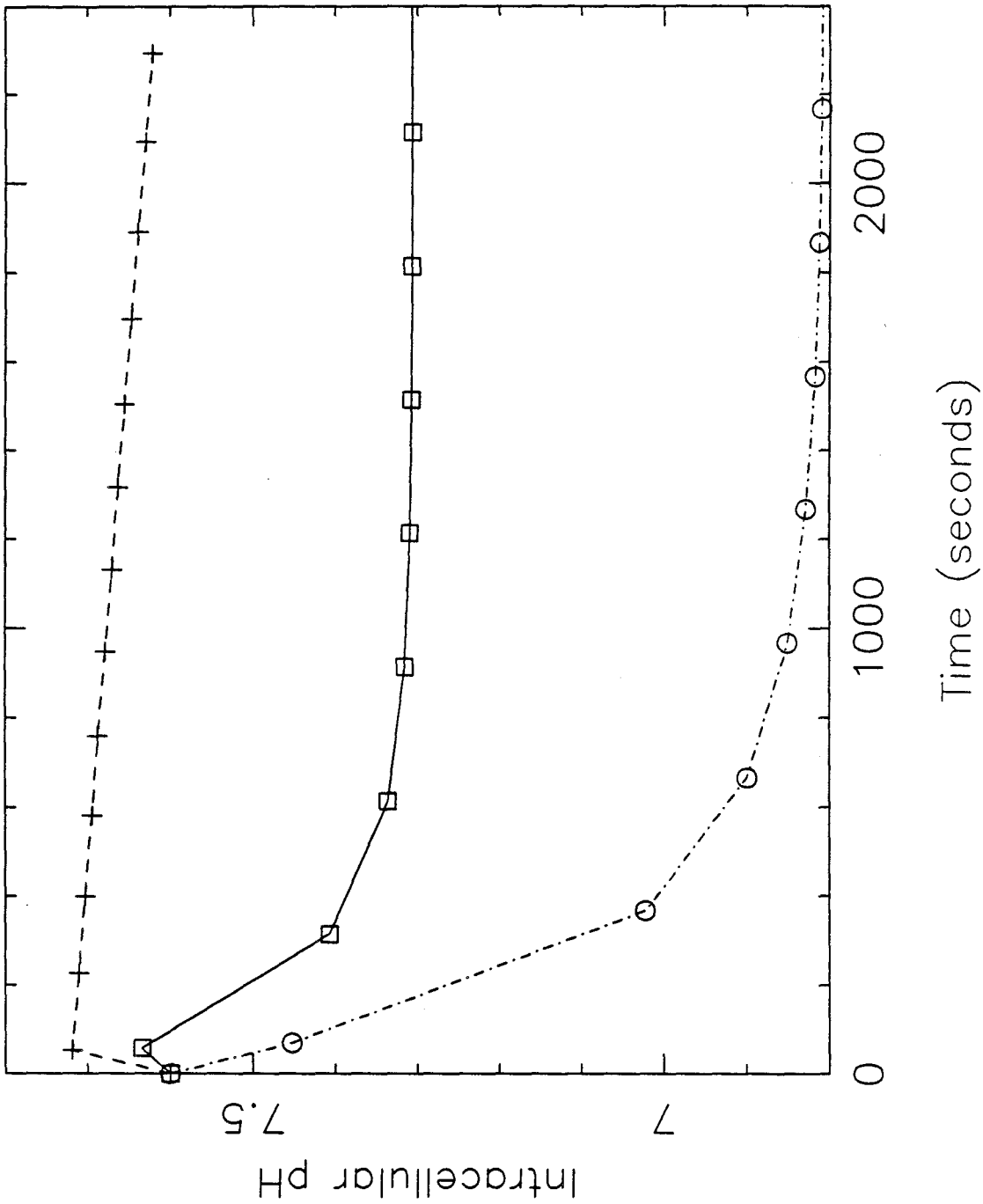

Figure 5B

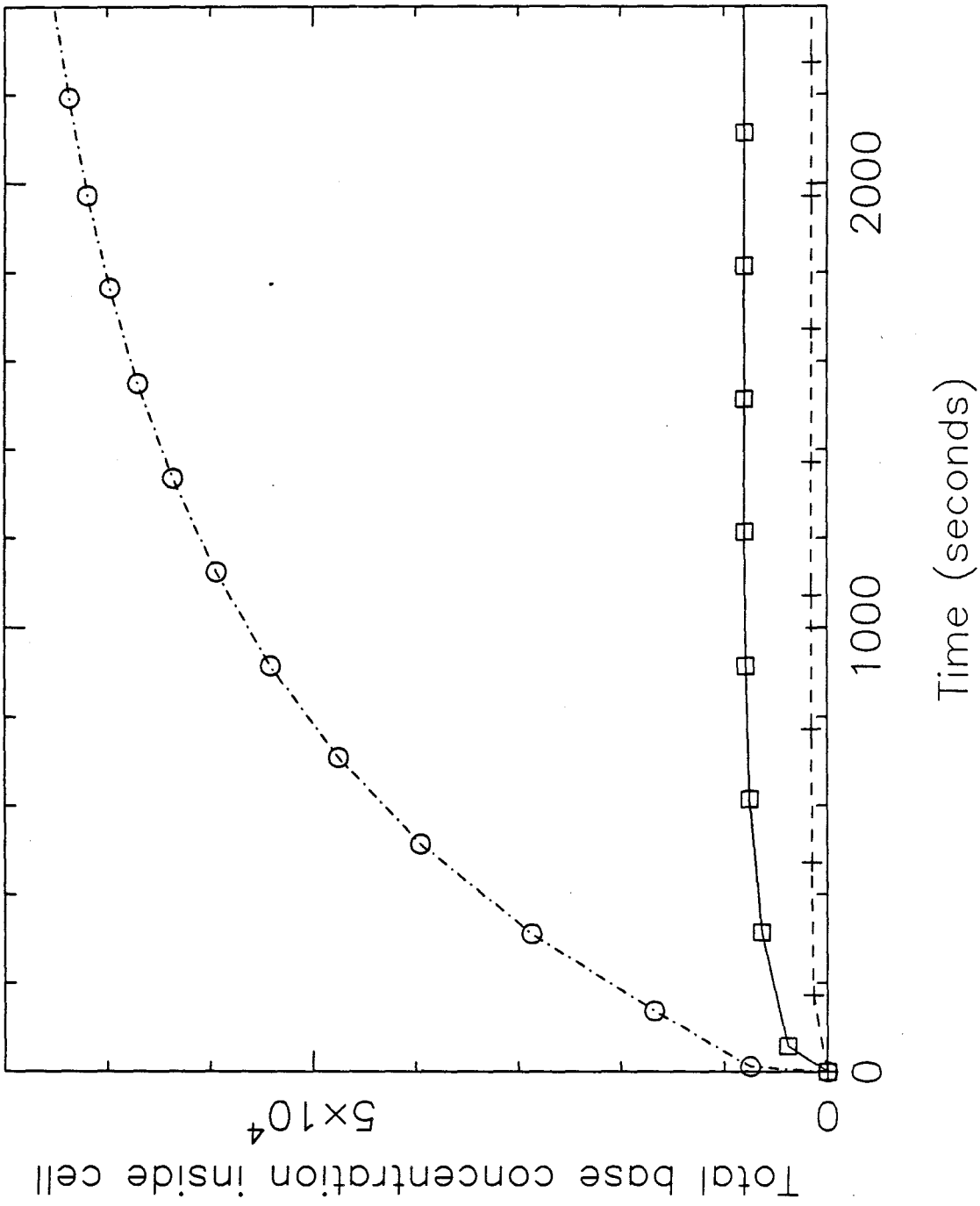
Total base concentration inside cell
5×10⁴
0
0
1000
2000
Time (seconds)

Figure 6A

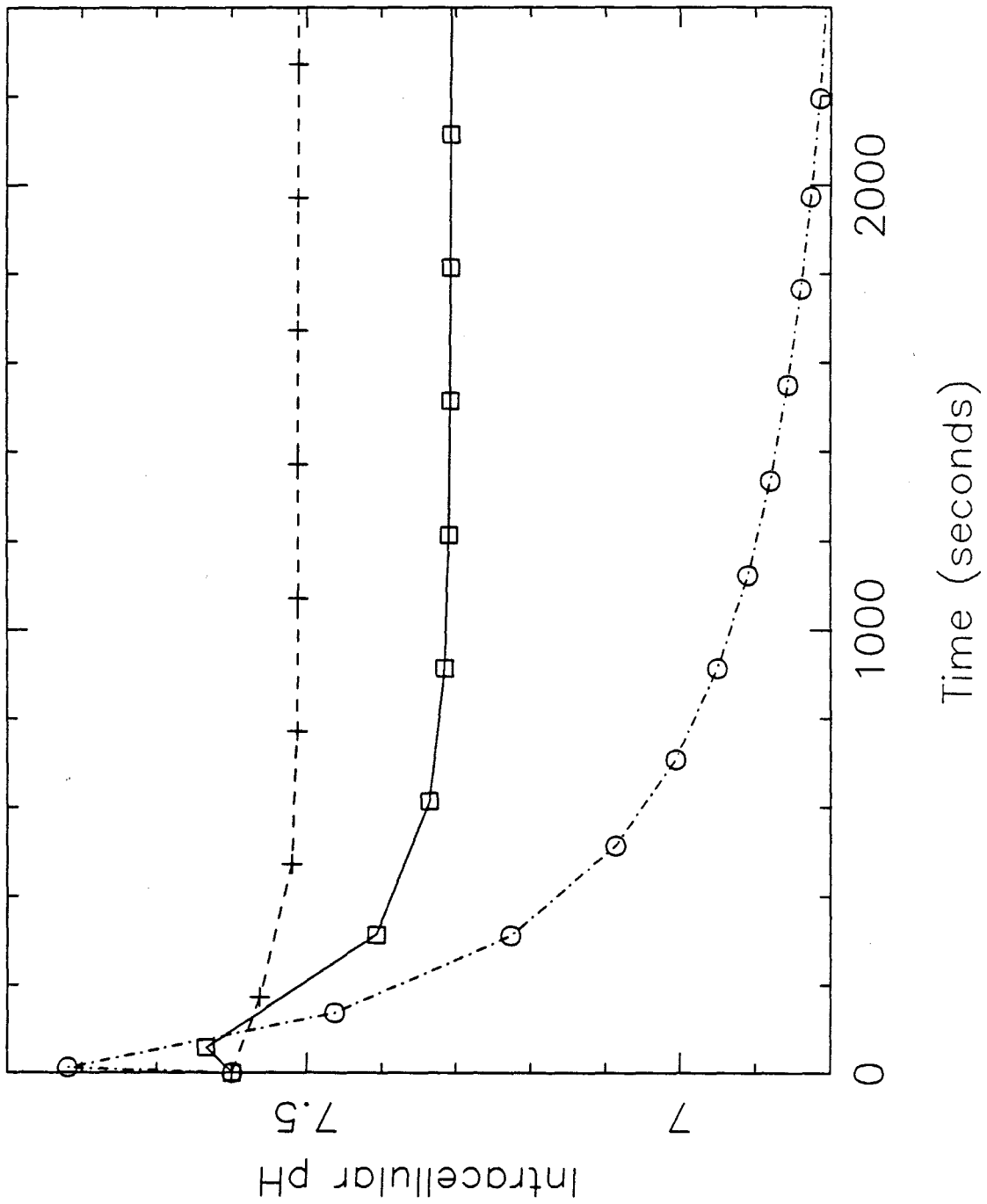

Figure 6B

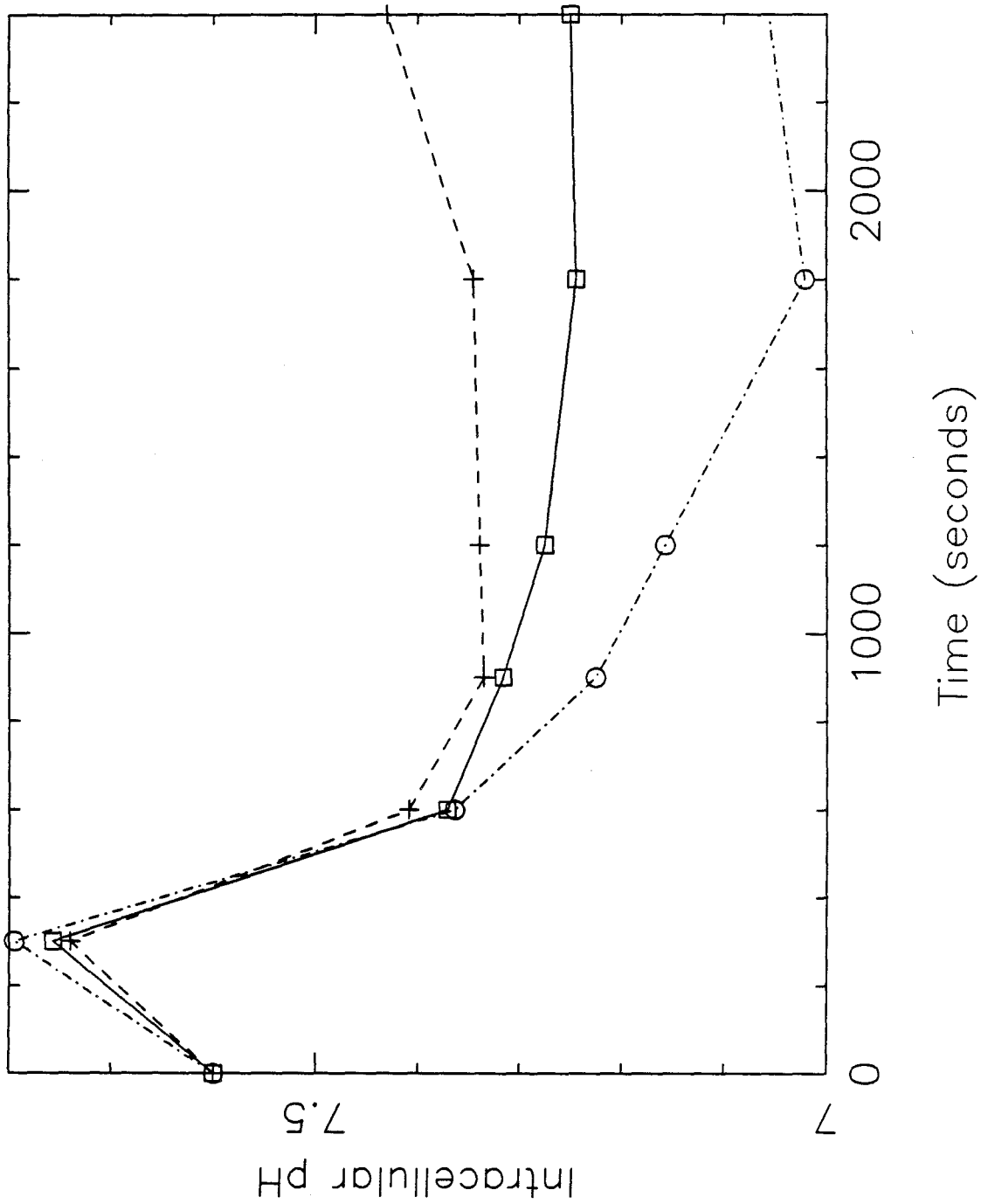

Figure 7

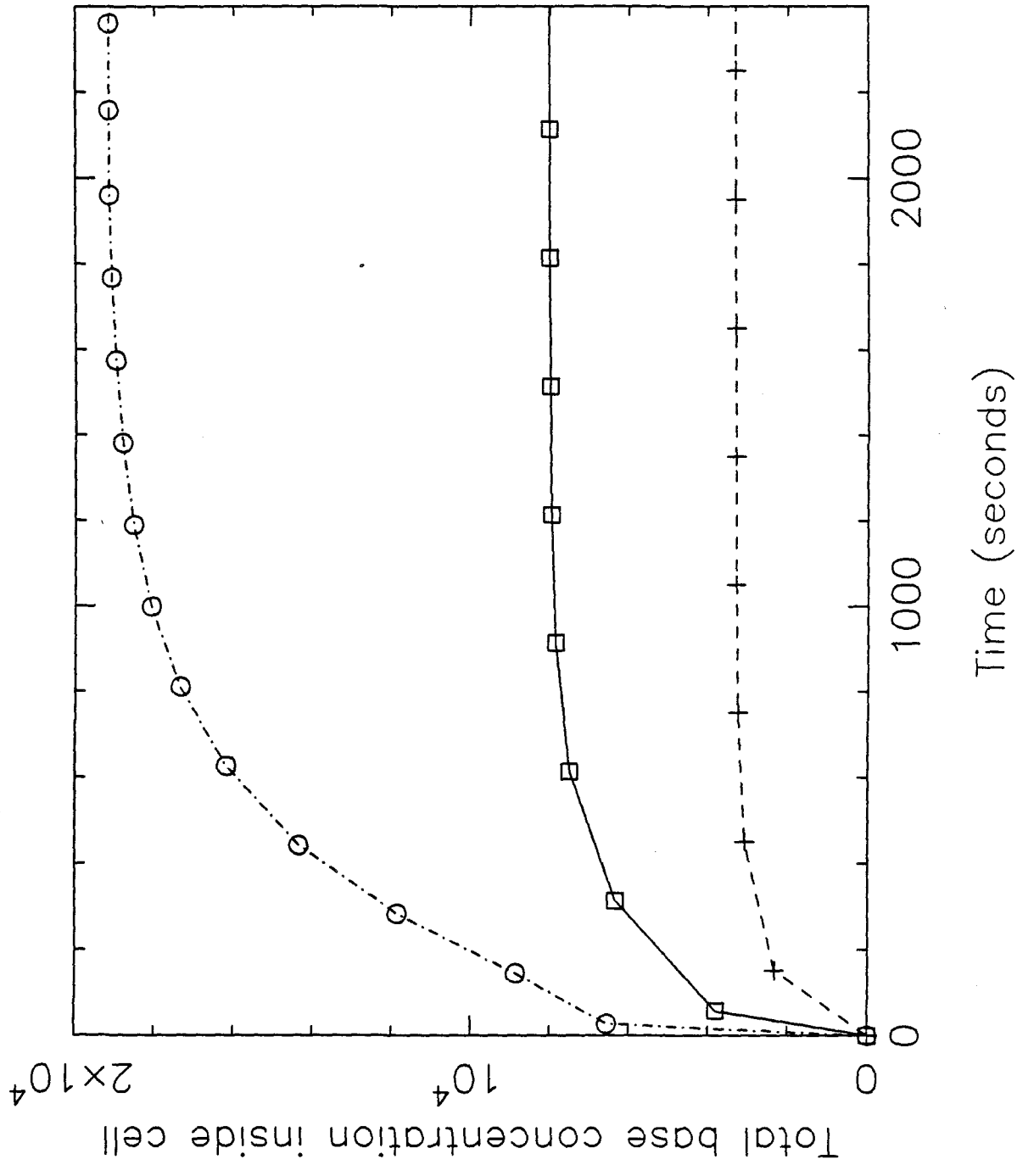
Total base concentration inside cell
0
10⁴
2×10⁴
0
1000
2000
Time (seconds)

Figure 8A

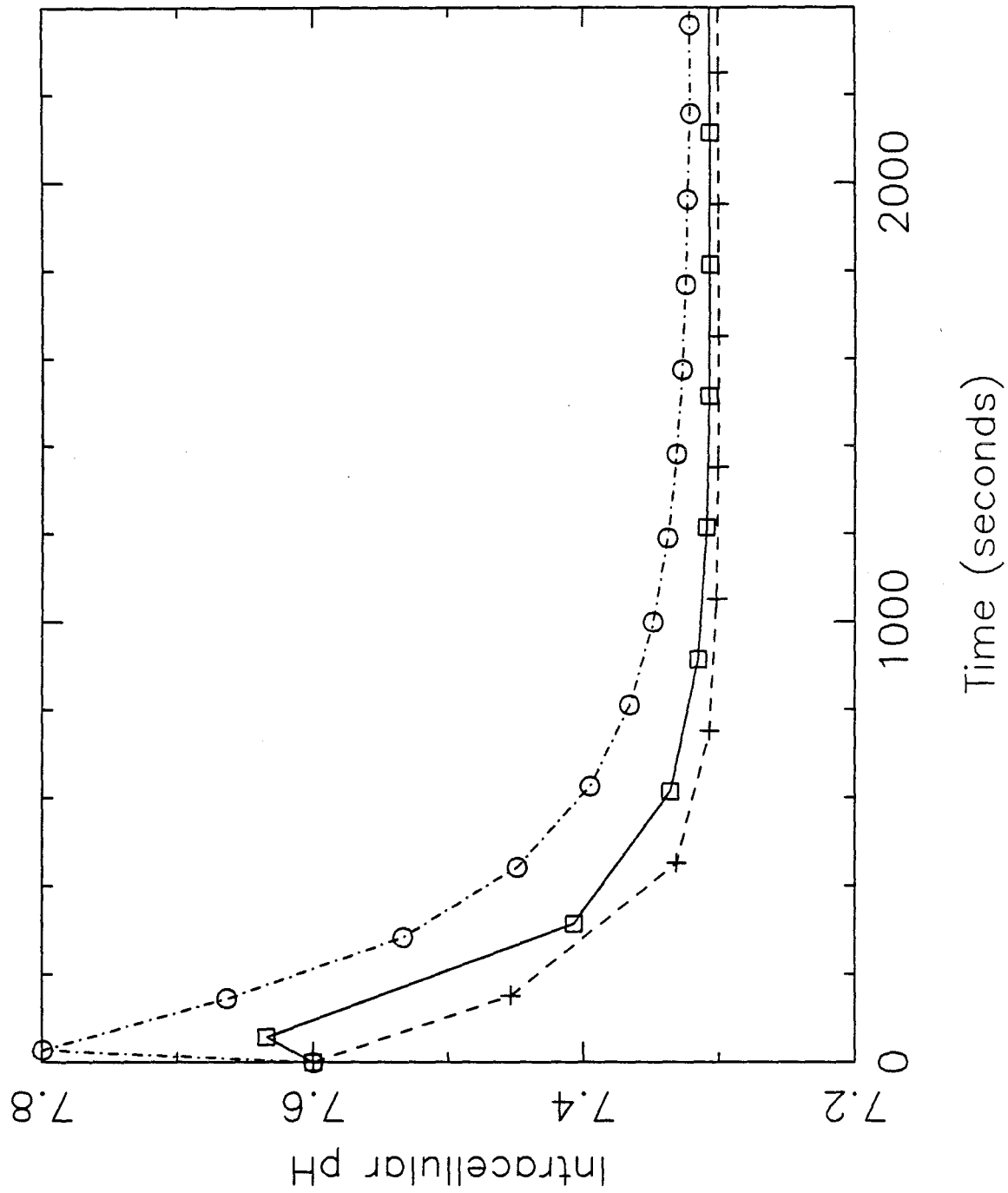

Figure 8B

CHAPTER 7.

Conclusions

Part A. Flow effects on the viability and lysis of suspended mammalian cells

1) When suspended mammalian cells were subjected to multiple passes through a turbulent flow device consisting of a sudden contraction into a short length of capillary tubing, the cells either broke or remained viable. 100 passes through the flow device had no effect on the growth rate of the surviving cells implying that exposure to the flow had no long-term sublethal effects.

2) A constant fraction of cells is lysed per pass through the turbulent flow device. This is the specific lysis rate.

3) The threshold value of the average wall shear stress level in the turbulent flow device at which significant lysis begins to occur is 1800dyn/cm^2. Above this value, the specific lysis rate increases with the average wall shear stress level.

4) The specific lysis rate increases with the residence time per pass in the turbulent flow device, indicating that the effects of the turbulent flow in the tube are significant relative to the extensional flow at the inlet.

5) The threshold value of the Kolmogorov length scale in the turbulent flow device, the size of the smallest turbulent velocity fluctuations, was found to be 3.5 μm, which is on the order of the cell diameter. This is in agreement with common theories on hydrodynamic effects on particles in turbulent flow.

6) A decrease in the serum level in which the cells are grown and subjected to flow trauma from 10% to 5% leads to an increase in the specific lysis rate in the turbulent flow device, suggesting that serum exerts a protective effect on cells during exposure to flow trauma.

7) The specific lysis rate of hybridoma cells in the turbulent flow device was higher than that of myeloma cells, implying that damage due to flow is cell-line dependent.

8) The threshold value of the average wall shear stress level was the same in the turbulent and laminar flow devices, implying that it is an important parameter governing cell damage.

9) However, the threshold value of the average wall shear stress level is not the only parameter governing lysis, since increases in the viscosity of the medium, which increase the average wall shear stress level in the laminar flow device, have no effect on the specific lysis rate in this device.

10) Increases in the viscosity of the medium, which increase the Kolmogorov length scale in the turbulent flow device, have no effect on the specific lysis rate in this device, indicating that the Kolmogorov length scale is not the only parameter governing lysis in turbulent flow.

Part B. Ammonium ion effects on hybridoma cell physiology

1) The addition of NH_4Cl causes cytoplasmic acidification, the extent of which depends on the NH_4Cl concentration.

2) There is a correlation between the effects of different NH_4Cl concentrations on growth and on pH_i. The addition of 10 mM NH_4Cl, which results in a 0.2-0.3 unit decrease in pH_i, causes severe growth inhibition.

3) The effects of NH_4Cl on growth and on pH_i were found to be independent of pH_e over the range 6.8 to 7.6, suggesting the importance of the mechanism of growth inhibition by NH_4^+ involving cytoplasmic acidification relative to that of the mechanism involving lysosomal alkalinization, discussed in the literature.

4) The addition of NH_4Cl leads to an increase in the average cell volume at pH_e 7.6 but not at pH_e values 6.8 and 7.2, implying that the lysosomal mechanism of growth inhibition is in effect at pH_e 7.6 but not at pH_e values 6.8 or 7.2.

5) Changes in pH_e over the range 6.8 to 7.6 have little effect on growth, while substantial growth inhibition occurs at pH_e 6.6.

6) Batch growth rates in flasks in an incubator and in a bioreactor at controlled pH and dissolved oxygen concentration were similar, implying that cultures in flasks were not oxygen-limited. Measurements of the effects of pH_e and NH_4Cl concentration on growth, metabolism, and antibody production also gave similar results for cells grown in flasks in the incubator or in the bioreactor.

7) Decreases in pH_e and increases in the NH_4Cl concentration result in decreases in glucose consumption in batch growth. It is hypothesized that this is due to inhibition of glycolysis by low pH_i, since previous measurements had shown that

both decreases in pH_e and increases in the NH_4Cl concentration lead to cytoplasmic acidification.

8) Decreases in pH_e inhibit glycolysis more than they inhibit growth, indicating that growth is not dependent on glucose consumption.

9) At all pH_e values, in the absence of NH_4Cl, glutamine is depleted at the time the maximum cell density is reached, suggesting that glutamine may be limiting cell growth.

10) In the case of pH_e decreases, decreases in the cell yield on glutamine are compensated by increases in the cell yield on glucose, while, in the case of increases in the NH_4Cl concentration, both the cell yield on glucose and the cell yield on glutamine decrease. This implies that the mechanism of growth inhibition is different in the two cases, and that NH_4Cl has some additional effect on cells other than causing cytoplasmic acidification. This finding points to some role for the alternate mechanism of growth inhibition by NH_4^+, that involving lysosomal alkalinization.

11) Changes in pH_e and in the NH_4Cl concentration, which cause growth inhibition, have no effect on the specific antibody production rate, underlining the fact that antibody production is not growth- related.

12) Using a mathematical model for the effects of NH_4Cl on pH_i, it is found that the cell permeability to NH_4^+ required to obtain a steady-state cytoplasmic acidification of the magnitude we observed is 3.5×10^{-7} cm/s, which is on the order of typical cell permeabilities to K^+.

13) A mathematical model for the effects of NH_4Cl on pH_i is consistent with the salient features of the experimental results, using parameter values taken from the

literature and a single fitted parameter, the cell permeability to NH_4^+. The features of pH_i changes upon NH_4Cl addition, which the model is consistent with, include the transient characteristics, the dependence on the NH_4Cl concentration and the lack of dependence on pH_e. The agreement between simulation results and experimental data implies that the assumptions made in developing the model could be valid (including the assumption that the Na^+/H^+ exchanger is the main pH_i regulating system in the cell) and that the mechanism proposed for NH_4^+ effects on pH_i used to formulate the mathematical model could be correct.